NAS9-14315
T-1067
LINE ITEM NO. 8
MA-129T
R-9807

NASA CR-
144409

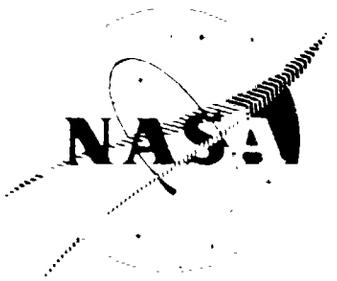

ORBITAL MANEUVERING ENGINE

FEED SYSTEM COUPLED STABILITY INVESTIGATION

FINAL REPORT

1 SEPTEMBER 1975

Prepared For

National Aeronautics and Space Administration
Lyndon B. Johnson Space Center
Houston, Texas 77058

Rockwell International
Rocketdyne Division
6633 Canoga Avenue
Canoga Park, California 91304

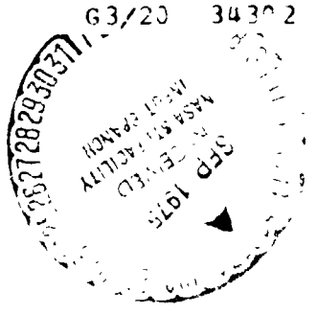

DISTRIBUTION LIST

Addresses	Copies
NASA/Lyndon B. Johnson Space Center R&T Procurement Branch Attn: C. S. Parks, Mail Code BC73(40) Houston, TX 77058	1
NASA/Lyndon B. Johnson Space Center Technical Library Branch Attn: Retha Shirkey, Mail Code JM6 Houston, TX 77058	4
NASA/Lyndon B. Johnson Space Center Management Services Division Attn: John T. Wheeler, Mail Code AT3 Houston, TX 77058	1
NASA/Lyndon B. Johnson Space Center Primary Propulsion Branch Attn: F. D. Freeburn, Mail Code EP2 Houston, TX 77058	30

FOREWORD

This document was prepared by Rocketdyne, a Division of Rockwell International Corporation, in accordance with Article I and Line Item No. 8 of the Data Requirements List of Contract NAS9-14315 with the National Aeronautics and Space Administration. The contract period of performance was 6 August 1974 to 6 July 1975. The NASA/JSC Technical Monitor was Mr. F. D. Freeburn. The Rocketdyne Program Manager was Mr. R. H. Helsel for the first three months; he was replaced by Mr. R. D. Paster for the remainder of the program. Mr. J. A. Nestlerode served as the Principal Engineer, assisted by Dr. D. R. Kahn.

Several technical people at Rocketdyne performed work or served as consultants regarding specific areas of the various program tasks: Mssrs. J. K. Hunting, R. L. Nelson, and L. E. Sack with respect to the feed system hydrodynamics, Mr. F. R. Linow with respect to combustion dynamics, Mr. M. D. Schuman with respect to combustion dynamics, chamber dynamics, engineering model formulation, and computer programming, and Mr. K. W. Fertig with respect to numerical analysis, computer programming,and checkout.

ABSTRACT

This report summarizes the technical effort conducted during an eleven-month program to develop and verify a digital computer model for NASA/JSC which can be used to analyze and predict engine/feed system coupled instabilities in pressure-fed storable propellant propulsion systems over a frequency range of 10 to 1000 Hz.

The analytical approach to modeling the feed system hydrodynamics, combustion dynamics, chamber dynamics, and overall engineering model structure is described and the governing equations in each of the technical areas is presented. This is followed by a description of the generalized computer model in which the specifics of the hydrodynamics, combustion dynamics, and chamber dynamics are formulated into discrete subprograms and integrated into an overall engineering model structure.

The operation and capabilities of the engineering model are verified by comparing the model's theoretical predictions with experimental data from an OMS-type engine with known feed system/engine chugging history. The latter data were obtained at White Sands Test Facility on Rocketdyne hardware during Task XII of the SS/OME Reusable Thrust Chamber Program (NAS9-12802).

The program is concluded with the successful operation of the engineering model on the NASA/JSC Univac 1110,EXEC-8 computer system and by extensive documentation of the model in the form of a computer user's guide and final report.

CONTENTS

ILLUSTRATIONS

TABLES

NOMENCLATURE

A	Area
A_n	Nozzle admittance; flow area of n^{th} line segment
c	Acoustic velocity
c_f	Pipe and restraint factor
c_p	Specific heat at constant pressure
c_v	Specific heat at constant volume
C_D	Drag coefficient
d_j	Liquid jet diameter at the atomization plane
D	Diameter
$\mathcal{D}$	Molecular diffusivity
e	Pipe wall thickness
E	Young's modulus
$\vec{F}$	Drag force vector
g	Gravitational [illegible]
h	Enthalpy
ΔH_{vap}	Latent heat of vaporization
i, J	$\sqrt{-1}$
I	Identity tensor
j,k,n	Summation indices
k	Thermal conductivity
l,ℓ	Length
m	Mass
$\dot{m}$	Mass flowrate

M	Mach number
MR	Mixture ratio
MW	Molecular weight
N	Number concentration of droplets
Nu_H, Nu_M	Nusselt numbers for heat and mass transfer
p,P	Pressure
Pr	Prandtl Number
Q	Spray or droplet heating rate
r	Radius
R	Resistance of fluid element
R_u	Universal gas constant
R	Response factor
t	Time
T	Temperature
$\vec{u}$	Velocity vector
v	Axial component of velocity
v_j	Liquid jet velocity
V	Volume
$\dot{w}$	Mass flowrate
x	Axial coordinate
x_K	Klystron distance (oxidizer or fuel jet)
y	Mass fraction
Z	Heat blockage parameter

GREEK LETTERS

β	Fluid bulk modulus
γ	Ratio of specific heat capacities
μ	Viscosity
ρ	Density
τ	Time delay
τ_K	Klystron time constant (oxidizer or fuel jet)
$\underline{\underline{\tau}}$	Stress tensor
ω	Complex frequency

SUPERSCRIPTS

$(\bar{})$	Time-average value of variable; or concerned with one-dimensional solution
$(\tilde{})$	Oscillatory component of variable, f(x,t)
$(\,)'$	Oscillatory component of variable, g(x)
*	Sonic flow condition
fu	Fuel
ox	Oxidizer
t	Tangential

SUBSCRIPTS

c	Chamber
d, ds	Droplet, droplet surface
eff	Effective value for turbulent flow
f	Film
fu	Fuel
g	Gas

inj	Injector, at the injector face
j	Jet or droplet group; concerned with j^{th} propellant species
k	Droplet group
l,ℓ	Liquid
n	Concerned with n^{th} droplet group, or n^{th} generalized line segment in feed system
Ø	Based on overall injection mixture ratio during steady-state operation
ox	Oxidizer
s	Fuel or oxidizer spray; at the droplet surface
v,vap	Vapor or vaporization

SECTION I

INTRODUCTION AND SUMMARY

Historically, during the development of pressure-fed propulsion systems, feed system/engine coupled instabilities have been frequently encountered. Resolution of these problems usually included increasing injector pressure drop to decouple the feed system from the combustor, the result being substantial system weight penalties. A dynamic computer model would be a useful tool in obviating coupled stability problems during the development of the Space Shuttle Orbit Maneuvering System (SS/OMS). A model could be used both as a system design tool to optimize component location and pressure profile (minimize system weight) and a system development tool to define test programs for assessing stability margins of the OMS.

Models have been constructed to study specific problems on specific engine configurations. Under a previous contract, NAS9-10319, a generalized propulsion system model for very low frequencies was constructed to provide a modular digital computer program for simulating transient operation in pressure-fed rocket engine systems (Ref. 1). The use of the program was demonstrated by modeling the Apollo Ascent and Descent engines and the Rocketdyne SE5-5 Propulsion System.

This document is the final report of an eleven-month program conducted by Rocketdyne to develop and verify an engineering digital computer model for the NASA/JSC which can be used to analyze feed system/engine coupled instabilities in pressure-fed, storable propellant, propulsion systems over a frequency range of 10 to 1000 Hz (frequencies lower than the chamber transverse frequencies). The model is sufficiently general so that it may be readily applicable to present and future engine and propulsion programs. For scaling purposes the baseline configuration chosen is the OMS engine. The model has been written for use on the NASA/JSC Univac 1110, EXEC-8 system, and provides NASA a tool which can be used to:

1. Conduct preliminary design tradeoff for feasibility studies prior to propulsion concept selection.
2. Guide the design of propulsion systems to ensure stability at all operating ranges and with minimum penalties.
3. Guide testing programs by predicting the least stable operating regimes thereby reducing the number of stability tests required.
4. Provide stability verification in the event system changes are made and hot-fire verification is impractical.
5. Diagnose problems on existing systems and evaluate potential solutions.

The specific end products of this effort are as follows:

1. A digital generalized computer model for investigating coupled instability in a pressure-fed propulsion system. The model is suitable for use in evaluating the stability of of the Space Shuttle OMS (Orbital Maneuvering System) in its various flight configurations and over its planned operating conditions. The structure of the model is modular such that it can be adapted to various configurations without major modifications. The output format of the model is such that the margin of stability is apparent rather than a simple stable/unstable prediction. Specific frequencies and modes of oscillations are also obtainable from the model.
2. Checkout of the model on the NASA/JSC (Johnson Spacecraft Center) Univac 1110, EXEC-8 computer and verification by comparing of a WSTF OMS engine and test rig with known feed system/engine chugging or buzzing history.
3. Complete documentation of the model effort including:
   a. A final report describing the effort involved in developing the model.
   b. A computer manual consisting of
      - A user's section designed for the engineer who desires to apply the model to a given engine system.

- A programmer's section for elucidation of the programming details, i.e., format, subroutining structure, program numerical limits, etc.
- An engineering section explaining the physical implications of the mathematics involved, the assumptions, range of validity and realistic limitations.

4. Discussions and recommendations for additional areas of investigation either for the improvement in the model or in application of the model to benefit existing or future propulsion programs. One such item is a test plan for the empirical determination of appropriate values of the variables describing the injection and combustion process. Areas of application of the model include analysis of the several OMS flight configurations, investigations of any coupled stability phenomena which might be incurred in the OMS system to determine their causes and to arrive at the most expeditious solutions, and to elucidate the coupled stability margin as a function of operating conditions.

The program was accomplished in three phases:

I. Model Evaluation and Formulation

II. Computer Model Development

III. Model Verification and Documentation

A logic flow diagram of the completed effort is shown in Fig. 1 .

In the initial phase, a detailed assessment of the available techniques for modeling the propulsion system's hydrodynamics, combustion dynamics and chamber dynamics was conducted. Recommendations for the characterization technique to be used in each of the technical areas were made and the dynamic equations were formulated. The results of Phase I were presented at a briefing held at NASA/JSC on 15-16 November 1974 and summarized in detail in a Phase I report, "Engineering Model Characterization Evaluation Interim Report" (Ref. 2).

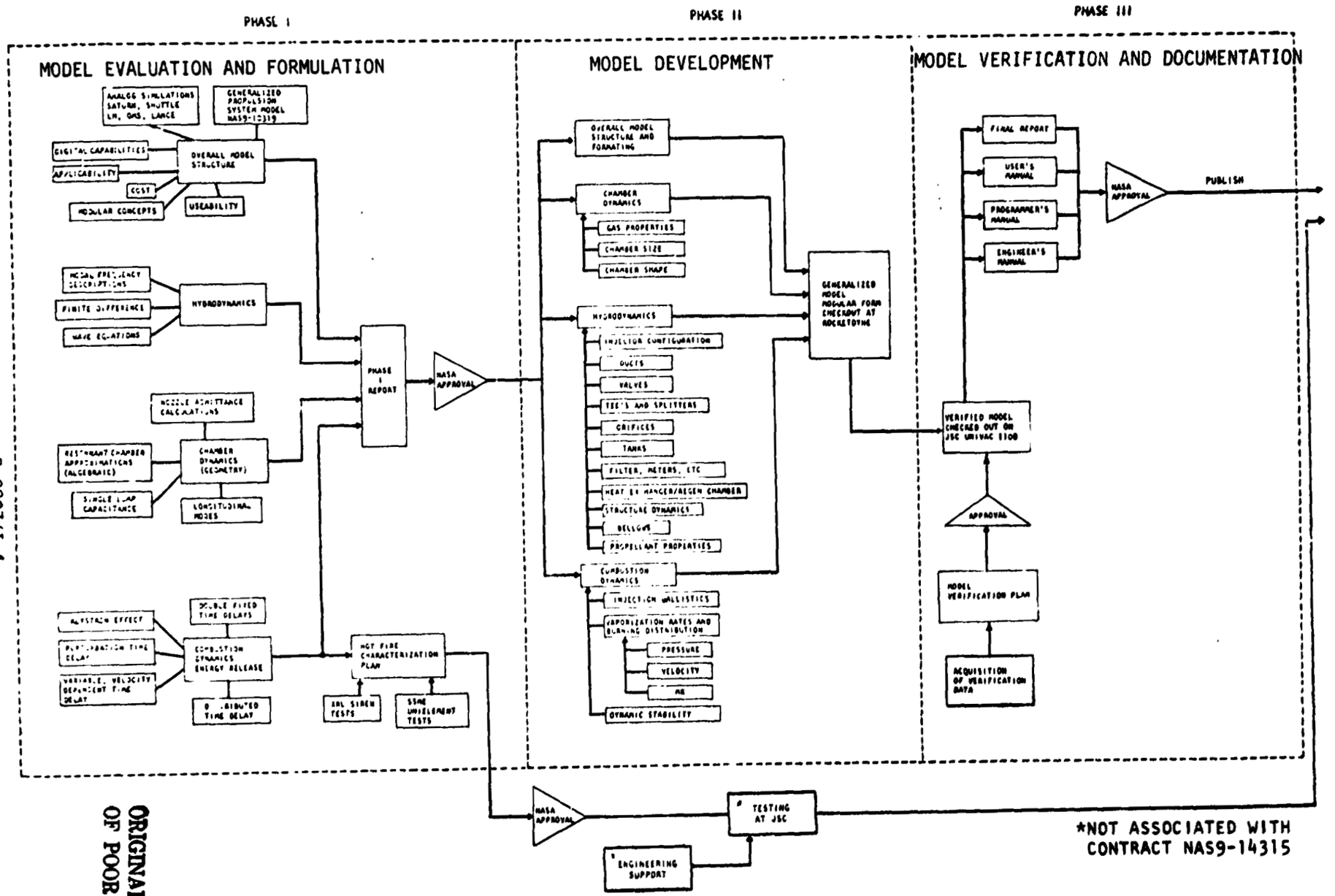

Figure 1. Logic Diagram of OME/Feed System Coupled Stability Program

In the second phase, the specifics of the hydrodynamics, combustion and chamber dynamics were programmed as discrete subprograms and integrated into an overall engineering structure to provide a usable, cost efficient computer package. Each subprogram was debugged and checkout cases were run to verify the computer logic formulation. The overall model was satisfactorily executed and reasonable values obtained for the model output parameters. A program review meeting was held at NASA/JSC on 10 April 1975 to support the results of Phase II.

In the third phase, the operation and capabilities of the engineering model were verified and the model's theoretical predictions were compared with experimental data from an OMS-type engine with known feed system/engine chugging history. The latter data were obtained at White Sands Test Facility (WSTF) on Rocketdyne hardware during Task XII of the Space Shuttle/OME Reusable Thrust Chamber Program (NAS9-12802). The particular sequence of data chosen involved a series of integrated thrust chamber tests in which the level of chamber pressure was progressively reduced until chugging occurred and included the effect of mixture ratio on the minimum pressure levels. All pertinent WSTF hot-fire test data to be used during model verification were summarized in an "Engineering Model Verification Plan," submitted to NASA/JSC on 7 May 1975. Included in the report were details of Rocketdyne's thrust chamber and injector (like doublet No. 1), schematics of the fuel and oxidizer configuration, and complete steady-state operating data for each of the seven verification analyses which were conducted.

A total of seven model verification analyses were completed using the Feed System Coupled Stability Model based upon the WSTF integrated chamber low pressure tests. In each given test case, the frequency and stability predicted by the engineering model were compared to the experimental data. The model was found to be in agreement with the experimental data in predicting engine stability or instability in six of the seven analyses. In comparing the experimental and calculated frequencies for the unstable tests, the calculated unstable frequencies were found to be approximately 16% lower than the experimental values. These discrepancies can be attributed in part to the assumptions used in modeling the feed system and

to the lack of experimentally determined combustion characterization parameters which are required as input data to the model. The calculations completed thus far have shown that the model is highly sensitive to changes in the hydrodynamics system as well as to certain combustion parameters (such as the Klystron constant).

The program was concluded with the conversion of the engineering model from Rocketdyne's IBM 370 computer to the NASA/JSC Univac 1110, EXEC-8 computer system and successful operation of the engineering model using the WSTF verification analyses. Model documentation in the form of the present final report and a computer user's manual constituted the end products of the contract.

The work performed within all of the foregoing tasks is summarized in this document. The presentation of the subject matter is organized as a task-by-task description rather than a detailed discussion of the computer program. The latter is extensively described in a separate companion document, entitled "OME/Feed System Coupled Stability Model, Computer User's Manual" (Ref. 3).

SECTION II

MODEL EVALUATION AND FORMULATION

FEED SYSTEM HYDRODYNAMICS

Introduction

Liquid propellant rocket engines require a feed system to carry propellants from storage vessels to the combustion zone. Careful consideration of the feed system is required to produce a complete engine system capable of high performance combined with stability. High performance systems are usually achieved by minimizing feed system losses, thus maximizing the overall thrust/weight ratio. Losses, however, such as orifices or high pressure drop injectors provide one of the most direct methods of providing dynamic stability in the lower frequency range. Often then, there must be a tradeoff between the static and dynamic performance of the system. Occasionally, a feed system may be tuned to force a stable coupling as in the use of quarterwave tubes, Helmholtz resonators or Quinke tubes. These are passive systems introduced to provide a resonance out-of-phase with an otherwise unstable system resonance. Analytical methods are helpful in (1) predicting the dynamics of the coupled feed system, (2) providing a method for understanding test data, and (3) providing a "logical" test facility where, after correlation with test data, the effect of system changes may be evaluated.

The dynamics of a propellant feed system are concerned with either the determination of the feed system pressures and flowrates as a function of time or of characterizing the system frequency response. Evaluating the dynamics of a feed system

requires an extension of steady-state pressure drop-flow calculations to include inertance and capacitive characteristics of the flowing system. The inertance term, as is implied, is the tendency of the fluid to resist changes in its velocity due to pressure forces. Similarly, the capacitance of the fluid is the tendency of the fluid to resist changes in its pressure, despite changes in flowrate. Both the inertance and capacitance effects are time dependent and together describe the ability of a given fluid system to exhibit preferred or characteristic frequencies.

Analytical Approach

The feed system analysis was initially directed toward determining which modeling technique could best provide the data in a form consistent with the input requirements for the combustion dynamics model. As described in a later section, the appropriate output from the feed system model should be gain and phase as a function of the chamber pressure perturbation.

Originally three approaches were considered: modal descriptions, lumped parameter and continuous parameter representations. It became apparent that the advantages of the modal descriptions lie in their adaptation to analog computer simulations. The lumped parameter approach is limited in obtaining high frequency response for long line lengths (many lumps are required). However, it remains a plausible way for handling discrete feed system elements and can be tied into the continuous parameter representation which has been selected.

Two methods of analyzing the continuous parameter representation were subsequently studied. Both yield output in the form of feed system gain and phase as a function of frequency. These were a Fourier transform method and a linear frequency response method (Fig. 2). By the first method, a set of nonlinear dynamic equations

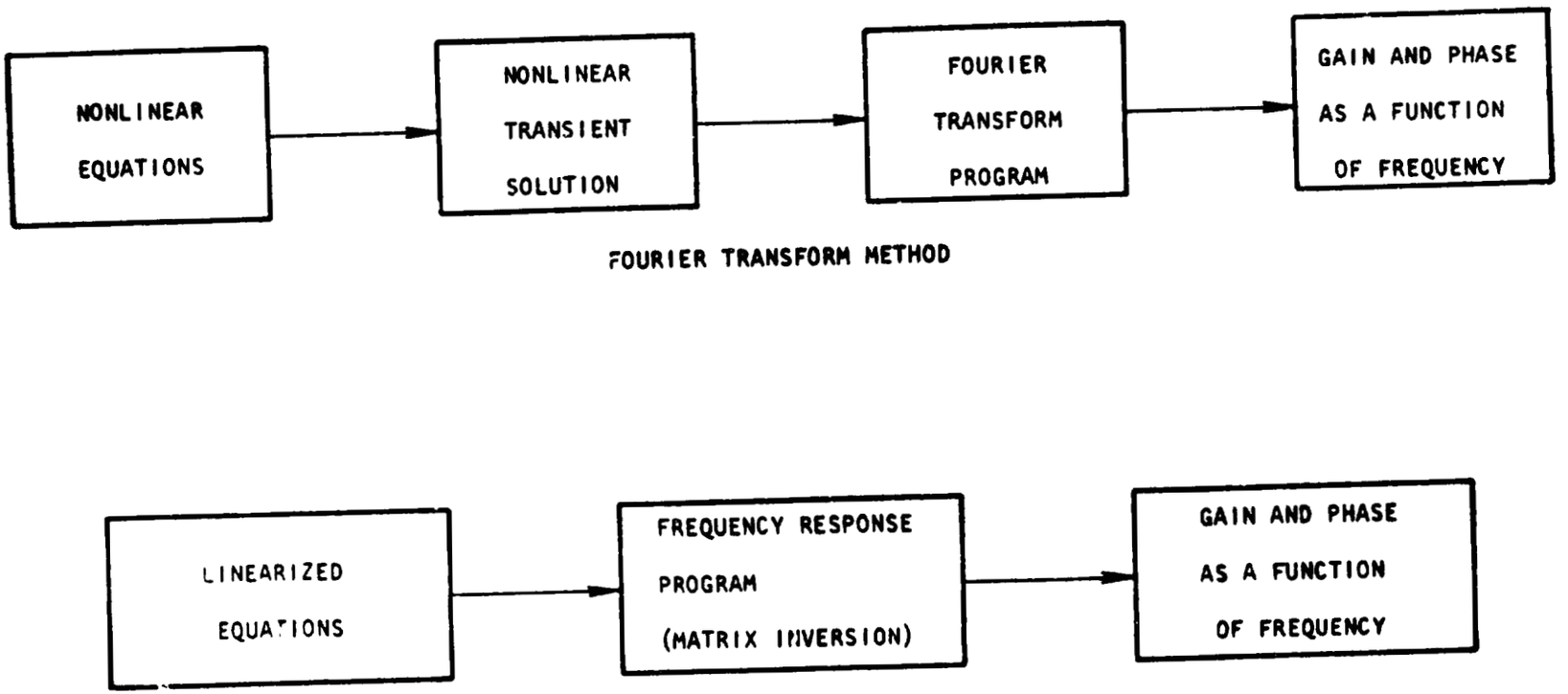

Figure 2. Comparison of Feed System Modeling Techniques Using a Continuous Parameter Representation

is used to generate a nonlinear transient solution. A Fourier transform computer program produces Fourier transforms of the transient data and the input signal. The ratio of these transforms, which is the system transfer function, is then evaluated over a frequency range and results in the system frequency response. Preliminary analysis demonstrated that the Fourier transform program output was accurate provided that the input data was recorded with sufficient accuracy and that at least five samples were taken per cycle at the highest frequency of interest. That is, if 1000 Hz is the upper frequency limit, the time transient would have to be sampled every 0.0002 seconds.

Employing the second method, the feed system dynamic equations are linearized and subsequently arranged in matrix form. The coefficient matrix and input matrix serve as input data to a frequency response computer program, which then yields the required system frequency response.

To determine the applicability of the two methods of dynamic characterization depicted in Fig. 2, a wave equation description of a four-segment baseline feed system was developed. Details of the analysis of the Fourier transform and linear frequency response methods for this baseline feed system have been given in Ref. 2. The results indicated that either method was capable of adequately describing the feed system dynamics. However, the linearized frequency response method was preferred because it provided greater numerical stability, was more flexible and required less computer time. It was therefore decided that the latter approach would be used in the formulation of the generalized OME feed system model.

Development of the Waterhammer Equations

Consider the differential control volume of a fluid element in a duct shown in Fig. 3.

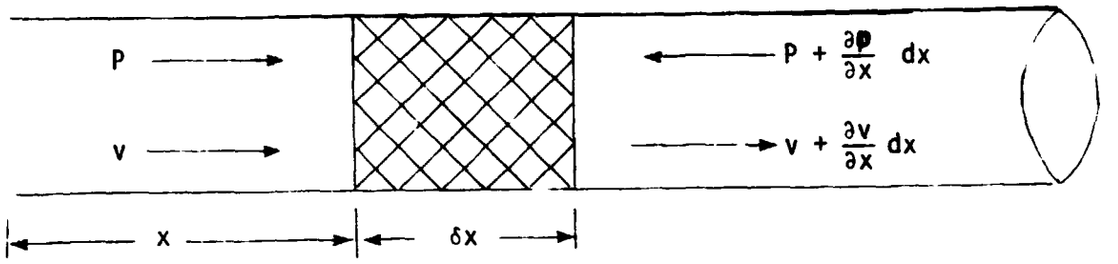

Fig. 3. Differential Pressures Developed Across the Incremental Length of a Fluid Element

Fluid compressibility and Newton's second law leads to the following pair of differential equations:

$$\frac{\partial p}{\partial t} = -\beta \frac{\partial v}{\partial x} = - c^2 \rho \frac{\partial v}{\partial x} \qquad (1)$$

$$\frac{\partial p}{\partial x} = -\rho \frac{\partial v}{\partial t} = - \frac{\beta}{c^2} \frac{\partial v}{\partial t} \quad , \qquad (2)$$

where

p = fluid pressure, N/m^2 ($lb/in.^2$)
v = fluid velocity, m/sec (in./sec)
β = fluid bulk modulus, N/m^2 ($lb/in.^2$)
ρ = fluid density, kg/m^3 ($lb/in.^3$)
c = acoustic velocity = $(\beta/\rho)^{1/2}$

There are several ways in which to solve these equations. The solution method presented here follows that of Ezekiel (Ref. 4). The general form of the solution that satisfies either of equations (1) and (2) is

$$p = F_1 \left(t + \frac{x}{c}\right) + F_2 \left(t - \frac{x}{c}\right) \qquad (3)$$

where F_1 and F_2 are arbitrary functions.

Taking the partial derivative of p with respect to x and t separately and substituting the results in equations (1) and (2) gives:

$$\frac{\partial v}{\partial x} = -\frac{1}{\beta}\frac{\partial p}{\partial t} = -\frac{1}{\beta}\left[F_1'\left(t+\frac{x}{c}\right) + F_2'\left(t-\frac{x}{c}\right)\right] \qquad (4)$$

$$\frac{\partial v}{\partial t} = -\frac{1}{\rho}\frac{\partial p}{\partial x} = -\frac{1}{\rho c}\left[F_1'\left(t+\frac{x}{c}\right) - F_2'\left(t-\frac{x}{c}\right)\right] \qquad (5)$$

where

$$F'(\xi) = \frac{\partial F(\xi)}{\partial \xi} \quad .$$

The expression for v is obtained from either equation (4) or (5):

$$zv = -F_1\left(t+\frac{x}{c}\right) + F_2\left(t-\frac{x}{c}\right) \qquad (6)$$

where

$$z \equiv (\rho\beta)^{1/2} \quad . \qquad (7)$$

Letting the subscript o denote x=0, the upstream position, and the subscript L denote x=L, the downstream position, and defining $\tau = L/c$ as the signal propagation time between the two positions, equations (3) and (6) become

$$p_o = F_1(t) + F_2(t) \qquad (8)$$

$$p_L = F_1(t+\tau) + F_2(t-\tau) \qquad (9)$$

$$zv_o = -F_1(t) + F_2(t) \qquad (10)$$

$$zv_L = -F_1(t+\tau) + F_2(t-\tau) \qquad (11)$$

Combining Eqs. (8) and (10), and Eqs. (9) and (11) separately, yields four additional relations:

$$p_o + zv_o = 2F_2(t) \qquad (12)$$

$$p_o - zv_o = 2F_1(t) \qquad (13)$$

$$p_L + zv_L = 2\,F_2(t-\tau) \qquad (14)$$

$$p_L - zv_L = 2\,F_1(t+\tau). \qquad (15)$$

Eliminating the functions F_1 and F_2 gives the final result as:

$$\left[p_o + zv_o\right]_{(t-\tau)} = p_L + zv_L \qquad (16)$$

$$\left[p_L - zv_L\right]_{(t-\tau)} = p_o - zv_o \qquad (17)$$

Consider now Fig. 4, which depicts a generalized line segment forming a portion of a feed system with many such segments.

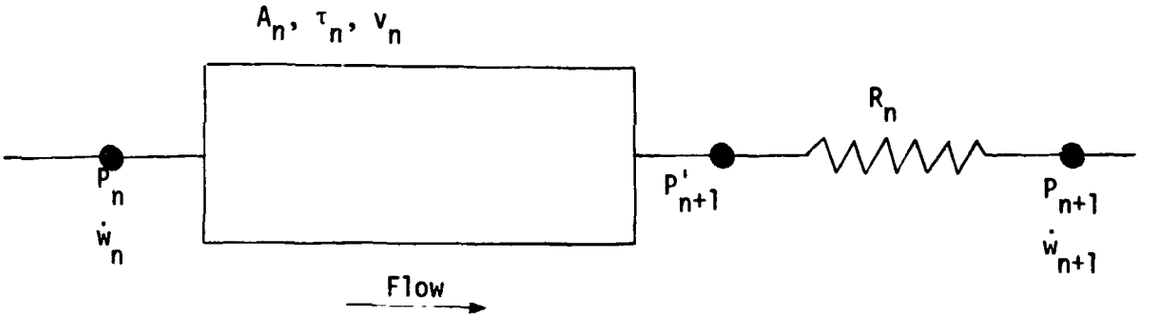

Figure 4. Generalized Line Segment

The equations which describe the pressure and flows as functions of time and of each other for the generalized line segment are obtained from Eqs. (16) and (17):

$$p_n - \left(\frac{v_n}{A_n g}\right)\dot{w}_n = \left[p'_{n+1} - \left(\frac{v_n}{A_n g}\right)\dot{w}_{n+1}\right]_{(t-\tau_n)} \qquad (18)$$

$$p'_{n+1} + \left(\frac{v_n}{A_n g}\right)\dot{w}_{n+1} = \left[p_n + \left(\frac{v_n}{A_n g}\right)\dot{w}_n\right]_{(t-\tau_n)} \qquad (19)$$

The expression, $t - \tau_n$, indicates values at τ_n seconds before, and

$$p'_{n+1} = p_{n+1} + R_n |\dot{w}_n| \dot{w}_n \qquad (20)$$

$$\dot{w}_n = \rho_n A_n v_n \,. \qquad (21)$$

Equations (18) and (19) are solutions of the wave equation, and equation (20) is the flow through a nonlinear fluid resistance. Letting

$$\alpha_n = \frac{v_n}{A_n g}$$

these equations can be combined to give:

$$p_n - \alpha_n \dot{w}_n = \left[p_{n+1} + R_n |\dot{w}_{n+1}| (\dot{w}_{n+1} - \alpha_n) \right]_{(t-\tau_n)} \qquad (23)$$

$$p_n + R_{n-1} |\dot{w}_n| \dot{w}_n + \alpha_{n-1} \dot{w}_n = \left[p_{n-1} + \alpha_{n-1} \dot{w}_{n-1} \right]_{(t-\tau_{n-1})} . \qquad (24)$$

Eliminating p_n and rearranging into quadratic form results in

$$R_{n-1} \dot{w}_n^2 + (\alpha_{n-1} + \alpha_n) \dot{w}_n - \left[p_{n-1} + \alpha_{n-1} \dot{w}_{n-1} \right]_{(t-\tau_{n-1})} \qquad (25)$$

$$+ \left[p_{n+1} + R_n |\dot{w}_{n+1}| (\dot{w}_{n+1} - \alpha_n) \right]_{(t-\tau_{n-1})} = 0$$

which can be solved for the appropriate solution using the quadratic formula. The tank end parameters are obtained using a solution of Eq. (23) only. The injector end solution is obtained using the quadratic formula for equation (25).

The linear model incorporated in the Hydrodynamics subprogram utilizes the same basic equations, (23) and (24), but in the following linearized form:

$$(\delta p_n) - \alpha_n (\delta \dot{w}_n) = \left[(\delta p'_{n+1}) - \alpha_n (\delta \dot{w}_{n+1}) \right]_{(t-\tau_n)} \tag{26}$$

$$(\delta p'_{n+1}) + \alpha_n (\delta \dot{w}_{n+1}) = \left[(\delta p_n) + \alpha_n (\delta \dot{w}_n) \right]_{(\tau-\tau_n)} , \tag{27}$$

where

$$(\delta p'_{n+1}) = (\delta p_{n+1}) + 2R_n \bar{\dot{w}}_{n+1} (\delta \dot{w}_{n+1}) . \tag{28}$$

These equations are then combined, resulting in

$$\alpha_n(\delta \dot{w}_n) - (\delta p_n) + \left[(\delta p_{n+1}) + (\bar{R}_n - \alpha_n)(\delta \dot{w}_{n+1}) \right]_{(t-\tau_n)} = 0 \tag{29}$$

$$(\bar{R}_n + \alpha_n)(\delta \dot{w}_{n+1}) + (\delta p_{n+1}) - \left[(\delta p_n) + \alpha_n (\delta \dot{w}_n) \right]_{(t-\tau_n)} = 0 , \tag{30}$$

where

$$\bar{R} = 2 R_N \bar{\dot{w}}_{n+1} \tag{31}$$

At the tank end, the term δp_n is zero for constant tank pressure. At the injector end, δp_{n+1} is the independent variable.

Injector Dynamics

The injector dynamics are included by treating the injector as a lumped compressible volume as shown in the figure below.

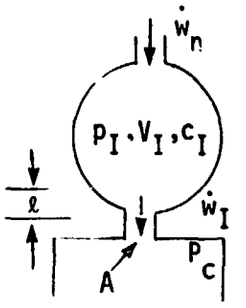

Figure 5. Schematic of the Injector as a Lumped Compressible Volume

The pressure in the injector manifold, p_I, is related to the entering flow, $\dot{w}_n$, from the upstream pipe segment and the injector flow, $\dot{w}_I$, as follows:

$$\frac{dp_I}{dt} = \frac{c_I^2}{V_I g} (\dot{w}_n - \dot{w}_I) \tag{32}$$

where V_I is the injector volume and c_I is the fluid sonic velocity.

The injector flow is controlled by the differential pressure across the injector as well as by the resistance and inertia of the injector orifices. Thus,

$$p_I - p_c = R_I \dot{w}_I^2 + \frac{\ell}{Ag} \frac{d}{dt} \dot{w}_I , \tag{33}$$

where p_c is the thrust chamber pressure, R_I is the injector hydraulic resistance and ℓ/Ag is the equivalent inertance of all the injector orifices combined, i.e.,

$$\frac{1}{\ell/Ag} = g \sum_{i=1}^{n} \frac{1}{\ell_i/A_i} . \tag{34}$$

In the preceding equation, ℓ_i and A_i are the length and area, respectively, of an individual injector orifice.

An additional factor which can have a significant effect on the response of the feed system to chamber pressure oscillations is injector face flexibility. This effect can be expressed as a change in injector volume proportional to a change in injector pressure drop:

$$\frac{d\,V_I}{dt} = K\left(\frac{d\,p_I}{dt} - \frac{d\,p_c}{dt}\right) \tag{35}$$

Also,

$$\frac{dp}{dt} = \frac{c^2}{g}\ \frac{d}{dt}\ \left(\frac{w}{V}\right)\ , \tag{36}$$

which can be rewritten as

$$\frac{dp}{dt} = \frac{c^2}{Vg}\ \dot{w} - \frac{c^2\,\rho}{Vg}\ \dot{V}\ . \tag{37}$$

Combining Eqs. (35) and (37) gives

$$\frac{d\,p_I}{dt} = \frac{c_I^2}{V_I g}\ (\dot{w}_n - \dot{w}_I) - \frac{c_I^2\,\rho_I}{V_I g}\ \left[K\left(\frac{dp_I}{dt} - \frac{dp_c}{dt}\right)\right]\ , \tag{38}$$

which can be rewritten as

$$\left(1 + \frac{c_I^2\,\rho_I\,K}{V_I\,g}\right)\ \frac{dp_I}{dt} = \frac{c_I^2}{V_I g}\ (\dot{w}_n - \dot{w}_I) + \frac{c_I^2\,\rho_I\,K}{V_I\,g}\ \frac{dp_c}{dt} \tag{39}$$

This expression reduces to Eq. (32) if no injector flexibility exists ($K = 0$).

Two-Phase Flow Acoustic Velocity

In the waterhammer equations the acoustic velocity, c, of the fluid appears in two places; (1) directly in the constant relating flow to pressure, and (2) indirectly in the time delay value, τ, which equals ℓ/c seconds, where ℓ is the pipe segment length. The acoustic velocity of a fluid is a property of that fluid. However, its effective value can be reduced by the elastic walls of the flow passage or by the entrainment of gas and vapor in the liquid (two phase flow). Gas in the liquid can appear from two sources. One source is direct entrainment from mixing of gas and liquid in the propellant tank, while the other can result from the evolution of dissolved gas as the pressure drops along the feed system.

Given the steady-state pressure at each point in the feed system and data on the solubility of the pressurant gas in the propellant as a function of pressure and temperature, the amount of gas in the fluid can be determined for each feed system segment. Then, knowing the amount of gas in the liquid, the effective acoustic velocity of the mixture may be calculated.

Assuming isentropic compression of the gas, the change in volume of the gas is

$$dV_g = - \frac{V_g}{Kp} \, dp, \tag{40}$$

and for the liquid

$$dV_\ell = \frac{V_\ell}{\beta} \, dp \tag{41}$$

Defining a constant, $\alpha \equiv \frac{V_g}{V_\ell}$

the following relation is obtained:

$$\frac{dV_t}{V_t} = \frac{- dp}{\left[\frac{1 + \alpha}{\frac{1}{\beta} + \frac{\alpha}{Kp}} \right]} \tag{42}$$

The bracketed term is the compressibility of the mixture. The density of the mixture can be shown to be

$$\rho_m = \frac{\alpha \rho_g + \rho_\ell}{(1 + \alpha)} \quad . \tag{43}$$

The acoustic velocity of a liquid in an elastic pipe is

$$c = \sqrt{\frac{1}{\frac{\rho}{g}\left(\frac{1}{\beta} + \frac{c_f}{eE}\right)}} \tag{44}$$

Using the above expressions for density and compressibility, the acoustic velocity, can be written as

$$c = \left[\frac{1}{\frac{\rho_m}{1+\alpha}\left(\frac{\alpha}{\rho_\ell c_\ell^2} + \frac{1}{\rho_g c_g^2} + \frac{1+\alpha}{q}\frac{c_f}{Ee}\right)}\right]^{\frac{1}{2}} \tag{45}$$

This expression can be used to define the acoustic velocity of a feed system segment with two phase flow. For an all liquid system, $\alpha = 0$ and the same equation can be used.

In the Hydrodynamics subprogram the effect of the wall compressibility term, $\frac{c_f}{Ee}$, on the fluid acoustic velocity is handled automatically (assuming input values of $\frac{c_f}{Ee}$ are provided for each feed system segment). However, the program does not compute the effects of two-phase flow. If such flow occurs in the feed system being modeled, an effective fluid acoustic velocity must be pre-calculated for each affected segment. Equation (45) above, with the $\frac{c_f}{Ee}$ term set equal to zero can be used for this calculation.

Simulation of Branch Lines

In the Hydrodynamics subprogram, branched lines are handled by assuming that each branch has zero internal volume and that its flows are incompressible. Thus, the pressures at the end of all segments which meet at a branch are set equal. The continuity of flow is then used to provide the additional equations in combination with the waterhammer equations to solve for the overall feed system dynamic response.

COMBUSTION DYNAMICS

The objective of this evaluation was to select an analytical technique to describe the low and intermediate frequency dynamics of the physico-chemical processes leading to the combustion of storable propellants. The selected technique must not only be an accurate description of the combustion dynamics, but must be in a form that mathematically couples with the analytical descriptions of the feed system hydrodynamics and the thrust chamber acoustics. The selected technique must also include the effects of injection geometry, propellant properties and engine operating conditions. No single technique that accomplished these requirements was readily available. Instead, a combination of existing combustion response models, steady-state combustion models, and empirical correlations were integrated into a mathematical combustion dynamic description which satisfied the technical requirements of the engineering model. Before elucidating the details of the combustion dynamics formulation, a general discussion of propellant combustion is presented.

Qualitative Understanding of Combustion Processes

Propellant combustion is usually recognized as being vaporization-rate limited and so is distributed spatially throughout the combustion chamber. For clarity and convenience, the combustor may be divided into a series of discrete zones as shown in Fig. 6 for a typical configuration. Certainly, transition from one zone to the next cannot be sharply defined, but is gradual. The positions and abruptness of these transitions are influenced by design variable, propellant combination and operating conditions.

Immediately adjacent to the propellant injector, the injection/atomization zone is least amenable to analytical description. With liquid injection concentrated at discrete sites, large gradients exist in all dimensions with respect to propellant mass fluxes and concentration, degree of atomization and spray dispersion, and properties of the gaseous medium. Spray droplets here are usually cold so the vaporization and burning rates are low. Gases in this zone are primarily either gaseous-injectants or recirculated combustion gases from the next zone downstream.

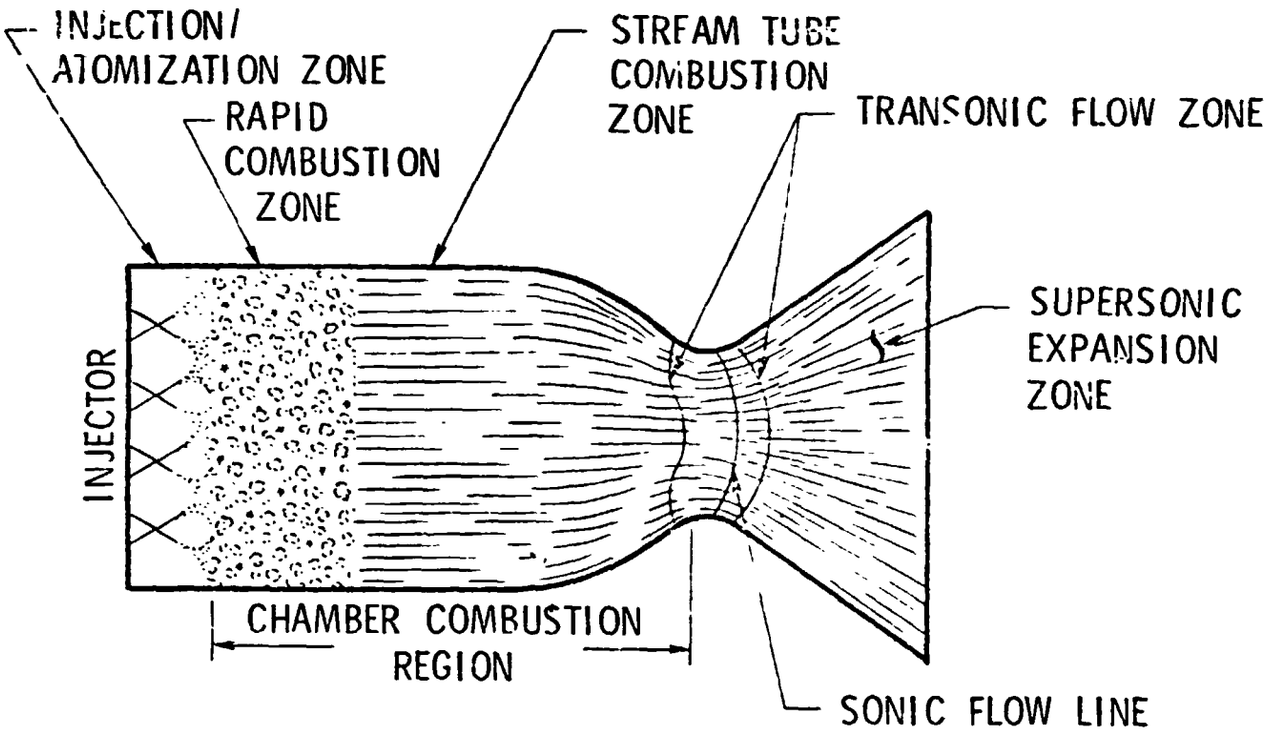

Figure 6. Subdivision of Combustion Chamber Into Zones for Analysis - Steady-State Operation

The primary atomization process is gradual to some extent and requires a finite zone length for completion, which is typically on the order of 1/2 to 2 inches. Spray formation and its dispersion from the (approximately point-source) injection sites proceeds simultaneously. Frequently straight line ray dispersion may be a good approximation, although interactions between sprays from neighboring injection sites may turn the sprays.

Completion of primary atomization and convective heating of spray droplets enhance vaporization rates leading to comparatively high chemical reaction rates in the rapid combustion zone. Upon burning, the volume of a liquid propellant element is increased 100-fold or more. This expansion forces transverse flows from high-burning-rate sites to low-burning rate sites as well as producing an axial acceleration. This provides some mixing but the sprays follow the gases only sluggishly, so spray mass flux gradients are primarily defined by injector-imposed geometric dispersion and interspray mixing. Lateral gas flows will be generated as long as appreciable spray flux gradients persist, but eventually they become small compared with axial flow velocities and the combustion field takes on a stream tube flow appearance.

In the stream tube combustion zone, the flow lacks the forced transverse convective components that are dominant in the earlier zones. Continued mixing depends upon turbulent exchange between neighboring, parallel-flowing situations, but flow velocities here are high, residence times are short, and turbulent mixing is not very effective. To a good approximation, mixing can be entirely neglected and the two-phase flow treated formally as stream tubes. As sprays are accelerated and depleted, combustion rate per unit chamber length decays with increasing distance. Chemical reaction rates, on the other hand, remain high well into the exhaust nozzle. Then as the combustion products expand through the nozzle, diminishing pressures and temperatures lower the gas-phase chemical reaction rates. Two-dimensional flow effects are also important in the transonic and supersonic flow zones. For most high-combustion-efficiency rockets, spray combustion effects are negligible compared with gas dynamic effects in these downstream zones.

Combustion Analysis

In the past, the combustion response has been modeled with a simple time delay(s) (Ref. 5 through 11). This time delay represents the time required for the propellants to travel at their injected velocity from the point where they are injected to another point where they burn, and implies the burning is concentrated at a fixed plane some arbitrary distance from the injector face. The procedure outlined above is obviously an oversimplification of the burning process which is distributed in some fashion throughout the combustion chamber.

Steady-state combustion models (Ref. 12 and 13 for example) provide insight to determine the droplet burning distribution as well as additional information required to relate the distribution to a combustion response as a function of frequency. Combustion models are designed to march incrementally down the combustion chamber from a set of specified initial conditions. In so doing, the model calculates the rate at which the propellants are consumed as a function of the axial position in the combustion chamber (burning rate profile).

The analytical technique selected to describe the combustion dynamics is based on employing the mathematical expressions used in the steady-state combustion models (in particular the JANNAF DER program, Ref. 13). These mathematical expressions are expanded into time average and oscillatory components and are described in the following sections. For more detail, the reader is referred to Appendix B.

Atomization Process. A very essential part of the combustion field initialization is the assignment of propellant spray droplet sizes and flowrates. Analytical descriptions of the atomization process are not available but empirical correlations that relate droplet diameter to injector geometry and flow conditions are available (Refs. 14, 15, and 16). For like-doublets, one empirical relationship is (Ref. 14).

$$D_d = 4.85 \times 10^4 \, v_j^{-0.75} \, (p_c/p_j)^{-0.52} \, d_j^{0.57} \qquad (46)$$

where v_j is the liquid jet velocity and d_j is the liquid jet diameter at the atomization plane. (For steady-state analysis, the velocity is the injection velocity and the diameter is the orifice diameter.)

For purposes of the current analysis, the atomization process is described by

$$D_d = K(d_j)^a_{x=x_{imp}} \quad (v_j)^b_{x=x_{imp}} \tag{47}$$

where x_{imp} is the location of the atomization plane or the impingement point. Expanding Eq. 47 into time-averaged and oscillatory parts, yields the oscillatory droplet diameter

$$\frac{\tilde{D}_d}{\bar{D}_d} = a\left(\frac{\tilde{d}_j}{\bar{d}_j}\right)_{x=x_{imp}} + b\left(\frac{\tilde{v}_j}{\bar{v}_j}\right)_{x=x_{imp}} \tag{48}$$

In order to evaluate the oscillatory droplet diameter, the oscillatory liquid jet diameter and velocity (and therefore the jet flowrate) are required at the atomization plane. Therefore, the dynamics of the fluid from the injector to the atomization plane, the Fenwick and Bugler Klystron effect (Ref. 17) is required. The dynamics of the propellant transport process to any location in the chamber are described by the continuity and momentum equations (for constant density):

$$\frac{\partial}{\partial t}(A_j) + \frac{\partial}{\partial x}(A_j v_j) = 0 \tag{49}$$

$$\frac{\partial}{\partial t}(A_j v_j) + \frac{\partial}{\partial x}(A_j v_j^2) = 0 \tag{50}$$

Expanding the preceding equations into time average and oscillatory parts and integrating between the injector face and any location in the chamber yields

$$\left(\frac{\tilde{v}_j}{\bar{v}_j}\right) = e^{i\omega x/\bar{v}_j}\left(\frac{\tilde{\dot{m}}_j}{\bar{\dot{m}}_j}\right)_{inj} \tag{51}$$

$$\left(\frac{\tilde{A}_j}{\bar{A}_j}\right) = \frac{-i\omega x}{\bar{v}_j}\; e^{i\omega x/\bar{v}_j}\left(\frac{\tilde{\dot{m}}_j}{\bar{\dot{m}}_j}\right)_{inj} \tag{52}$$

$$\left(\frac{\tilde{\dot{m}}_j}{\bar{\dot{m}}_j}\right) = e^{i\omega x/\bar{v}_j}\left[1 - \frac{i\omega x}{\bar{v}_j}\right]\left(\frac{\tilde{\dot{m}}_j}{\bar{\dot{m}}_j}\right)_{inj} \tag{53}$$

where ω is the complex frequency and the oscillatory injection rate, $(\tilde{\dot{m}}_j)_{inj}$ is determined by the feed system dynamics. Equation 53 is the oscillatory flowrate at x and is usually referred to as the Klystron effect (Ref. 17). The Klystron time delay, τ_K, is therefore given by

$$\tau_{K_j} = \frac{x_{K_j}}{\bar{v}_j} \tag{54}$$

Considerable amplification of the injector face flow oscillations are possible when the Klystron effect is present and could explain the periodic burst of acoustic resonances called resurging and the steep-fronted waves seen in low and intermediate frequency instabilities.

Droplet Vaporization. Theories of droplet combustion (Refs. 12, 18, 19) are available which may be used to evaluate the extent of coupling between droplet burning rate and local pressure and velocity fluctuations. In general, droplet burning is enhanced by increased turbulence levels or by periodic directional variations in velocity, because droplets are relatively heavy and resist following gas streamlines.

Calculation of the spray heating and vaporization is usually accomplished through specification of the corresponding individual droplet processes and summation over all the droplets that constitute the spray(s) being analyzed. The calculation of single droplet evaporation is usually based on a spherically symmetric model of simultaneous heat transfer and mass

transfer across the gas side boundary, or film, separating the liquid droplet from the surrounding hot combustion gas. Forced convection and resultant nonspherical transfer processes are accounted for through empirical Nusselt number correlations for both heat and mass transfer.

Based on the derivations presented in Ref. 12, the droplet vaporization rate for the $k^{\underline{th}}$ droplet group size may be expressed as

$$\dot{m}_{vap_k} = \frac{(6)\ Z_k\ k_{f_k}\ Nu_{H_k}\ m_k}{\rho_{\ell_k}\ D_{d_k}^{\ 2}\ c_{p_{v_k}}} \tag{55}$$

where

$$Z_k \equiv \frac{c_{p_{v_k}}\ Nu_{m_k}\ P\ MW_{v_k}\ D_{v_k}}{k_{f_k}\ Nu_{H_k}\ R_u\ T_{f_k}}\ \ln\left(\frac{p}{p - p_{v_k}}\right) \tag{56}$$

The fuel or oxidizer droplet spray continuity equation is

$$\sum_k \frac{d}{dx}\ (A\ \rho_k\ v_k) = -\ A \sum_k \rho_k\ \frac{\dot{m}_{vap_k}}{m_k} \tag{57}$$

where ρ_k is the spray density, v_k is the droplet velocity and m_k is the mass of a single droplet.

For steady-state combustion models, the preceding equations are numerically integrated allowing the droplet diameter, D_{d_k}, to vary along the length of the combustor. In order to simplify the integration for stability analysis, the droplet diameter was held constant and the droplet number flowrate was assumed to vary (for more detail see Appendix B). Combs (Ref. 20) has shown that changing from a variable droplet diameter to a variable droplet number flowrate yields approximately the same results for steady-state vaporization. Therefore, substituting Eq. 55 into Eq. 57 and letting

$$\rho_s \equiv \sum_k \rho_k \tag{58}$$

$$v_s \equiv \frac{1}{\rho_s} \sum_k (\rho_k v_k) \tag{59}$$

$$\tau_s \equiv \frac{\rho_{\ell_s} c_{p_{v_s}} D_s^2}{(6) Z_s k_{f_s} Nu_{H_s}} \tag{60}$$

$$D_s^2 \equiv \frac{\dot{m}_{s_{inj}}}{\sum_k \dot{m}_{k_{inj}} / D^2_{d_{k_{inj}}}} \tag{61}$$

yields

$$\frac{d}{dx}(A\rho_s v_s) = -\frac{A\rho_s}{\tau_s} = -A\dot{m}_{vap_s} \tag{62}$$

Integrating Eq. 62 between the start of vaporization (x_0) and any general location (x) and substituting the resulting expression into Eq. 62 yields the spray vaporization rate

$$\dot{m}_{vap_s} = \frac{(\dot{m}_s)_{x=x_{K_s}}}{A \tau_s v_s} \exp\left[-\int_{x_0}^{x} \frac{dx}{\tau_s v_s}\right] \tag{63}$$

Expanding Eq. 63 into time average and oscillatory parts yields

$$\bar{\dot{m}}_{vap_s} = \frac{(\bar{\dot{m}}_s)_{x=x_{K_s}}}{A \bar{\tau}_s \bar{v}_s} \cdot \exp\left[\frac{-(x-x_0)}{\bar{\tau}_s \bar{v}_s}\right] \tag{64}$$

$$\tilde{\dot{m}}_{vap_s} = \bar{\dot{m}}_{vap_s}\left[\frac{(\tilde{\dot{m}}_s)_{x=x_{K_s}}}{(\bar{\dot{m}}_s)_{x=x_0}} - \frac{\tilde{\tau}_s}{\bar{\tau}_s} - \frac{\tilde{v}_s}{\bar{v}_s} + \int_{x_0}^{x}\left(\frac{\tilde{\tau}_s}{\bar{\tau}_s} + \frac{\tilde{v}_s}{\bar{v}_s}\right)\frac{dx}{\bar{\tau}_s \bar{v}_s}\right] \tag{65}$$

where

$$\frac{\tilde{v}_s}{\bar{v}_s} \cong \frac{(v_s)_{x=x_{K_s}}}{(\bar{v}_s)_{x=x_{K_s}}} \tag{66}$$

$$\frac{\tilde{\tau}_s}{\bar{\tau}_s} = 2\left(\frac{\tilde{D}_s}{\bar{D}_s}\right) - \frac{\tilde{Z}_s}{\bar{Z}_s} - \frac{\widetilde{Nu}_{H_s}}{\overline{Nu}_{H_s}} + \left(\frac{\partial \tau_s}{\partial MR}\right)\frac{\widetilde{MR}}{\bar{\tau}_s} \tag{67}$$

and the oscillatory spray droplet diameter (D_s) is given by Eq. 48 and the oscillatory flowrate is given by Eq. 53. The above formulation results in a linear oscillatory vaporization model similar to Crocco's n-τ model (Ref. 6). The formulation includes the effects of: (1) distributed energy release, (2) oscillations in the injection rate, (3) oscillations in droplet diameter, (4) oscillations in droplet temperature, (5) gas pressure and velocity oscillations, and (6) oscillations in the local mixture ratio.

Nusselt Number. It may be observed that one of the dominant terms in both the expressions for the average and oscillatory time delay is the Nusselt number. The Nusselt number, for longitudinal modes, is (Ref. 21).

$$Nu_H = 2.0 + 0.6\, Pr^{1/3} \left[\frac{\rho D_s}{\mu} |v - v_s|\right]^{1/2} \tag{68}$$

In order to evaluate the oscillatory Nusselt number, the oscillatory droplet spray velocity is required. The droplet spray velocity can be obtained from the drag equation.

$$m_s \frac{dv_s}{dt} = \frac{\pi}{8} \rho D_s^2 |v-v_s|(v-v_s) C_{D_s} \quad . \tag{69}$$

Let

$$\tau_{drag_s} \equiv \frac{\rho_{\ell_s} D_s^2}{(18)\,\alpha_s\,\mu} \quad . \tag{70}$$

where

$$\alpha_s \equiv \frac{C_{D_s}}{24} \left(\frac{D_s \rho}{\mu} |v - v_s| \right) \quad . \tag{71}$$

The oscillatory droplet spray velocity can be written as

$$\tilde{v}_s = \left[\frac{1 + i\omega\tau_{drag_s}}{1 + (\omega\tau_{drag_s})^2} \right] \tilde{v} \tag{72}$$

and the oscillatory Nusselt number can be written as (for more detail, see Appendix B)

$$\frac{\tilde{Nu}_H}{\overline{Nu}_H} = \left(\frac{\overline{Nu}_H - 2}{\overline{Nu}_H} \right) \left[\frac{1}{2} \left(\frac{\tilde{D}_s}{\overline{D}_s} \right) + R_{F_\rho} \left(\frac{\tilde{\rho}}{\overline{\rho}} \right) + R_{F_v} \left(\frac{\tilde{v}}{\overline{c}} \right) \right] \tag{73}$$

where

$$\begin{aligned} R_{F_\rho} &\simeq \frac{1}{2} \\ R_{F_v} &\simeq \frac{1}{2\Delta M} \left[\frac{(\omega\tau_{drag_s})^2 - i(\omega\tau_{drag_s})}{1 + (\omega\tau_{drag_s})^2} \right] \end{aligned} \tag{74}$$

Calculations have been made which indicate that, for large droplet diameters, the average and oscillatory Nusselt numbers are quite sensitive to pressure and velocity oscillations. Therefore, the Nusselt number can have a significant effect on engine stability.

Droplet Heat Transfer Blockage Term. The oscillatory combustion time delay given by Eq. 67 requires the evaluation of the heat transfer blockage term (Z_s) which is related to the combustion gas and liquid vapor properties by Eq. 56. Because the vapor pressure (P_{v_s}) at the droplet surface is related to the droplet temperature, the blockage term also depends on the oscillatory droplet surface temperature inside the droplet which is given by:

$$\frac{\partial}{\partial t}\left(\rho_\ell \, c_{v_\ell} \, T_\ell\right) = \frac{1}{r^2} \frac{\partial}{\partial r}\left[r^2 \, k_{eff_\ell} \frac{\partial T_\ell}{\partial r}\right] \tag{76}$$

Therefore, the oscillatory heat transfer rate to the droplet can be related to the oscillatory droplet surface temperature by

$$\tilde{Q}_s = R_{T_s} \tilde{T}_s \tag{77}$$

where R_{T_s} is given in Appendix B. The droplet heating rate can also be written as (Ref. 12)

$$Q_s = Z_s \, k_{f_s} \, Nu_{H_s} \left[\frac{(T - T_s)}{(e^{Z_s} - 1)} - \frac{\Delta H_{vap_s}}{c_{p_{v_s}}}\right] (\pi D_s) \tag{78}$$

Assuming that

$$\left(\frac{d\bar{T}_s}{dt}\right) = 0 \qquad \text{(droplet at "wet bulb" temperature)} \tag{79}$$

and

$$\frac{\tilde{p}_v}{\bar{p}_v} = R_{p_v} \left(\frac{\tilde{p}}{\bar{p}}\right) , \tag{80}$$

etc. for the other variables, the response factor for the heat transfer blockage term can be related to droplet and gas properties and flow conditions (see Appendix B).

Examination of the response factor for the heat transfer blockage term indicates that this term can have a dominant effect on stability if the frequency is high and the effective thermal conductivity is low.

Generalized Vaporization Rate Expression

In order to maintain generality in representing the combustor dynamics, the spray vaporization rates (fuel and oxidizer) can be written as:

$$\tilde{\dot{m}}_{vap_s} = \bar{\dot{m}}_{vap_s} \left\{ c_{1_s}\left(\frac{\tilde{p}}{\bar{p}}\right)_{x=0} + c_{2_s}\left(\frac{\tilde{p}}{\bar{p}}\right) + c_{3_s}\left(\frac{\tilde{\rho}}{\bar{\rho}}\right)_{x=0} \right. \tag{81}$$

$$+ c_{4_s}\left(\frac{\tilde{\rho}}{\bar{\rho}}\right) + c_{5_s}(\widetilde{MR})_{x=0} + c_{6_s}(\widetilde{MR})$$

$$+ c_{7_s}\left(\frac{\tilde{v}}{\bar{c}}\right)_{x=0} + c_{8_s}\left(\frac{\tilde{v}}{\bar{c}}\right) + \int_{x_0}^{x} \left[c_{9_s}\left(\frac{\tilde{p}}{\bar{p}}\right)_{x=0} \right.$$

$$+ c_{10_s}\left(\frac{\tilde{p}}{\bar{p}}\right) + c_{11_s}\left(\frac{\tilde{\rho}}{\bar{\rho}}\right)_{x=0} + c_{12_s}\left(\frac{\tilde{\rho}}{\bar{\rho}}\right) + c_{13_s}(\widetilde{MR})_{x=0}$$

$$\left. \left. + c_{14_s}(\widetilde{MR}) + c_{15_s}\left(\frac{\tilde{v}}{\bar{c}}\right)_{x=0} + c_{16_s}\left(\frac{\tilde{v}}{\bar{c}}\right) \right] \frac{dx}{\bar{\tau}_s \bar{v}_s} \right\}$$

From the preceding sections, and Appendix B , the combustion coefficients (c_1 through c_{16}) can be defined in terms of injector geometry, flow conditions, etc.

CHAMBER DYNAMICS

During certain periods of a rocket engine's operation, conditions within the combustion chamber are time variant, i.e., the operation is not steady with respect to time. In the following sections, prime interest is focused on abnormal transient operation during unstable combustion, i.e., pressure oscillations in a combustion device which are sustained by the combustion process. Start and stop transients are not considered.

Classifications of Instability

The deviations from steady-state combustion which occur during unstable burning depend upon the kind of instability experienced. Liquid rocket instabilities are classified according to their dominant time-varying processes. They may be divided initially into two categories, depending upon whether the instability oscillation wave length is long or short compared with the chamber dimensions.

If the instability wave length is considerably longer than the chamber length and diameter, pressure disturbances propagate rapidly through the combustion space compared with rates of change due to the instability. As a result, wave motion in the chamber may be neglected and chamber pressure can be considered to vary only with time but not to vary spatially (i.e., P_c is a lumped parameter). These instabilities depend upon a fluid mechanical coupling between the propellant feed system(s) dynamics (fluctuating injection rates), the propellant combustion rates (delay times), and the combustion gas exhaust rates (pressure relaxation). Such instabilities can be further subdivided into various categories depending on the extent of wave motion in the feed system.

The breakpoint at which chamber wave motion becomes important is not abrupt. In reality, chamber wave motion is always present and, in effect, lumped chamber instabilities are really "zero order mode" limits of more general wave motion instabilities. In practice, it is found that the chamber gases can be considered to act as a lump until the frequency of oscillation exceeds

roughly one-fourth of the frequency of the lowest chamber acoustic resonance mode. At and above such frequencies wave motion becomes important and cannot be neglected in analysis. Chamber wave motion instabilities are characterized by wave-length of the oscillatory motion being comparable to the chamber dimensions. As with lumped chamber instabilities, the driving energy comes from oscillatory spray combustion. With wave motion instabilities, however, in addition to the effects of injection rate fluctuations, there is the combustion response of burning propellant sprays as they are disturbed by passage of a pressure wave through them. Wave motion may increase local burning rates by any of several mechanisms: (1) a pressure effect on the drop vapor gas phase burning rates; (2) enhanced mixing between gases and between sprays and gases; and (3) increased spray gasification rates. Increased spray gasification may be due to transient increases in convective flow velocities, to increased temperature or concentration gradients, and/or spray droplet shattering. The instability amplitude depends upon the magnitude of the response, and vice versa; typically, the interacting processes are driven to a limit represented by abrupt, essentially complete consumption of the propellant sprays. This direct response can be so great that injection rate fluctuations may be of secondary importance. As a result this class of instability can also be further subdivided as to the importance of feed system coupling. In the absence of feed system coupling, the instability is referred to as "classical acoustic instability." Only feed system coupled instabilities are considered in this program.

Analytical Approach

Two methods of approach were considered for solving the chamber dynamics. The first method used a linear lump chamber coefficient. This method is valid only at low frequencies (less than 500 Hz) and results in a set of nonlinear algebraic equations to be solved.

The second method employed a first-order perturbation model to define the chamber frequency and growth coefficient along with the oscillatory pressure

distribution in the chamber. This method is valid for all frequencies of interest in the present program (10 to 1000 Hz). For the oscillatory variables, solutions of the form $\tilde{\phi} = \phi' e^{-i\omega t}$, where ω is the complex frequency, were assumed. These forms yielded a set of nonlinear differential equations which were numerically integrated between the injector face and the nozzle inlet plane. Using iteration techniques and the requisite boundary conditions at the injector and nozzle inlet plane, the chamber frequency and growth coefficient were obtained.

Consideration of the degree of complexity in solving the governing equations by each of the above methods, as well as the range of validity of each approach, resulted in choosing the first-order perturbation models as the best method for describing the chamber dynamics. In the following paragraphs, the solutions to the first-order perturbation model stability equations are presented without showing their derivations. The reader is referred to Appendix C for a complete derivation of the chamber model equations.

First-Order Perturbation Model

The perturbation technique is a useful mathematical tool to simplify nonlinear partial differential equations. Assuming a variable ϕ can be expressed as:

$$\phi = \bar{\phi} + \tilde{\phi} \tag{82}$$

where $\bar{\phi}$ and $\tilde{\phi}$ represent the time-averaged and oscillatory components, respectively, and letting $\tilde{\phi}\tilde{n} << \bar{\phi}\bar{n}$, results in a set of equations of reduced complexity.

The assumptions used in the derivations of the chamber model equations are: (1) ideal gas flow is a valid state equation, (2) dilute sprays occupy a negligible fraction of the chamber volume; (3) the spray can be represented by a finite number of dropsize groups; each dropsize group contains a large number of locally identical drops; and, each size group constitutes a separate liquid phase and exchange terms between liquid phases are not

included; (4) drag contributes only kinetic energy to the spray energy equation; (5) secondary "shear" breakup of drops is not included; (6) no body forces; (7) one-dimensional axial flow; (8) diffusion, thermal and viscous gradients are negligible; and (9) droplet drag forces and heat transfer to the droplets are negligible.

Based upon these assumptions and following the perturbation technique described above, the equations for longitudinal instabilities can be written as (see Appendix C).

(a) Gas Continuity

$$\rho'\left(\frac{-i\omega}{c_{\phi}}\right) + \frac{dv'}{dx} + \frac{v'}{A\bar{\rho}}\frac{d(A\bar{\rho})}{dx} + \left(\frac{\bar{v}}{c_{\phi}}\right)\frac{d\rho'}{dx} + \frac{\rho'}{A\bar{\rho}\,c_{\phi}}\frac{d}{dx}(A\bar{\rho}\,\bar{v}) = \frac{(\dot{m}'_{vap_{ox}} + \dot{m}'_{vap_{fu}})}{\bar{\rho}\,c_{\phi}} \tag{83}$$

(b) Gas Momentum

$$v'\left(\frac{-i\omega}{c_{\phi}}\right) + \frac{v'}{c_{\phi}}\frac{d\bar{v}}{dx} + \frac{\bar{v}}{c_{\phi}}\frac{dv'}{dx} - \frac{\rho'}{\bar{\rho}\,c_{\phi}^2}\frac{d\bar{p}}{dx} + \frac{p'}{\bar{\rho}\,c_{\phi}^2}\frac{d\bar{p}}{dx} + \frac{\bar{p}}{\bar{\rho}\,c_{\phi}^2}\frac{dp'}{dx} = 0 \tag{84}$$

(c) Equation of State

$$p' = \rho' + T' + \frac{\overline{\rho T}}{\bar{p}}\left(\frac{\partial R}{\partial MR}\right)_{\phi} MR' \tag{85}$$

(d) Gas Energy

$$p'\left(\frac{-i\omega}{c_{\phi}}\right) + \left(\frac{\bar{v}}{c_{\phi}}\right)\left[\frac{dp'}{dx} + \frac{p'}{\bar{p}}\frac{d\bar{p}}{dx}\right] + \frac{v'}{\bar{p}}\frac{d\bar{p}}{dx} + \gamma_{\phi}\left[\frac{dv'}{dx} + \frac{v'}{A}\frac{dA}{dx}\right] \tag{86}$$

$$+ \frac{\gamma_{\emptyset}\, p'}{\bar{A}\, c_{\emptyset}} \frac{d}{dx}(\bar{A}\bar{v}) = \frac{(\gamma_{\emptyset} - 1)}{\bar{p}\, c_{\emptyset}} \left\{ \dot{m}'_{vap_{ox}} \left[\Delta h_{ox} - \left(\frac{\partial h}{\partial \overline{MR}}\right)_{\emptyset} (2\,\overline{MR} + 1) \right] \right.$$

$$+ \dot{m}'_{vap_{fu}} \left[\Delta h_{fu} + \left(\frac{\partial h}{\partial \overline{MR}}\right)_{\emptyset} (\overline{MR})^2 \right] - 2\,\bar{\dot{m}}_{vap_{ox}} \left(\frac{\partial h}{\partial \overline{MR}}\right)_{\emptyset} MR'$$

$$\left. + 2\,\bar{\dot{m}}_{vap_{fu}}\, \overline{MR} \left(\frac{\partial h}{\partial \overline{MR}}\right)_{\emptyset} MR' \right\}$$

(e) Gas Mixture Ratio

$$MR' \left(\frac{-i\omega}{c_{\emptyset}}\right) + \left(\frac{\bar{v}}{c_{\emptyset}}\right) \frac{d\,MR'}{dx} + \left[\left(\frac{\bar{v}}{c_{\emptyset}}\right) \rho' + v'\right] \frac{d\,\overline{MR}}{dx} \qquad (87)$$

$$= \frac{(\overline{MR} + 1)}{\bar{\rho}\, c_{\emptyset}} \left[\dot{m}'_{vap_{ox}} - \overline{MR}\, \dot{m}'_{vap_{fu}}\right]$$

$$+ \frac{1}{\bar{\rho}\, c_{\emptyset}} \left[\bar{\dot{m}}_{vap_{ox}} - (2\,\overline{MR} + 1)\, \dot{m}_{vap_{fu}}\right] (MR')$$

The preceding set of ordinary differential equations are numerically integrated once the complex frequency is specified, between the injector face and the nozzle inlet plane. The method of calculating the complex frequency for the perturbation model, based on nozzle admittances calculated from upstream and downstream variables, is discussed in the Computer Model Development Section under the Engineering Model.

SECTION III
MODEL DEVELOPMENT AND SOLUTION

FEED SYSTEM HYDRODYNAMICS

Introduction

Prior to the development of the generalized hydrodynamics model, a trip to McDonnell Douglas/St. Louis was made to obtain design and operating mode data for the OMS, PBK and RCS feed systems. The data included layouts and dimensions for all the lines in the propellant flow paths, as well as information related to propellant properties and system operating pressures, for the various system operating modes.

The data were found to be satisfactory for definition of the generalized feed system model such that suitable representation of the OMS feed system could be employed.

Generalized Feed System Model

Based upon the design and operating mode data for the OMS, PBK and RCS systems, a generalized feed system model was developed for use in the Hydrodynamics subprogram and is shown in Fig. 7. The system is comprised of 30 individual line segments, each denoted in Fig. 7, as the lines between the black dots. As described in Section II, a continuous parameter representation of each line segment is obtained through the use of separate sets of waterhammer equations. Each line segment can have a different line length, area, wall compliance, fluid acoustic velocity and resistance, and hence can model a wide variety of feed system components by merely choosing the appropriate values from these parameters. Also included in the generalized model are lumped parameter descriptions of two injectors (designated O and F on Fig. 7). Parameters for the injectors are volume, resistance, inertance, fluid acoustic velocity and face flexibility. A list of feed system components which may be included in the generalized OME feed system analysis are given in Table 1.

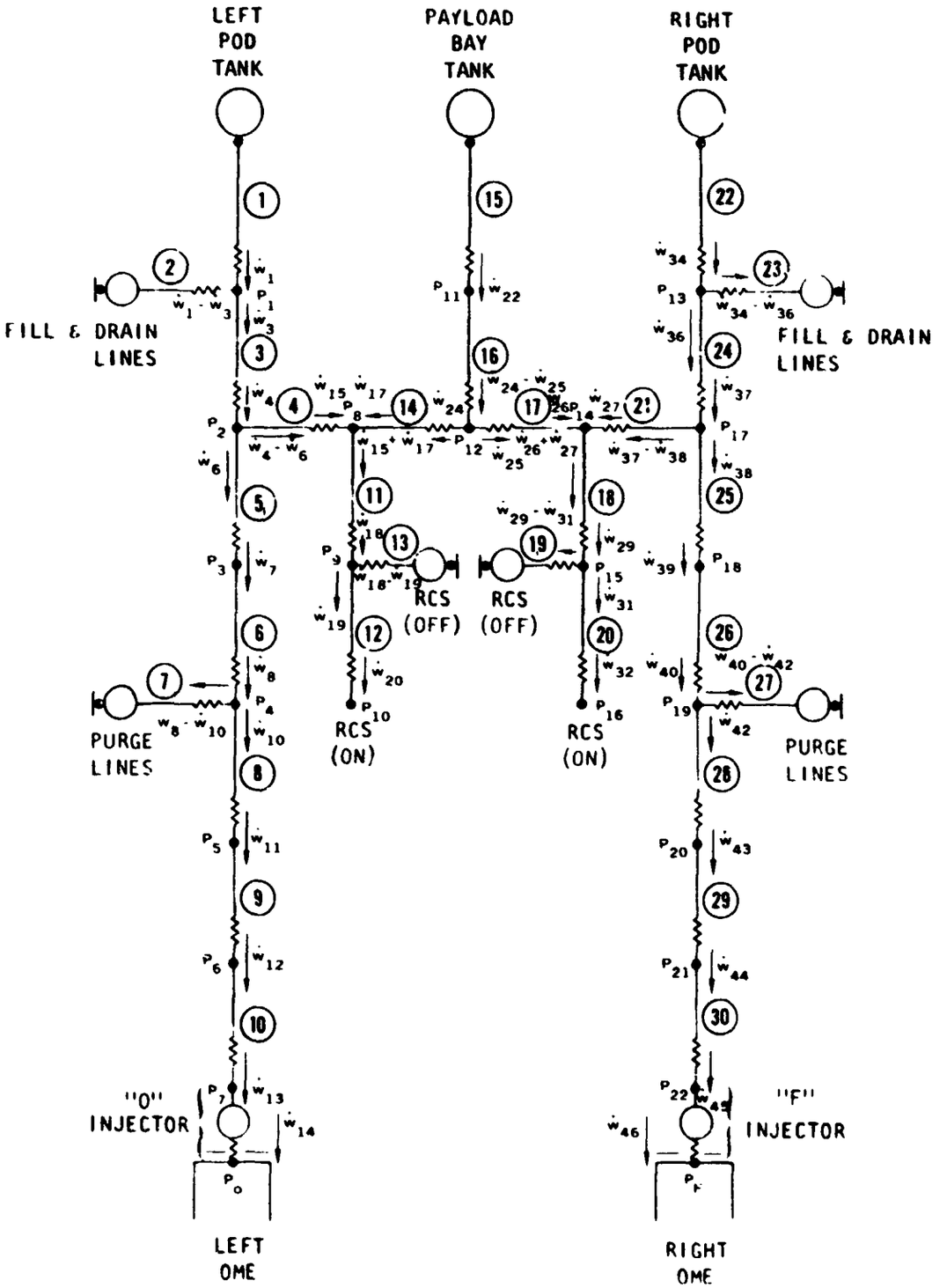

Figure 7. Generalized OME Feed System Schematic

TABLE 1. FEED SYSTEM FEATURES MODELED BY THE GENERALIZED OME HYDRODYNAMICS MODEL

- Propellant Tanks
- Propellant Feedlines
- Gas/Propellant Heat Exchanger
- Orifices
- Screen Filters
- Flow Control Valve (variable area cavitating venturi)
- Propellant Shutoff Valve
- Flexible Bellows
- Propellant Injector
- Rocket Engine Thrust Chamber
  - Ablative Cooled
  - Regeneratively/Film Cooled
- Rocket Engine Nozzle
- Propellant Accumulators
- Propellant Acquisition System
- Propellant Properties
  - Variable Density and Temperature
  - Pressure
  - Quality
  - Pressurizing Gas Saturation
- Structural Inputs

The system of 57 equations describing the generalized feed system depicted in Fig. 7 is provided in Appendix A. It should be noted that the Hydrodynamics subprogram solves the complete system of equations each time it is called. Thus the frequency response of the entire system is calculated each time. It has been shown, however, that simpler feed systems, representing only a portion of the Fig. 7 schematic, can be modeled by merely assigning values to the parameters of the unneeded line segments which will exclude them from having any effect on the system frequency response (Ref. 2). This is accomplished automatically by the Hydrodynamics subprogram via the assignment of very large resistances and very short lengths to all line segments for which no data is entered.

Solution Method

The system of equations describing the generalized feed system is solved using standard matrix techniques. A subroutine (FRESP) in the Hydrodynamics subprogram (HYDRDY) solves for the variables X_i in the following relationship:

$$[C] \cdot \{X\} = a \cdot [Y]$$

where {X} represents the column matrix of independent variables (pressures and flowrates), and Y is a single input variable that represents a unit value of the injector end combustion chamber pressures. The matrix [a] then relates the specific pressure input to each applicable equation that contains combustion chamber pressure ([a] may contain both static and dynamic terms.) The matrix [C] is simply the coefficients of the linear differential equations that represent the physical system. The values of the coefficients for the [a] and [C] matrices are computed by the subroutine HYDRDY.

The FRESP matrices can be expressed as:

$$\left[C_{ijk}\, S^{k-1} \right]_j \cdot \{X_j\} = \left[a_{ik}\, S^{k} \right] \cdot Y \qquad (88)$$

with the differential operator defined as $S = J\omega$, where $J = \sqrt{-1}$ and ω is the frequency. The matrices may be broken down to provide real matrices and imaginary matrices.

$$\left\{\left[C_{ij1} - C_{ij3}\,\omega^2 + C_{ij5}\,\omega^4 - \ldots\ldots \right] + J\left[C_{ij2}\,\omega - C_{ij4}\,\omega^3 + \ldots \right]\right\} \cdot \left[X_j \right] = \left\{\left[a_{i1} - a_{i3}\,\omega^2 + \ldots\ldots \right] + J\left[a_{i2}\,\omega - a_{i4}\,\omega^3 + \ldots \right]\right\} \cdot Y \qquad (89)$$

Since the time delay coefficients used in the differential equations are of the form $e^{-\tau S} \cdot X$, which is equivalent to $e^{-\tau j\omega} \cdot X$, and since $e^{-jy} = \cos(y) + j\sin(y)$, these terms may be added to the previously formed real and imaginary matrices to give:

$$\left\{\left[C_{ij1} - C_{ij3}\,\omega^2 + \ldots\ldots + \cos\left(\tau_{ij}\,\omega\right)\right] + J\left[C_{ij2}\,\omega - C_{ij4}\,\omega^3 + \ldots\ldots + \sin\left(\tau_{ij}\,\omega\right)\right]\right\} \cdot \left[X_j \right] = \left\{\left[a_{i1} - a_{i3}\,\omega^2 + \ldots\ldots + \cos\left(\tau_i\,\omega\right)\right] + J\left[a_{i2}\,\omega - a_{i4}\,\omega^3 + \ldots\ldots + \sin\left(\tau_i\,\omega\right)\right]\right\} \cdot Y \qquad (90)$$

and solved for $\left[X_i\right]$:

$$\left[X_i \right] = \left\{\left[C_{ij1} - C_{ij3}\,\omega^2 + \ldots\ldots + \cos\left(\tau_{ij}\,\omega\right)\right] + J\left[C_{ij2}\,\omega - C_{ij4}\,\omega^3 + \ldots\ldots + \sin\left(\tau_{ij}\,\omega\right)\right]\right\} \cdot \left\{\left[a_{i1} - a_{i3}\,\omega^2 + \ldots\ldots + \cos\left(\tau_i\,\omega\right)\right] + J\left[a_{i2}\,\omega - a_{i4}\,\omega^3 + \ldots\ldots + \sin\left(\tau\omega\right)\right]\right\} \cdot Y \qquad (91)$$

The matrices are multiplied and then solved for $[X_i]$ using a standard Gaussian elimination procedure for solving linear equations. The $[X_i]$ solution is still separated into real and imaginary components, and are simply combined to form a vector for each variable. The procedure is repeated for each frequency being considered.

Structure of the Hydrodynamics Subprogram

A functional block diagram of the Hydrodynamics subprogram (HYDRDY) is shown in Fig. 8. HYDRDY is called by the main program to calculate the frequency response characteristics of the feed system. Its functions include (1) reading of input data describing the physical attributes of the feed system components, (2) generation of a matrix of linear differential equations representing the complete feed system, (3) solution of the feed system equations to yield the amplitude and phase response of all feed system pressures and flowrates as a function of chamber pressure oscillation amplitude and frequency, and (4) generation of tabulated output of injector flowrate frequency response for use by the main program.

A basic assumption of subroutine HYDRDY is that the feed system being modeled can be represented by the generalized schematic of Fig. 7 (or by some portion of this schematic). This assumption is necessary because HYDRDY sets up and solves the complete set of simultaneous equations representing the Fig. 7 schematic. By assigning very high resistance and very short length values to any of the 30 numbered line segments of the generalized schematic, those segments can effectively be excluded from having any effect on the frequency response characteristics of the rest of the system. With this approach a wide variety of feed systems can be modeled with no changes to the program other than the input data.

Input control variable IR directs the reading of subroutine HYDRDY input data. If IR is zero or less, the program assumes that all required data has previously been read and the data read function is bypassed. If IR equals one or greater, provision is made to read in the appropriate data for the line segments and injector(s) to be included in the analysis.

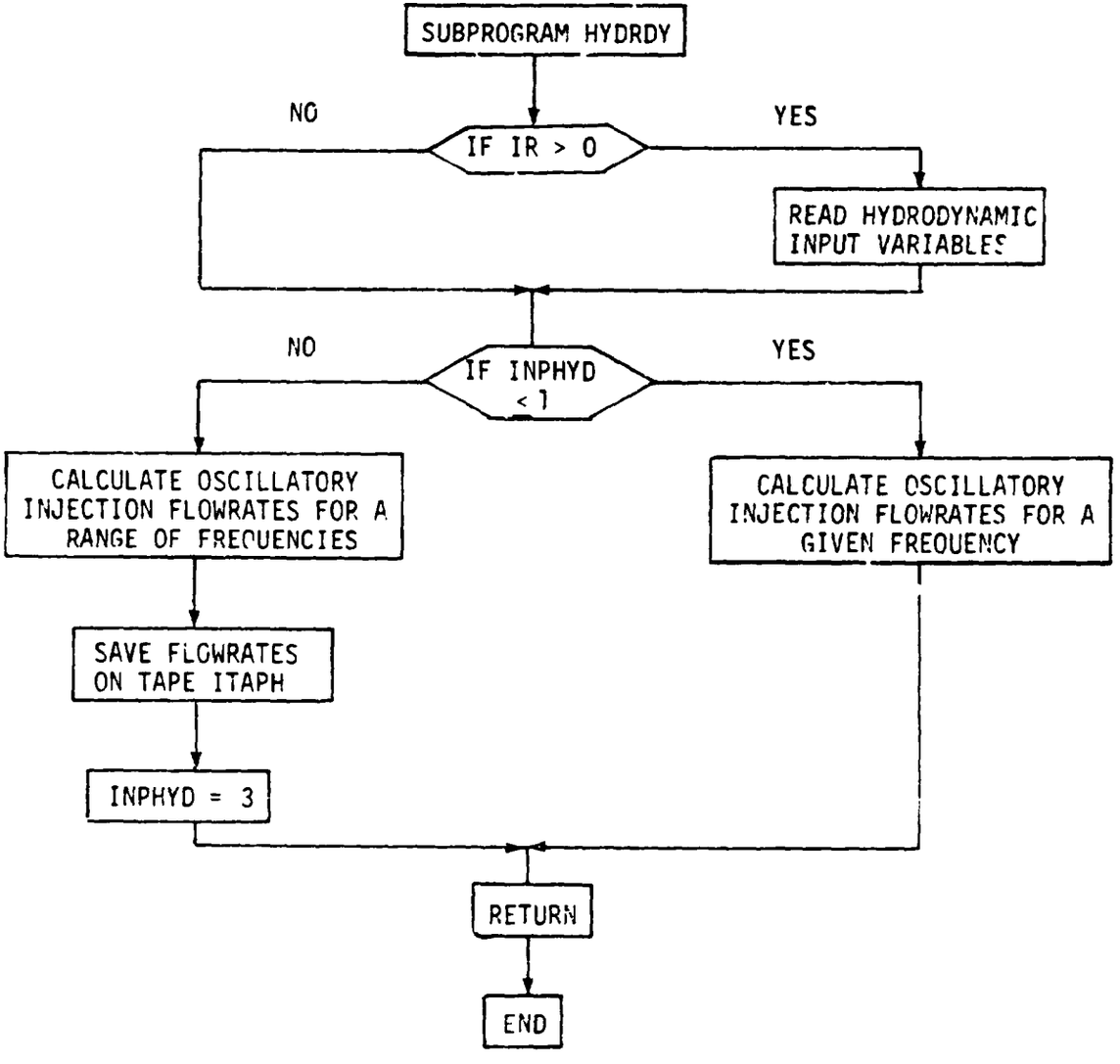

Figure 8. Block Diagram of Hydrodynamics Subprogram

Control variable INPHYD determines the procedure by which the oscillatory injection flowrates are calculated. If INPHYD is less than or equal to one, the hydrodynamic calculations are performed for one iteration step or frequency. If INPHYD is greater than one, the hydrodynamic calculations are performed for a range of frequencies and the results stored on tape.

Simultaneous solution of the 57 linear waterhammer and injector equations describing the complete Fig. 7 generalized feed system, at each specified input frequency, yields the oscillatory amplitude and phase response of all pressures and flowrates in the feed system to inputs via chamber pressure oscillations at that frequency. It should be noted that although output from a single call to HYDRDY contains values for both "oxidizer" and "fuel" oscillatory injection flowrates (at one or more frequencies), the output values actually refer to the "O" and "F" injectors of the Fig. 7 schematic. Thus, unless both oxidizer and fuel feed systems can simultaneously be modeled with the Fig. 7 layout, it is necessary to call HYDRDY twice - once for the oxidizer feed system and once for the fuel feed system.

A complete description of the Hydrodynamics subprogram, as well as detailed information related to all input variables, is given in the CME/Feed System Coupled Stability Model, Computer User's Manual (Ref. 3).

COMBUSTION DYNAMICS

Structure of the Combustion Dynamics Subprogram

A block diagram of auxiliary programs required to evaluate particular combustion parameters is presented in Fig. 9. Equilibrium properties of the combustion gases are evaluated using the NASA ODE computer program, or an equivalent program. An existing Distributed Energy Release combustion model (JANNAF computer program DER) which uses the combustion gas properties, chamber and nozzle geometry, injector geometry, and engine operating conditions is used to calculate distributed combustion parameters. The distributed vaporization rates calculated by the DER computer program are used to evaluate the average droplet vaporization "time delays", Nusselts numbers, and other important steady-state parameters required by the combustion dynamics subprogram. Output from the DER program, oscillatory injection flowrates, engine operating conditions, propellant properties, chamber geometry, and the Klystron constants are input data for the combustion dynamics subprogram.

A functional block diagram of the Combustion Dynamics subprogram (CØMBDY) is shown in Fig. 10. CØMBDY is called by the main program to calculate the combustion coefficients required by the chamber dynamics routine. Its functions include (1) reading of input data describing the physical attributes of the combustion process, (2) solution of the combustion equation to yield combustion coefficients and (3) generation of tabulated output of combustion coefficients as a function of frequency for use by the chamber dynamics routine.

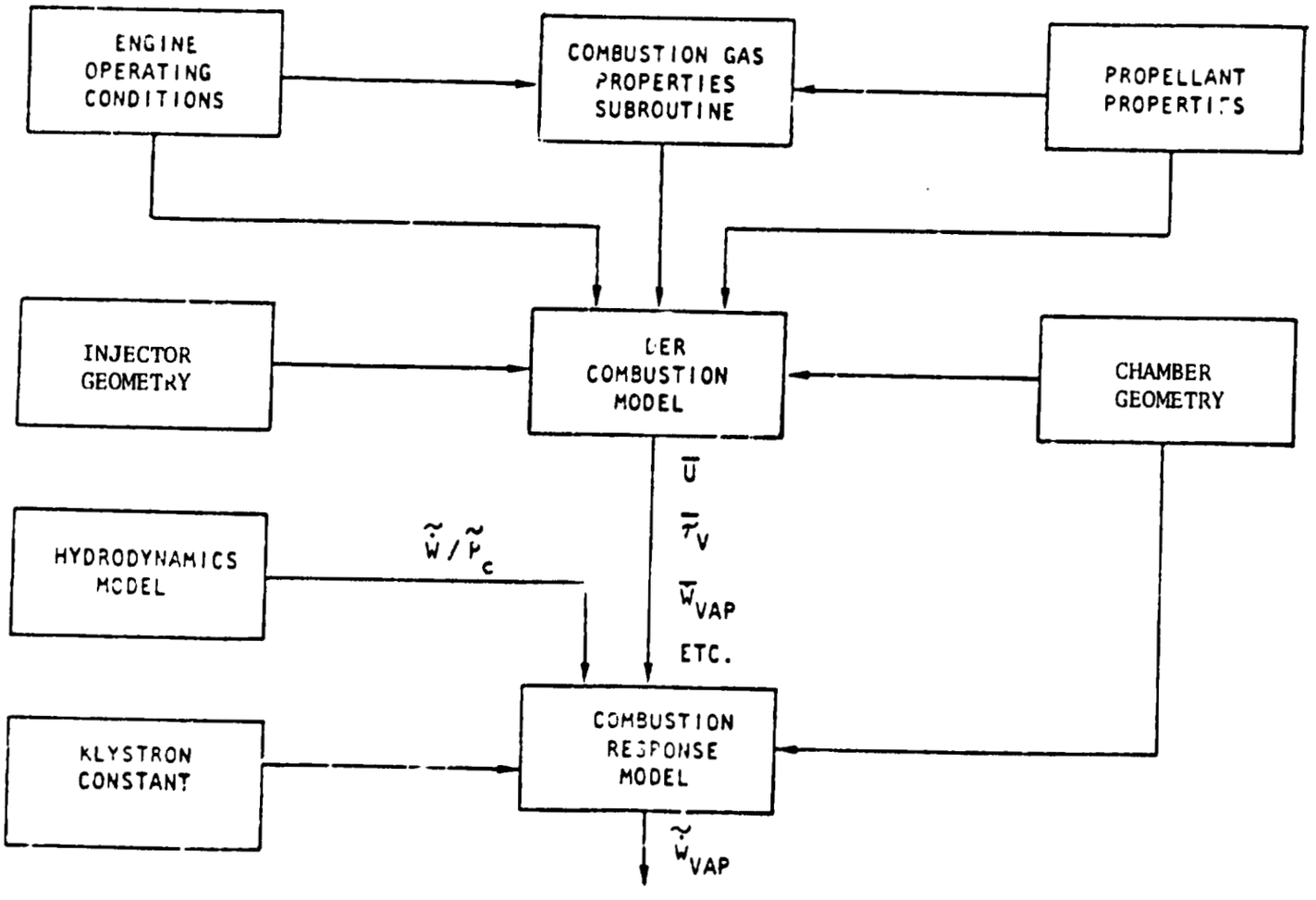

Figure 9. General Structure of Combustion Dynamics Model

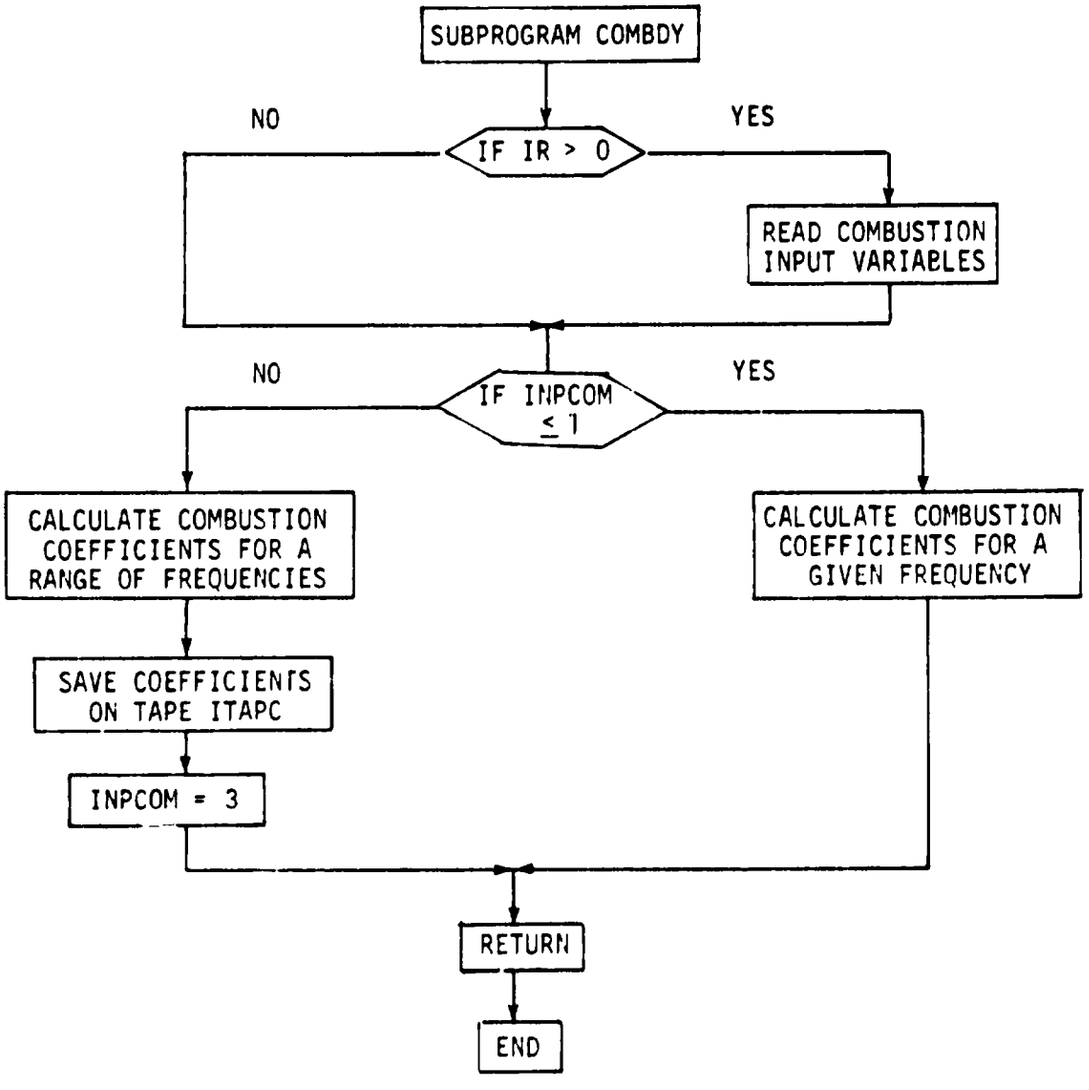

Figure 10. Block Diagram of Composition Dynamics Subprogram

Input control variable IR directs the reading of subroutine CØMBDY input data. If IR is less than or equal to zero, the program assumes that all required data has previously been read and the data read functions are bypassed. If IR is greater than or equal to one, provision is made to read in the appropriate data for evaluating the combustion effects to be included in the analysis.

Control variable INPCØM determines the procedure by which the combustion coefficients are calculated. If INPCØM is less than or equal to one, the combustion coefficient calculations are performed for only one frequency. If INPCØM is greater than one, the combustion coefficients calculations are performed for a range of frequencies and the results stored on tape.

A complete description of the combustion dynamics subprogram, as well as detailed information related to all input variables, is given in the OME/Feed System Coupled Stability Model, Computer Manual (Ref. 3).

Combustion Coefficient Evaluation

The main purpose of the combustion dynamics subprogram is the evaluation of the combustion coefficients which appear in the generalized vaporization rate expression(p.II-28). Basically, the coefficients are evaluated by substituting the oscillatory equation for the combustion processes into the oscillatory vaporaization rate expression and then comparing the resulting equations with the generalized vaporization rate expression.

For example, the oscillatory spray velocity is

$$\frac{v_s}{\bar{v}_s} = e^{i\omega x_{k_s}/\bar{v}_s} \left(\frac{\dot{m}}{\bar{\dot{m}}}\right)_{inj_s} \qquad (2$$

Since

$$\left(\frac{\dot{m}}{\bar{\dot{m}}}\right)_{inj_s} = G_{inj_s} \left(\frac{p}{\bar{p}}\right)_{inj} \tag{93}$$

the oscillatory spray velocity can be written as

$$\frac{v_s}{\bar{v}_s} = e^{i\omega x_{k_s}/\bar{v}_s} \; G_{inj_s} \left(\frac{p}{\bar{p}}\right)_{inj} \tag{94}$$

To eliminate the time dependency from the preceeding expression, recall

$$\phi = \phi \cdot e^{-i\omega\tau} \tag{95}$$

therefore

$$\frac{v_s}{\bar{v}_s} e^{i\omega x_{k_s}/\bar{v}_s} = G_{inj_s} e^{i\omega x_{k_s}/\bar{v}_s} \left(\frac{p}{\bar{p}}\right)_{inj} e^{i\omega\tau}$$

$$= G_{inj_s} \left[\left(\frac{p}{\bar{p}}\right)_{inj} e^{-i\omega\,(\tau - x_{k_s}/\bar{v}_s)}\right] \tag{96}$$

The bracketed term in the preceeding expression is just the injector end pressure evaluated at earlier time ($x_{k_s}/\bar{v}_s$); therefore, the oscillatory spray velocity can be written as

$$\frac{v_s}{\bar{v}_s} = G_{inj} \left(\frac{p}{\bar{p}}\right)_{x=0} \tag{97}$$

where $\left(\frac{p}{\bar{p}}\right)_{x=0}$ includes all time phases which is consistent with the method which is used in the chamber dynamics equations.

Using similar methods to evaluate the other oscillatory combustion processes, the generalized combustion coefficients are

$$c_{1_s} = R_{m_s} - R_{u_s} - 2 R_{D_s} + \left(\frac{\overline{Nu}_s - 2}{\overline{Nu}_s} \right) \frac{R_{D_s}}{2} \tag{98}$$

$$c_{4_s} = R_{F\rho_s} \left(\frac{\overline{Nu}_s - 2}{\overline{Nu}_s} \right) \tag{99}$$

$$c_{6_s} = - \left(\frac{\partial \bar{\tau}_s}{\partial MR} \right) \frac{1}{\bar{\tau}_s} \tag{100}$$

$$c_{8_s} = R_{Fu_s} \left(\frac{\overline{Nu}_s - 2}{\overline{Nu}_s} \right) \tag{101}$$

$$c_{9_s} = 2 R_{D_s} - \left(\frac{\overline{Nu}_s - 2}{\overline{Nu}_s} \right) \frac{R_{D_s}}{2} + R_{u_s} \tag{102}$$

$$c_{12_s} = - c_{4_s} \tag{103}$$

$$c_{14_s} = - c_{6_s} \tag{104}$$

$$c_{16_s} = - c_{8_s} \tag{105}$$

$$c_2 = c_3 = c_5 = c_7 = c_{10} = c_{11} = c_{13} = c_{15} = 0 \tag{106}$$

where the subscript s denotes the fuel or oxidizer and

$$R_{m_s} = G_{inj_s}\left(1 - \frac{i\omega x_{k_s}}{\bar{v}_s}\right) \tag{107}$$

$$R_{u_s} = G_{inj_s} \tag{108}$$

$$R_{D_s} = \left[b_s - a_s \frac{i\omega x_{imp_s}}{\bar{v}_s}\right] G_{inj_s} \tag{109}$$

It should be noted that the oscillatory heat blockage term has been neglected based on work presented in Refs. 22 and 23 which indicates that this term is not important at low frequencies.

Combustion Characterization Test Plan

One of the inherent analytical limitations of the Feed System-Coupled Stability Model is to be found in the determination of the complete set of combustion parameters required as input data to the combustion dynamics subprogram. The combustion dynamics model has been formulated to permit variables obtained from real combustion systems to be related to the mathematical model. The Klystron constant, which results from the analysis of the oscillatory fluid dynamic properties from the injector to the atomization plane (Ref. 17), is one example of a parameter that must be experimentally determined for the particular combustion system being investigated.

Originally, the experimentation needed to obtain the combustion parameters was to be conducted by NASA concurrently with the present program's effort. To aid in these determinations, and as partial fulfillment of the requirements of Contract NAS9-14315, a "Combustion Characterization Test Plan" (Ref. 24) was written which defined in detail the test objectives, test

hardware, test procedures, and data requirements necessary to obtain empirical characterization of stability-related propellant injection parameters and sensitive operating conditions for OME-type combustor hardware. The propellant injection parameters to be included were nozzle admittance, injection admittance, Klystron response, and total combustion time lag. A test series was proposed that involved four subscale injector configurations (three like-doublet units and a triplet injector) in conjunction with a heat sink combustor using the N_2O_4/MMH propellant combination. Details of the series of 36 tests were outlined for the determination of stability limits for the four injector configurations. A series of 48 tests was also recommended to determine the combustion response of two of the injectors over a range of chamber pressure, mixture ratio, and frequency.

The above plan was subsequently changed due to delays in conducting the experimental program. As a result, the combustion parameters required by the present computer model for use in model verification were estimated using the best available experimental data.

CHAMBER DYNAMICS

Structure of the Chamber Dynamics Subprogram

A block diagram of auxiliary programs required to evaluate the gas flow variables and the chamber dynamics is presented in Fig. 11. An existing Distributed Energy Release combustion model is used to calculate distributed combustion parameters which are employed in defining the steady-state flow variables. The combustion dynamics subprogram supplies combustion coefficients for evaluating the oscillatory distributed energy release along with other important combustion parameters, such as the vaporization time delays, Klystron constants, etc. Additional input required by the chamber dynamics subprogram are the chamber geometry and the nozzle admittance based on downstream conditions.

Output from the chamber dynamics subprogram are oscillatory chamber gas variables as a function of distance from the injector face and a comparison between the nozzle admittance calculated based upon both upstream and downstream conditions. A complete description of the combustion dynamics subprogram, and other supporting routines, is given in the OME/Feed System Coupled Stability Model, Computer Manual (Ref. 3).

Solution Method

The ordinary differential equations describing the oscillatory solution are solved using a second order implicit finite difference method. This method has the advantage of being simple to implement and modify, as well as being unconditionally stable for systems of equations which do not have exponentially growing solutions. The method as applied to the first order system

$$Y' = Ay + g \tag{110}$$

where Y and g are nxl vectors and A is an nxn matrix is as follows:

$$y_{i+1} = y_i + \frac{\Delta x}{2} A_{i+1/2} (y_i + y_{i+1}) + g_{i+1/2} \tag{111}$$

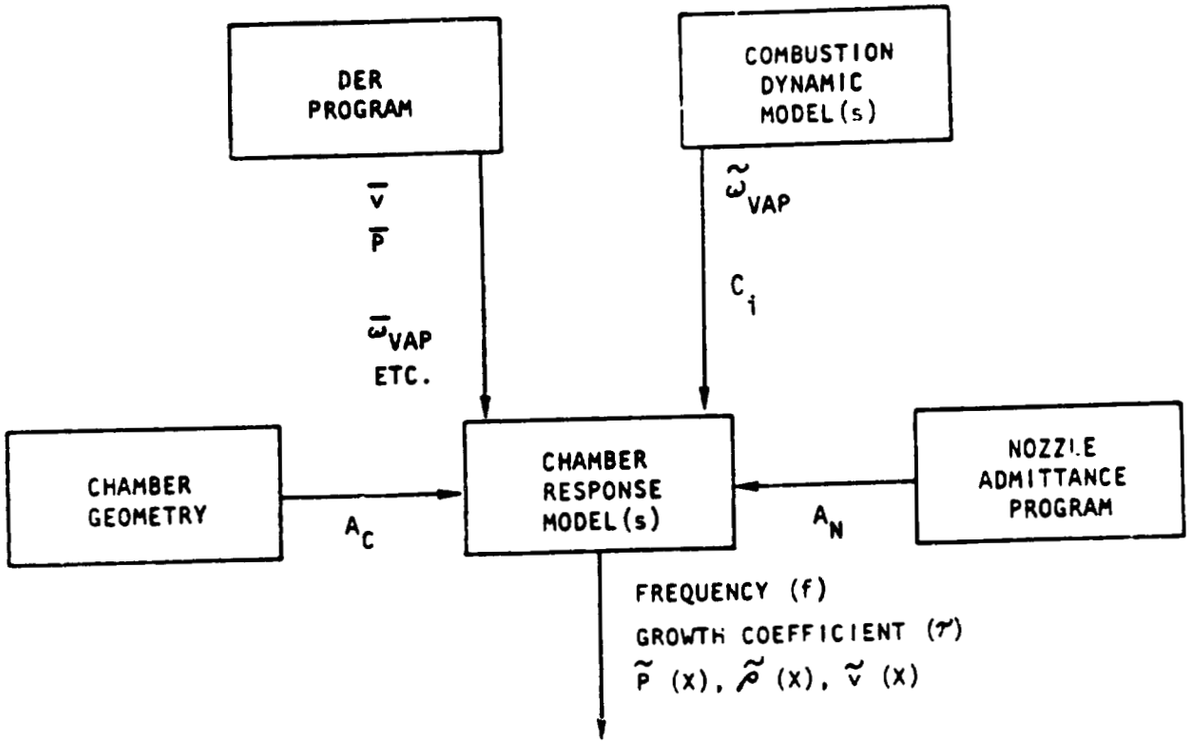

Figure 11. General Structure of Chamber Dynamics Model

Here, the subscript i refers to the i'th mesh point in the finite difference scheme, e.g., $x_i = x_0 + i\Delta x$. The y_i approximate the Y vector at x_i. That is $y_i \sim Y_i = Y(x_i)$. The subscript i+1/2 refers to evaluation at $x_i + \Delta x/2$; e.g., $A_{i+1/2} = A(x_i + \frac{\Delta x}{2})$.

That the above method leads to a second order approximation (error is proportional to Δx^3) can be shown as follows:

Solving for y_{i+1} yields

$$y_{i+1} = (I - \frac{\Delta x}{2} A_{i+1/2})^{-1} (I + \frac{\Delta x}{2} A_{i+1/2}) y_i + \Delta x (I - \frac{\Delta x}{2} A_{i+1/2})^{-1} g_{i+1/2} \tag{112}$$

Without loss of generality, assume i = 0.

From the two expansions

$$Y_1 = Y_{1/2} + \frac{\Delta x}{2} Y'_{1/2} + \frac{\Delta x^2}{8} Y''_{1/2} + o(\Delta x^3) \tag{113}$$

$$Y_0 = Y_{1/2} - \frac{\Delta x}{2} Y'_{1/2} + \frac{\Delta x^2}{8} Y''_{1/2} + o(\Delta x^3) \tag{114}$$

the following are obtained

$$Y_1 = Y_0 + \Delta x\, Y'_{1/2} + o(\Delta x^3) \tag{115}$$

and

$$Y_{1/2} = (Y_0 + Y_1)/2 + o(\Delta x^2) \tag{116}$$

Let $y_0 = Y_0$; it is necessary to show $y_1 = Y_1 + o(\Delta x^3)$ in order to demonstrate second-order accuracy.

From the differential equation (110), one obtains

$$g_{1/2} = Y'_{1/2} - A_{1/2} Y_{1/2} \tag{117}$$

Substituting (117) into (112) and noting $y_0 = Y_0$ yields

$$y_1 = \left(I - \frac{\Delta x}{2} A_{1/2}\right)^{-1} \left(I + \frac{\Delta x}{2} A_{1/2}\right) Y_0 + \Delta x \left(I - \frac{\Delta x}{2} A_{1/2}\right)^{-1} \tag{118}$$

$$\left(Y'_{1/2} - A_{1/2} Y_{1/2}\right) = \left(I - \frac{\Delta x}{2} A_{1/2}\right)^{-1} \left\{Y_0 + \Delta x\ Y'_{1/2} + A_{1/2}\ \Delta x\ (1/2\ Y_0 - Y_{1/2})\right\} \tag{119}$$

Using (115) and (116) gives the result

$$y_1 = Y_1 + \left(I - \frac{\Delta x}{2} A_{1/2}\right)^{-1} o(\Delta x^3) \tag{120}$$

$$= Y_1 + o(\Delta x^3)$$

Consider now the stability of the finite difference formula (111) for systems which do not have exponentially increasing solutions; that is, the real part of each of the eigenvalues of A is negative. To prove that they are stable for this situation, define the error $\varepsilon_i = Y_i - y_i$ and consider the two equations given by (111) and

$$Y_{i+1} = \left(I - \frac{\Delta x}{2} A_{i+1/2}\right)^{-1} \left(I + \frac{\Delta x}{2} A_{i+1/2}\right) Y_i +$$

$$\Delta x \left(I - \frac{\Delta x}{2} A_{i+1/2}\right)^{-1} g_{i+1/2} + o(\Delta x^3) \quad , \tag{121}$$

the latter resulting from (120). Subtracting (111) from (121) yields

$$\varepsilon_{i+1} = \left(I - \frac{\Delta x}{2} A_{i+1/2}\right)^{-1} \left(I + \frac{\Delta x}{2} A_{i+1/2}\right)\varepsilon_i + o(\Delta x^3) \tag{122}$$

Let $B = \frac{\Delta x}{2} A_{i+1/2}$. The method is stable if and only if the matrix $(I-B)^{-1}$ $(I+B)$ has a spectral radius less than one, for this would produce (Ref. 25)

$$\lim_{n\to\infty} \left[(I-B)^{-1} (I+B)\right]^n = 0 \tag{123}$$

Since the eigenvalues of $(I-B)^{-1}(I+B)$ are just equal to $(1+\beta)/(1-\beta)$, where β is an eigenvalue of B, the spectral radius of $(I-B)^{-1}(I+B)$ is just

$$\max_{\beta} |(1+\beta)/(1-\beta)| \tag{124}$$

For this to be less than one,

$$|1+\beta|<|1-\beta| \tag{125}$$

for all β. This implies

$$1+\beta+\bar{\beta}+\beta\bar{\beta} < 1-\beta-\bar{\beta}+\beta\bar{\beta} \tag{126}$$

or

$$\beta+\bar{\beta} < -(\beta+\bar{\beta}) \tag{127}$$

$$\text{Real}(\beta) < 0 \tag{128}$$

Since $\beta = \frac{\Delta x}{2\alpha}$, where α is an eigenvalue of A, the method will be stable if all the eigenvalues of A have real parts less than zero, that is, the solutions to (110) are not exponentially increasing.

ENGINEERING MODEL

Structure of the Program

The general structure of the Engineering Model is depicted in Fig. 12 . The decision to adopt this structure was based on a trade-off of setup time, storage capabilities, and solution time. An equilibrium gas property program similar to NASA ODE computer program (Ref. 26), and the DER combustion model (Ref. 13) must be executed external to the stability program in order to obtain important input information. General input data to the program including geometric factors, engine operating conditions, propellant properties, starting location for vaporization, estimated complex frequency, and control variables are first input to the program. The control program will then execute the nozzle admittance and hydrodynamics subprograms each time through the program or calculate the admittance and/or oscillatory injector flowrates as a function of frequency and store the results on tape. Input data required by the nozzle admittance and hydrodynamic subprograms are read in the first time these programs are executed. Next, the combustion dynamics and steady-state subprograms are called. The combustion dynamics subprogram inputs combustion data the first time it is executed and the steady-state subprogram is only executed the first time through the program. The chamber dynamics subprogram then numerically integrates the chamber dynamic equations from the injector plane to the nozzle inlet plane and calculates the nozzle admittance based on upstream conditions. This admittance is then compared with the nozzle admittance based on downstream conditions. Numerical methods are then used to calculate a new estimate for the complex frequency and the above procedure repeated until the two admittances agree within a prescribed limit.

Output of the model includes a prediction of the oscillatory frequency and information related to the stability or damping coefficient (decrement) of that frequency for the particular propulsion-fed system. In addition, at each solution point, the amplitude and phase angle for the oscillatory pressure ratio, velocity ratio, temperature ratio, and mixture ratio are given as a function of distance from the injector face.

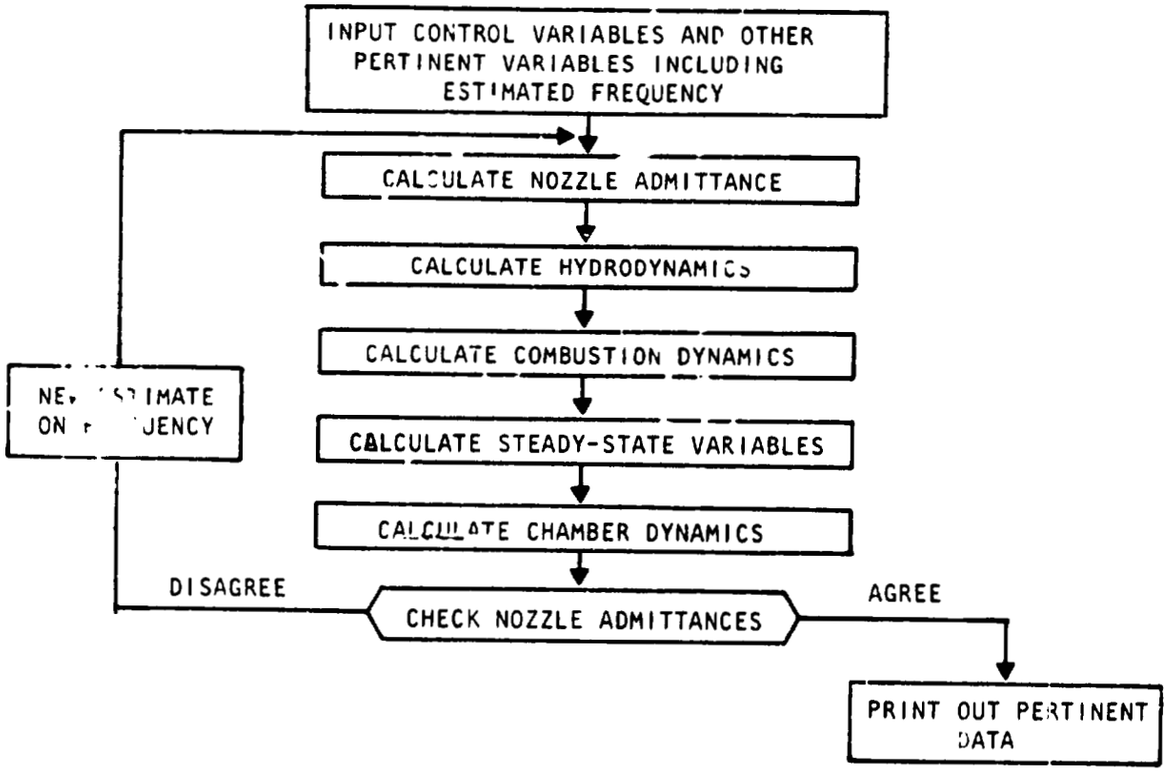

Figure 12. General Structure of the Engineering Model

Determination of Complex Frequency: Numerical Solution Method

The complex frequency, ω, is determined such that the boundary condition in the nozzle is satisfied. Specifically, the admittance is required to be continuous across the interface between the combustion zone and the zone immediately downstream of the combustion zone. In the downstream zone, the nozzle admittance, A_{N_D}, is computed from a nozzle admittance program. In the upstream combustion zone, the nozzle admittance, A_{N_U} is computed from the oscillatory flow parameters determined by the chamber dynamics. The complex frequency must be such that

$$A_{N_D} = A_{N_U} \tag{129}$$

Let $\omega = x + iy$ and $F = A_{N_U} - A_{N_D} = u + iv$. The numerical problem is to find x and y such that

$$u(x,y) = 0 \tag{130}$$

$$v(x,y) = 0 \tag{131}$$

Several methods were considered for solving this system of equations. Because F is not an analytic function of ω, the complex form of the Newton-Raphson method may not always work. On the other hand, one could use the two-dimensional form of Newton-Raphson (Ref. 27), but since the derivatives of u and v with respect to x and y must be computed numerically, the two-dimensional Newton-Raphson method will require three functional evaluations of F at each ω, i.e., (x,y), $(x + \Delta x,y)$, and $(x,y + \Delta y)$. Alternatively, a far more efficient method is to use the two-dimensional form of the secant method (Ref. 27) since this does not require the evaluation of any derivatives. Specifically, this method approximates the u and v surfaces with linear functions u_L and v_L (planes) based on three previous guesses for ω, $[(x_1,y_1), (x_2,y_2), (x_3,y_3)]$. The next guess for ω, (x_4,y_4), is determined from the equations $u_L(x_4,y_4) = v_L(x_4,y_4) = 0$. The new value of ω then replaces one of the previous three values, normally the one with the largest error as measured by the absolute value of $F(x_j,y_j)$, and the iteration

is continued until convergence is reached. The actual equations for the above process take the following form. Let $\omega_j = x_j + iy_j$, $u_j = u(x_j,y_j)$, and $v_j = v(x_j,y_j)$ for $j = 1,2,3$.

1. Determine π_j, $j = 1,2,3$, such that

$$\pi_1 + \pi_2 + \pi_3 = 1 \tag{132}$$

$$\pi_1 u_3 + \pi_2 u_2 + \pi_3 u_1 = 0 \tag{133}$$

$$\pi_1 v_3 + \pi_2 v_2 + \pi_3 v_1 = 0 \tag{134}$$

2. Compute $\omega_4 = \pi_1\omega_3 + \pi_2\omega_2 + \pi_3\omega_1$. (135)

3. Compute u_4 and v_4, based on x_4 and y_4.

4. Test for convergence, i.e., require that $\min_j |\omega_j - \omega_4|/|\omega_4| < \varepsilon_1$ and $|F_4| < \varepsilon_2$.
   If the process has not converged, continue with steps 5, 6, and 7.
5. Determine the j between 1 and 3 such that $u_j^2 + v_j^2$ is maximum.
6. Replace ω_j, u_j, and v_j by ω_4, u_4, and v_4, respectively.
7. Go to 1.

Operationally, steps 4 and 5 may be altered to replace the ω's cyclically, i.e., $\omega_i \to \omega_{i-1}$, $u_i \to u_{i-1}$, $v_i \to v_{i-1}$. In fact, the computer program as written alternates between these two procedures every three iterations in order to avoid any possible cycling that may occur.

The above algorithm has been found to be very efficient when the first three guesses are relatively near an actual solution. The difficult problem was to develop a searching algorithm which determines the regions in the ω plane where solutions exist.

One possible procedure would be to utilize the fact that the surface $u^2 + v^2$ has an absolute minimum at each solution. Using any reasonable value of ω as a first guess, one might be tempted to employ a gradient, or modified

gradient, method to march along the surface until one came near a relative minimum. Unfortunately, this procedure fails because the surface $u^2 + v^2$ has many relative minima which are not actual solutions. The reason for the large number of relative minima (and maxima) for this surface is undoubtedly due to the coupling between the combustion processes and the feed system oscillation in conjunction with the very rapid change of the feed system response as a function of frequency. The searching algorithm must be able to discriminate between those relative minima that are not solutions and those that are. Such a procedure was developed for this program. It takes advantage of the fact that a large portion of the computations required are only a function of the real part of ω, i.e., they use x as an independent variable and do not depend upon y. Thus y may be changed without having to redo many of the calculations within the program.

Intuitively, the idea is to increment x through a range of values, while determining y at each x according to the criterion mentioned below, until it is determined that a solution has been crossed. This determination employs the use of a test function which changes sign when a root is crossed in the same manner that a single equation in one unknown changes sign as it goes through a zero. The task of developing a defining criterion for y and a test function for x would be easy if, for example, v were a strong function of y and u were a strong function of x. Then, for each x, y could be chosen such that $v(x,y) = 0$ and, as x is incremented, a solution would be crossed when $u[x,y(x)]$ changes sign. Unfortunately, neither u nor v behaves this way.

To develop functions that do behave this way, the following procedure was developed. First, for each x choose y such that the absolute value of F is minimized. This can be done in several ways. The program uses a method that always guarantees finding a value if one exists. Essentially, the absolute value of F squared and its gradients are computed. The value of y is altered in the direction indicated by the gradient until either the gradient changes sign or is so close to zero that convergence has been reached. Once the gradient changes sign, Muller's method (Ref.28) is used to converge on the root. This is essentially a bisection method followed by inverse parabolic interpolation. For this searching process, it is not necessary to make the convergence criteria very tight, since only rough estimates are eventually needed in order to start the two-dimensional secant method described earlier.

Now that a criterion for y has been established, it is only necessary to find a test function that will change sign when a solution is crossed while incrementing x. Such a function is given by

$$uu_x + vv_x \tag{136}$$

This function acts as a very good test function because it represents the coordinate direction in the u,v plane along which the vector (u,v) changes most with x. When this coordinate changes sign as one goes from, say, x_1 to x_2 with y_1 and y_2 chosen so that the length of the vector (u,v) is minimized, then it is very likely that a solution has been crossed. Exceptions to this rule occur when one is near relative minima of the surface $u^2 + v^2$ that are not zero. To see this, consider the actual equations that are being solved. In order that the vector (u,v) is minimum for each y, it is necessary that $\partial(u^2 + v^2)/\partial y = 0$. That is, $uu_y + vv_y = 0$. Combining this with the above equation, we see we are finding an x and y such that the matrix equation

$$\begin{pmatrix} u_x & v_x \\ u_y & v_y \end{pmatrix} \begin{pmatrix} u \\ v \end{pmatrix} = \begin{pmatrix} 0 \\ 0 \end{pmatrix} \tag{137}$$

is satisfied. The matrix is just the transpose of Jacobian of u and v with respect to x and y.

This equation can be satisfied if either u and v are zero, or the Jacobian is singular. The Jacobian is necessarily singular at all relative minima of the surface $u^2 + v^2$ except those at $u = v = 0$. In order to differentiate between those solutions to (137) that are due to singularities of the Jacobian and those that are due to u and v vanishing, we employ two different tests. First of all, when a singularity point is crossed, the determinant of the Jacobian should change sign. If this occurs, then the program rejects this

point as a possible solution. Sometimes, however, the determinant does not change sign because either the convergence criterion used in the searching algorithm is too loose or because the singularity has a double root. In either case, the procedure is to test the condition number* of the transpose of the Jacobian matrix in the region near the suspected solution. If the condition number does not exceed a given input limit (e.g. , around 80), then the point in question is usually a solution.

Once it is determined that a potential solution has been crossed between x_1 and x_2, for example, the procedure is to (a) determine x_3 based on the method of false position using the test function given in (136), (b) determine y_3 to minimize $|F|$, and (c) use (x_1,y_1), (x_2,y_2), and (x_3,y_3) as the required first three guesses for the two-dimensional secant method. Operationally steps (a) and (b) are repeated (at least twice) until the total error, $|F|$, is less than a given fraction of $|A_{N_D}|$. This has been found to be necessary since occasionally one has to be quite close to a singularity before it can be discovered. Repeating steps (a) and (b) will result in a convergence to that singularity which will then be discovered by either the determinant changing sign or the condition number getting large. However, once the total error is reasonably small, the determinant remains of one sign, and the condition number is not large, it is almost certain that an actual solution exists and therefore the program proceeds to step (c).

The above procedure has been found to be most satisfactory for the conditions tested in this program. The search algorithm described above has several salient features. First, as mentioned earlier, the search method takes advantage of the fact that many of the computations in the program are not a function of the imaginary part of ω, namely y. Specifically, the hydro-

---

* The condition number of a matrix, A, is a measure of how sensitive a solution to the system Ab=c is to perturbations in c. It is equal to the square root of the ratio of the absolute value of the largest eigenvalue of A'A to the smallest eigenvalue of A'A. For singular matrices, the condition number is infinite. For matrices that are nearly singular, the condition number will be quite large.

dynamics of the feed system, the combustion dynamic coupling coefficients, and the major terms needed to compute the downstream nozzle admittance are all only a function of the real part of the frequency. This allows the minimization of $|F|$ with respect to y to proceed with high efficiency. Secondly, and more importantly, the procedure has been automated to the extent that the user only has to specify a frequency range and a maximum number of roots he desires in that range. The algorithm will start at the lower end of the frequency range and will increment through it until either the maximum number of roots are found or the upper end of the frequency range is reached. This is a very powerful property since it does not require the user to have a clear knowledge of the location of any of the roots in the ω plane.

SECTION IV
MODEL VERIFICATION

INTRODUCTION

The primary objective of Phase III of the OME/Feed System Coupled Stability Investigation was to verify the operation and capabilities of the Engineering Model, and to compare the model's predictions with experimental data from an OMS-type engine with known feed system/engine chugging or buzzing history. In the following sections, the experimental hot-fire test data which was used for comparing the model's operation and performance are described. Next, the methods of evaluating the combustion parameters and Klystron constant appearing in the combustion dynamics model are presented. Finally, a summary of the Feed System Coupled Stability Model results from each of the seven model verification tests is given. The computed output is compared to the experimental predictions and analyzed in terms of the applicability of the available experimental data to the OME system being modeled.

DESCRIPTION OF EXPERIMENTAL HOT-FIRE TEST DATA

Background

Rocketdyne has recently completed an extensive and comprehensive program for NASA/Johnson Spacecraft Center (NAS9-12802) to determine the feasibility of and evaluate potential reusable thrust chamber concepts for the Space Shuttle Orbit Maneuvering Engine (OME). The program determined the applicability of various thrust chamber concepts to the Space Shuttle OME application. Feasibility was analytically predicted and experimentally demonstrated for the most promising reusable thrust chamber concept. This information will support NASA/JSC and shuttle vehicle contractor Orbit Maneuvering System (OMS) studies, and provide technical foundation for the final definition of the OMS. The technical effort started in June 1972 and was completed in February 1975.

Under Task XII of the SS/OME Reusable Thrust Chamber program a series of experimental tests was conducted at White Sands Test Facility to investigate:

(1) the start, shutdown, and restart characteristics of the integrated thrust chamber; and (2) OME thrust chamber operating characteristics at very low chamber pressures typical of propellant tank blowdown operation and without supplementary boundary layer coolant. Test Sequence 7 of this task involved a series of tests in which the level of chamber pressure was progressively reduced until chugging occurred and included the effect of mixture ratio on the minimum pressure level. Discrete 5-second tests were conducted (as opposed to continuous blowdown tests) to minimize facility hyperflow time. Cold fuel (45 F) was used to enhance the regenerative coolant safety factor at low chamber pressures. Tests 7-7 through 7-14 of this series were conducted with unsaturated propellant using the facility feed-system configuration which simulates the OMS.

Tests at 80 and 75 psia nominal chamber pressure resulted in chugging at start which damped out during the tests. At 65 psia nominal chamber pressure, the chug persisted throughout the test. Chugging was observed to occur at frequencies between 115 and 350 Hz.

After extensive review of Rocketdyne's hot-fire test data obtained at White Sands Test Facility for the SS/OME Reusable Thrust Chamber Program and following discussions with the NASA/JSC contract monitor, it was concluded that the data reported in Task XII (OME Integrated Thrust Chamber Tests) would be sufficient and appropriate for use in Phase III model verification of the current program. An "Engineering Model Verification Plan" (Ref. 29) was subsequently written which summarized all pertinent White Sands Test Facility hot-fire test data to be used during model verification. The report included (1) details of Rocketdyne's thrust chamber and injector (like-doublet No. 1), (2) schematics of the fuel and oxidizer feedline configurations, and (3) steady-state operating data for the seven planned verification analyses. A summary of the pertinent test hardware, test facility description, and hot-fire test data contained in this report is presented below. The reader is referred to Ref. 30 for a complete description of all test hardware, instrumentation, and experimental results pertaining to NAS9-12802, Task XII.

Test Hardware

The hardware used for the White Sands test program (Task XII) consisted of a regeneratively-cooled thrust chamber, full size and truncated radiation-cooled nozzles, and a like-doublet injector. The injector and chamber were designed to closely simulate the thermal and dynamic characteristics of OME flight-type hardware. All components were bolted together and sealed with either metallic or elastomeric O-rings, as appropriate.

Table 2 provides a summary of the regeneratively cooled chamber design characteristics. The combustion chamber had a length of 0.3734 m (14.7 in.) and a contraction ratio of 2:1 with a throat diameter of 0.1478 m (5.820 in.). The expansion area ratio of the regeneratively cooled nozzle was 7:1. A radiation-cooled Columbian nozzle with an expansion ratio of 9:1 was used for the tests at low chamber pressure (Test Sequence 7) to eliminate the chance of chamber damage due to high side loads. The inner wall and the lands of the chamber were 321 CRES, and the channels were closed out with electroformed nickel. The thrust chamber was designed for the heat flux profile shown in Fig. 13. Channel sizes were such that the minimum safety factor was approximately 1.5 at a fuel inlet temperature of 38.1° C (100° F), chamber pressure of 82.73 x 10^4 N/m^2 (120 psia), and propellant mixture ratio of 1.85. The coolant jacket itself was flightweight with nickel closeout thicknesses as thin as 0.064 m (0.025 in.) at the throat. The fuel inlet manifold was a heavyweight configuration to reduce cost, but simulated flight manifold volume. The coolant outlet manifold was more critical thermally and represented a typical flight design.

The completed regeneratively-cooled thrust chamber is shown in Fig. 14. Complete details of all instrumentation used during Task XII is given in Ref. 30. It should be noted that chamber pressure instrumentation was not configured to provide high response transient data. However, close coupled high-pressure, high-response transducers were used to record the transients in fuel and oxidizer injection pressures and fuel coolant jacket inlet pressure. Other principal instrumentation involved measurement of propellant flows, thrust, chamber skin temperatures, and P_c in acoustic cavities.

TABLE 2. DEMONSTRATOR THRUST CHAMBER DESIGN CHARACTERISTICS

COMBUSTOR	
Contraction Ratio	2:1
Length, m (in.)	0.3734 (14.7)
Contour	Tapered from 0.1778 m (7 in.) upstream of throat
NOZZLE	
Regen Section Expansion Ratio	to 7:1
Nozzle Extension Expansion Ratio	7:1 to 72:1
Contour	Flight parabolic
COOLANT	
Circuit	Counterflow
Number of Regen Coolant Channels	120
Coolant Pressure Drop, N/m^2 (psid)	10.34×10^4 (15)
Coolant Bulk Temperature, Rise, °C (°F)	81.4 (178)
Auxiliary Film Coolant	2.7% Total Propellant
Channel Dimensions at throat	
Width, m (in.)	0.0029 (0.114)
Height,m (in.)	0.0017 (0.068)
Channel Dimensions near injector	
Width, m (in.)	0.0029 (0.114)
Length, m (in.)	0.0011 (0.042)
MATERIALS	
Hot Wall (0.0008 m/0.030 in.) and Lands	CRES 321
Cold Wall (0.0008 m/0.030 in.)	Electroformed Nickel
Nozzle Extension	CRES

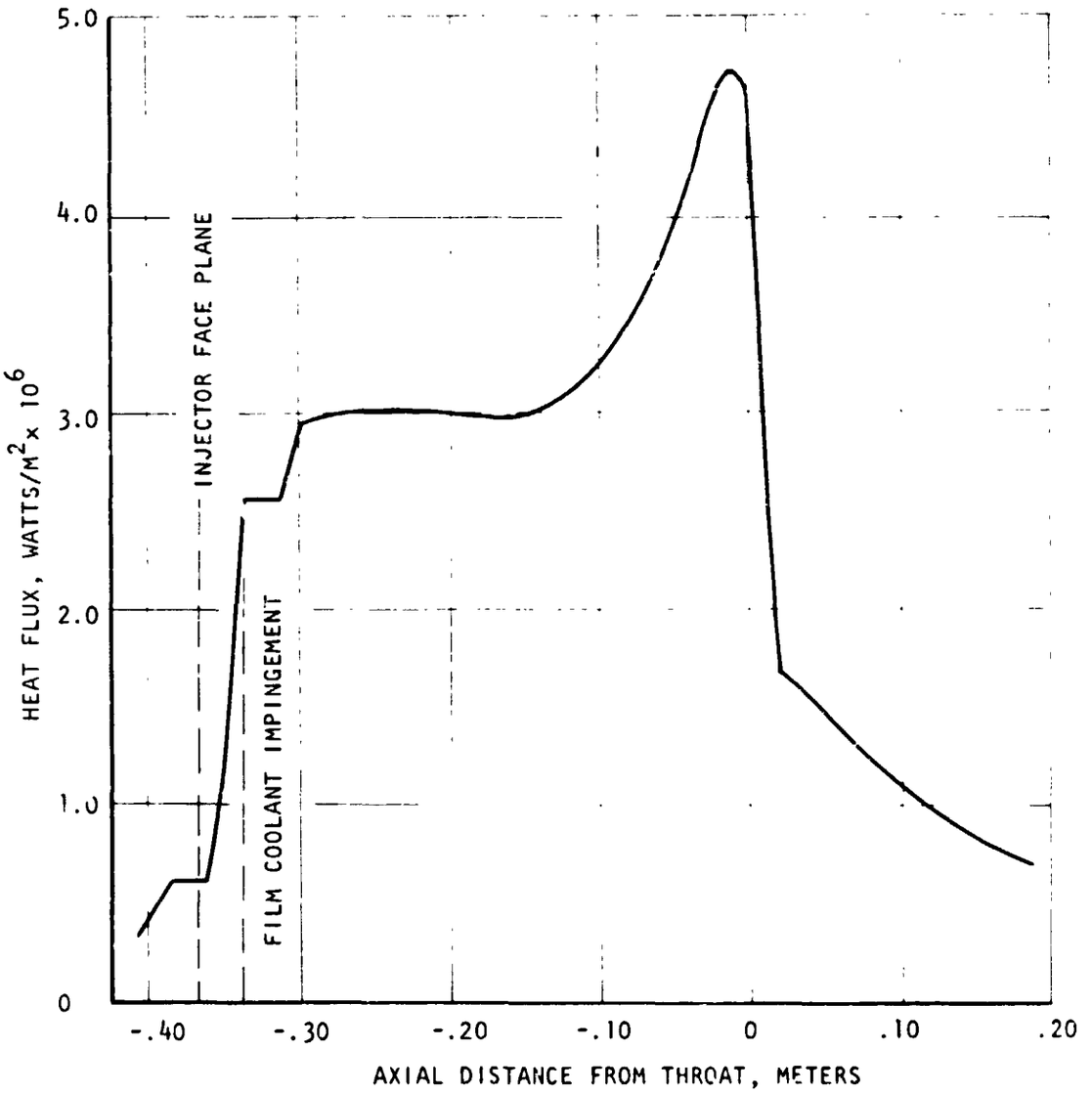

Figure 13. Heat Flux Profile Used as Basis for Integrated Thrust Chamber Design

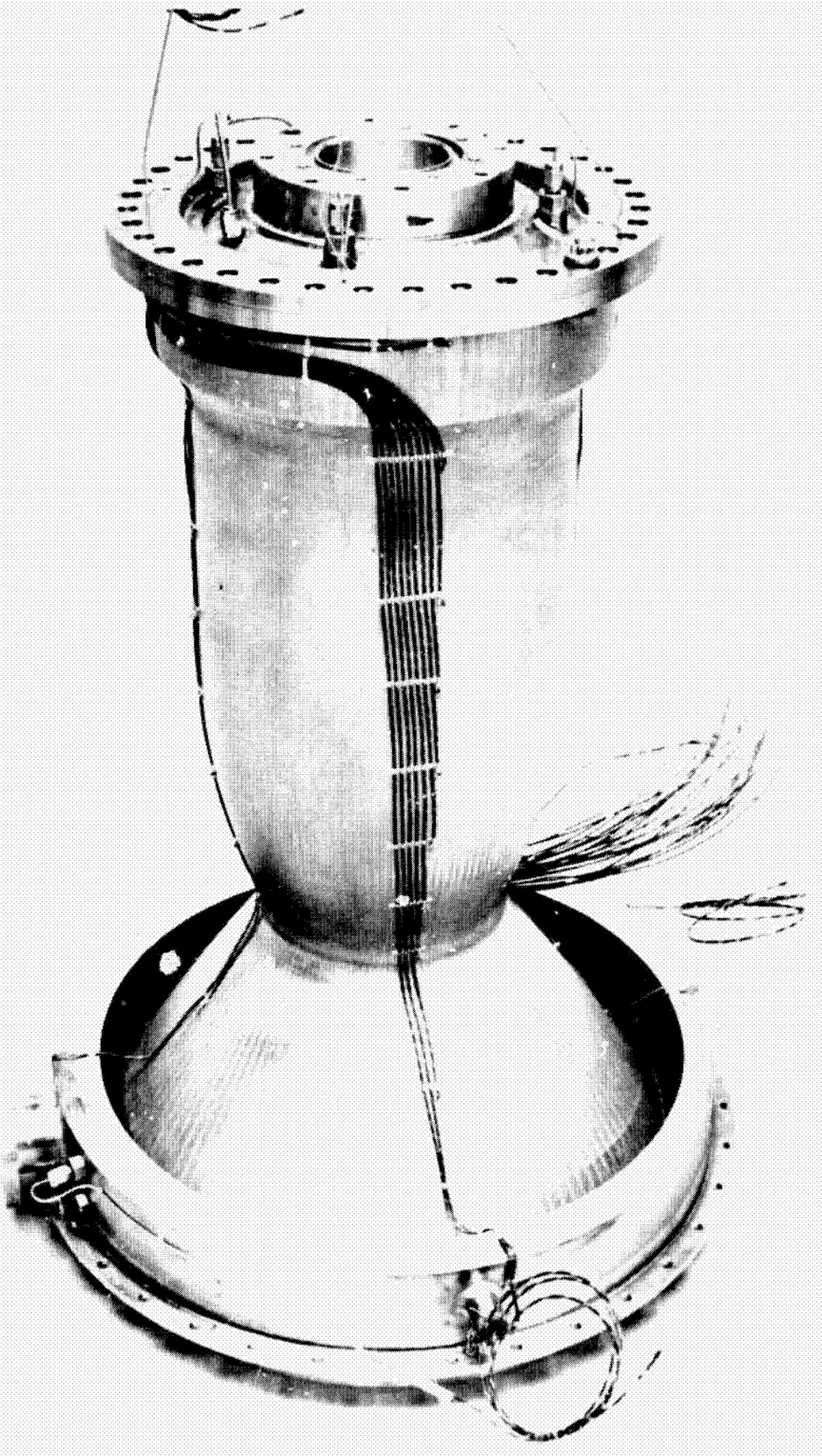

1S031-10/12/73-C1A*

Figure 14. Regeneratively Cooled Integrated Thrust Chamber Assembly

The injector used was a like-doublet (L/D No. 1), which had 186 elements arranged in nine rows. Oxidizer orifice diameters ranged from 0.0008 to 0.001 m (0.032 to 0.038 in.), while fuel orifice diameters ranged from 0.0007 to 0.0008 m (0.028 to 0.033 in.). The injector included 68 orifices (0.0005-m, 0.020-in. diameter) to provide boundary layer coolant amounting to 2.7 percent of the total propellant flow at nominal mixture ratio. Injector characteristics are summarized in Table 3.

The injection pairs of like-double No. 1 were designed with a fan impingement angle of 60°, an oxidizer-to-fuel fan inclination angle of 22.5°, and an element spacing of 0.0073 m (0.289 in.). These parameters are shown in Fig. 15. The nominal impingement height of the like-doublet pairs was 0.0048 m (0.188 in.). Detailed injector orifice data are presented in Table 4.

Test Facility

The thrust chamber assembly was tested at the White Sands Test Facility at Las Cruces, New Mexico. A simplified feed system schematic of the installation is shown in Fig. 16. Fuel (MMH) and oxidizer (NTO) were stored and conditioned in 7.57 m^3 (2000 gallon) propellant tanks external to the vacuum cell. The propellant was pumped from the external tanks to the two 0.227 m^3 (60 gallon) tanks inside the vacuum cell simulating the OMS tankage exits. Line sizes and lengths from the propellant tanks to the OME interface were configured so as to simulate OMS ducting. Dimensions of the actual fuel and oxidizer feedline configuration used during integrated hardware testing are given in Fig. 17 and 18. A flowmeter was located in each propellant feedline between the tanks and the engine interface. A common pressure source was used to pressurize both the internal and external propellant tanks.

The fuel sides of the two LM descent engine valves were used as the engine propellant control valves. Fuel valves were used for both fuel and oxidizer sides because these valves contained the actuators and the position indicators. Each valve was series and parallel redundant including upstream isolation valves and downstream shutoff valves. Positions were measured on one of the isolation valves and one of the shutoff valves for each propellant. The valves were located so as to provide a slight positive drain into the

TABLE 3. INJECTOR ../D No. 1 CHARACTERISTICS

Diameter, m (in.)	0.2083 (8.200)
Number of Elements	186
Number of Rows	9
Type of Elements	Like Doublet
Oxidizer Eleme ·meter, m (in.) (minimum/maximum)	0.0008/0.0010 (0.032/0.038)
Fuel Element Diameter, m (i...) (mini...m/maximum)	0.0007/0.0008 (0.028/0.033)
Pressure Drop @ Nominal Flows	
Oxidizer, N/m^2 (psi)	38.61×10^4 (56)
Fuel, N/m^2 (psi)	42.75×10^4 (62)
Number of Acoustic Cavities*	8/4
Mode Suppression	1st & 3rd Tangential, 1st Radial

* Cavities formed by chamber and injector

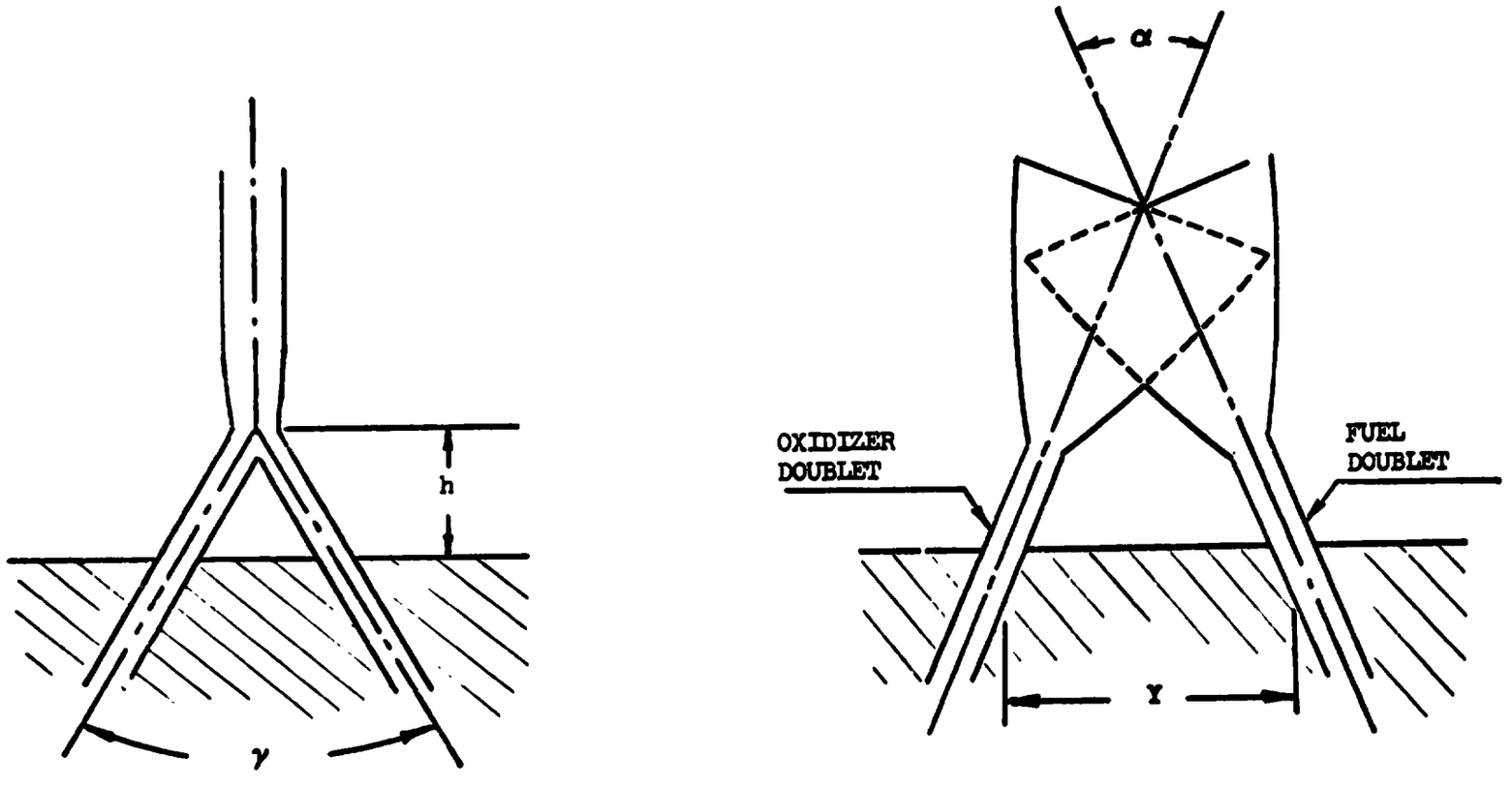

NOMINAL OME DESIGN PARAMETERS

α = FAN INCLINATION ANGLE - 22.5°

γ = FAN IMPINGEMENT ANGLE - 60°

Y = ELEMENT SPACING - 0.0073 m (0.289 in.)

h = IMPINGEMENT HEIGHT - 0.0048 m (0.188 in.) (NOMINAL)

Figure 15. Like Doublet No. 1 Element Configuration

TABLE 4. OME LIKE DOUBLET INJECTOR PARAMETERS, LIKE DOUBLET NO. 1

	INJECTION ROW									ACOUSTIC CAVITY DAM BLC
	1	2	3	4	5	6	7	8	9	
Oxid. Orifice Dia	.0345	←			→	.0345	.0321	.0332	.0379	-
Fuel Orifice Dia	.0300	←			→	.0300	.0279	.0289	.0330	.0200
No. of Elements	6	10	12	16	20	24	30	34	34	42
Element Spacing	.754	.688	.770	.725	.697	.679	.622	.618	.669	-
Row Radius	.720	1.095	1.470	1.845	2.220	2.595	2.970	3.345	3.620	-
Face Area Fract.	.0515	.0513	.0689	.0865	.1041	.1216	.1392	.1657	.2112	-
Flow Coverage	.0321	.0534	.0641	.0855	.1069	.1283	.1392	.1698	.2207	-
Flow/Area	.629	1.041	.931	.989	1.027	1.054	1.000	1.025	1.045	-
BLC % Fuel										1.3
Design Delta P										
Oxidizer	44.8	←							→	44.8	-
Fuel	52.8	←							→	52.8	52.8
1/2 Thrust/ Element	16.05	16.02	16.03	16.03	16.04	16.04	13.92	14.98	19.48	-

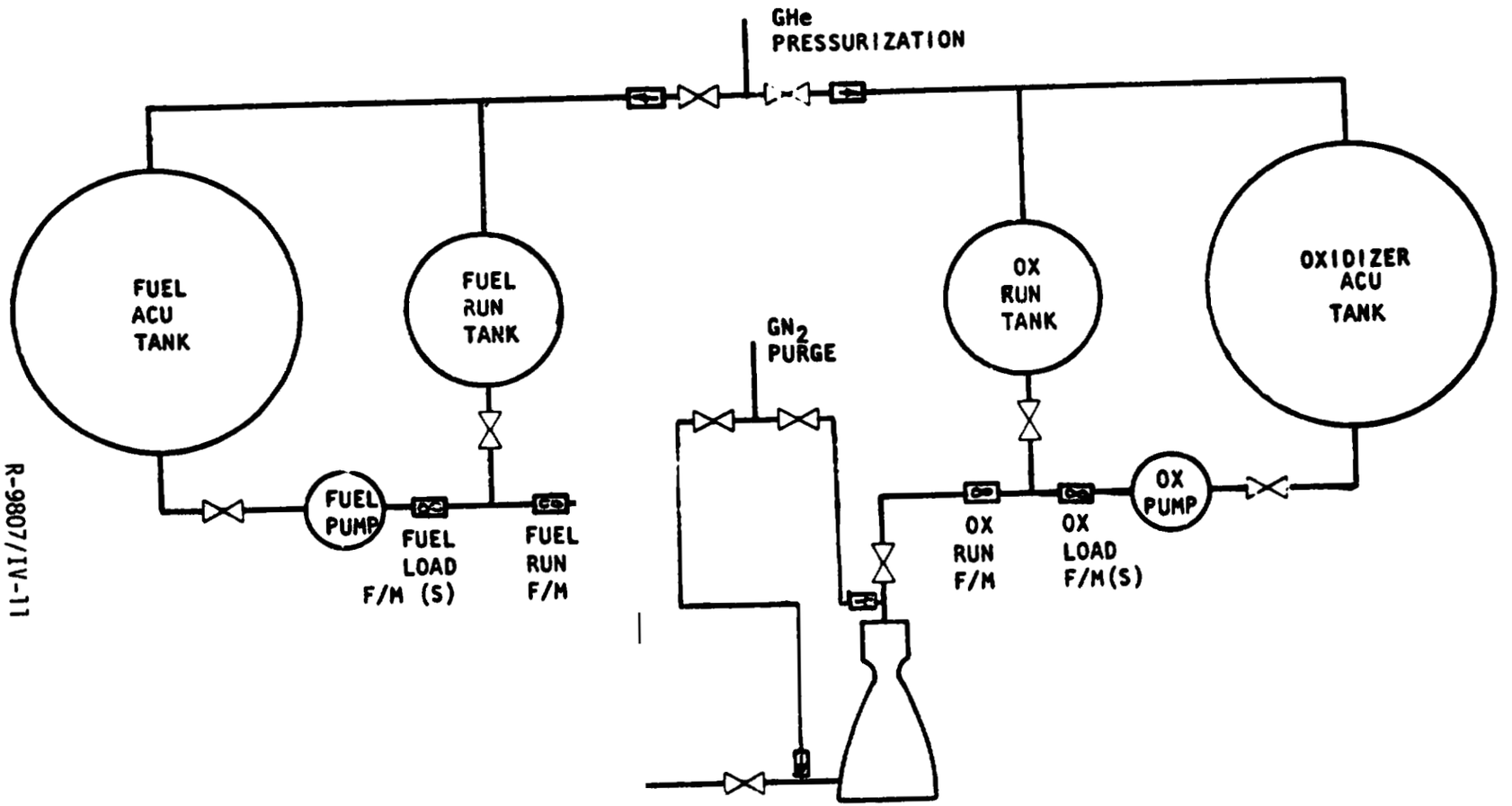

R-9807/IV-11

Figure 16. Simplified NASA/WSTF Propellant Feed System Schematic With Ducting to Simulate OMS

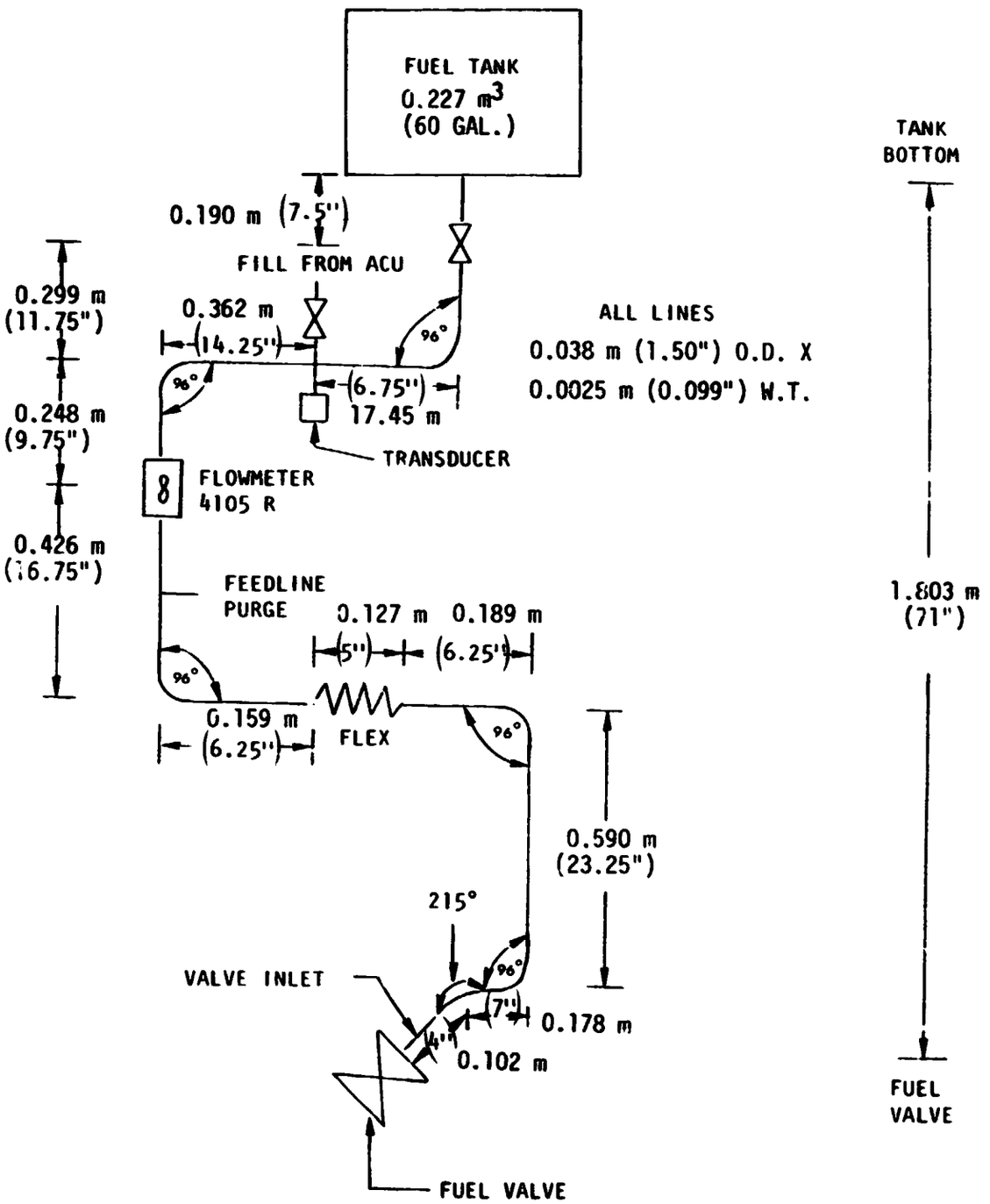

Figure 17. Rocketdyne Integrated Hardware Tests, Fuel Feedline Configuration Simulated APS POD Lines at White Sands Test Facility (3-74)

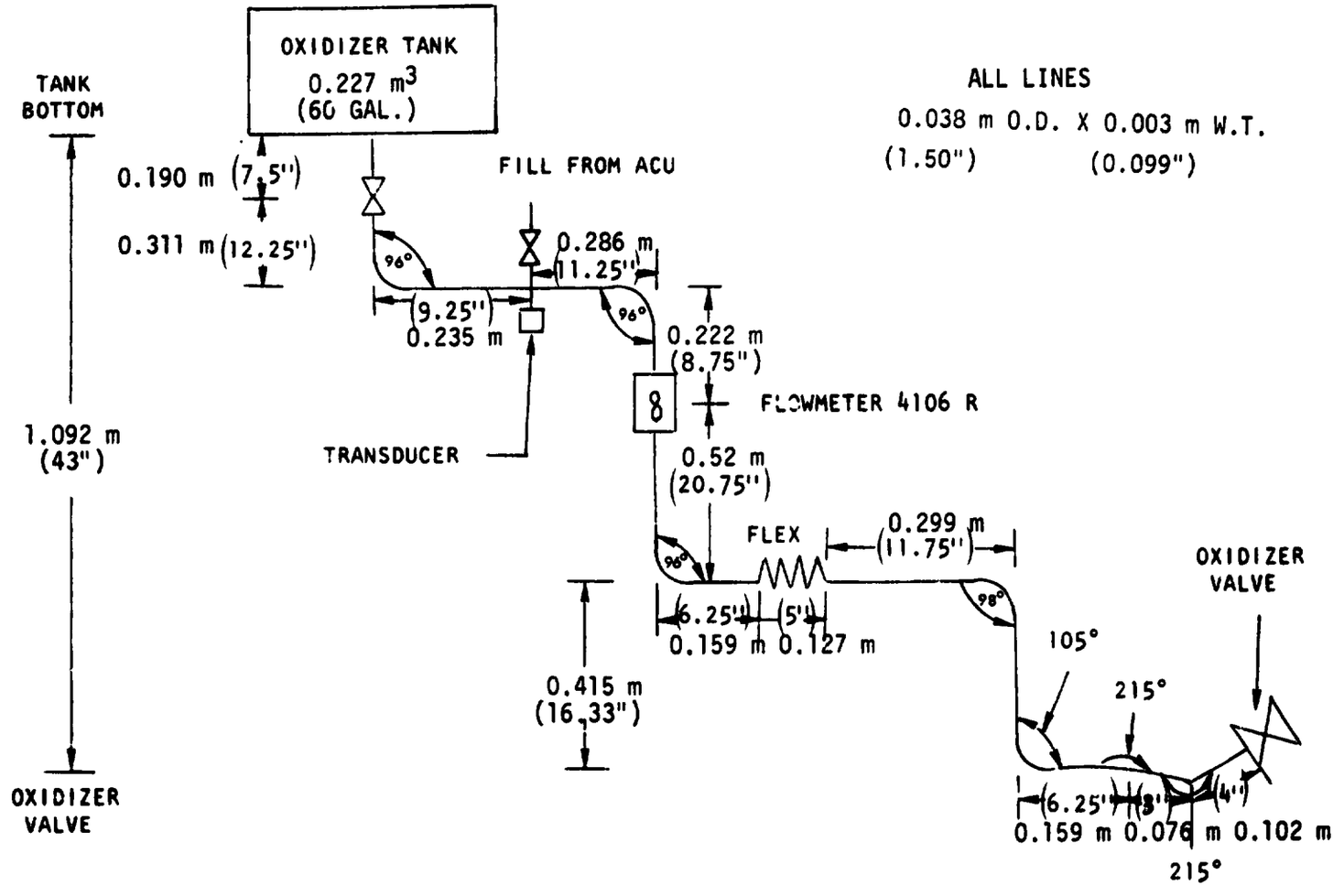

Figure 8. Rocketdyne Integrated Hardware Tests, Oxidizer Feedline Configuration, Simulated APS POD Lines at White Sands Test Facility (3-74)

engine inlets in an attempt to simulate the depletion which would occur after shutdown under zero 'g' conditions. The ducting between the valves and the engines was configured to simulate typical line volumes and sizes for the flight OME as shown in Fig. 19 .

Details of the test facility instrumentation and test stand operation are given in Ref. 30.

Hot-Fire Test Data

As stated earlier, one purpose of Test Sequence 7 was to investigate OME operation at very low chamber pressures typical of propellant tank blowdown operation. To prevent excessive side loads which might be associated with very low pressure operation, a 9:1 nozzle was used. In addition, the fuel temperature was reduced to approximately 7.5°C to provide a higher safety factor.

Tests 7-2 and 7-4 were moderately low-pressure tests conducted with the external facility propellant tanks. Tests 7-7 through 7-14 were conducted with unsaturated propellant using the facility feed-system configuration which simulates the OMS. Based on the stiffness factor, $\sqrt{\Delta P/\dot{w}}$ (where ΔP is the difference between propellant tank and chamber pressures, and $\dot{w}$ is the propellant flowrate) the feed system using external oxidizer tanks is 3% stiffer than the OMS simulated system and the feed system using external fuel tanks is 8% stiffer than the corresponding OMS system.

The range of chamber pressures, propellant flowrates, and mixture ratios employed in Tests 7-7 through 7-14 is shown in Table 5 . Measured and predicted injector pressure drops are tabulated. The measured pressure drops are the values recorded when no significant oscillations were occurring during the test. Predicted values are all referred to the measured values of Test 7-7 and ratioed according to the square of the flowrates. The difference between the measured and predicted pressure drops particularly at lower pressures may be the result of subtracting two high pressure measurements (injection and chamber pressures) to obtain a ΔP although

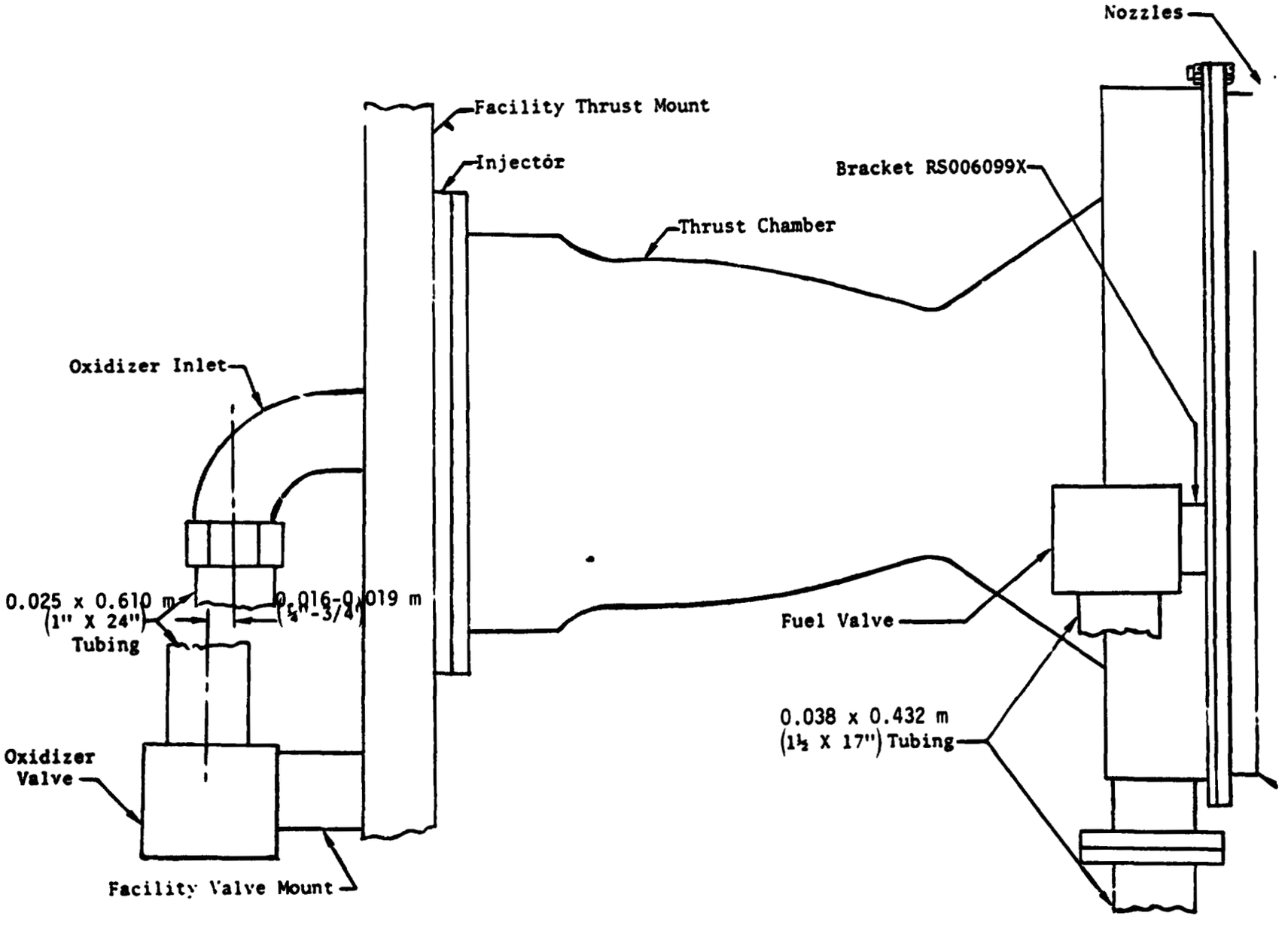

Figure 19. Propellant Inlet Ducting and Valves

TABLE 5. SS/OME REUSABLE THRUST CHAMBER PROGRAM (NAS9-12802)
TASK XII - DATA DUMP
INTEGRATED CHAMBER LOW-PRESSURE TESTS

	7-7	7-8	7-9	7-10	7-10A	7-11	7-12	7-14
CHAMBER PR, $N/M^2 \times 10^4$ (PSIA)	86.37 (126)	57.92 (84)	52.40 (76)	46.88 (68)	50.33 (73)	45.50 (66)	46.88 (68)	86.88 (126)
MIXTURE RATIO, O/F	1.68	1.7	1.8	1.8	1.5	1.6	1.9	1.66
FLOWRATE, KG/SEC (LB/SEC)								
OXID	5.62 (12.4)	3.76 (8.29)	3.36 (7.41)	2.88 (6.34)	3.08 (6.78)	2.73 (6.02)	2.98 (6.57)	5.53 (12.2)
FUEL	3.35 (7.39)	2.14 (4.72)	1.86 (4.10)	1.58 (3.48)	2.05 (4.53)	1.72 (3.79)	1.54 (3.40)	3.35 (7.39)
MEASURED INJ P,*								
$N/M^2 \times 10^4$ (PSI) OXID	38.61 (56)	13.10 (19)	7.58 (11)	--	--	--	--	35.16 (51)
FUEL	39.30 (57)	12.41 (18)	6.89 (10)	--	--	--	--	35.85 (52)
PREDICTED INJ. P,								
$N/M^2 \times 10^4$ (PSI) OXID	38.61 (56**)	16.55 (24)	13.79 (20)	10.34 (15)	11.72 (17)	8.96 (13)	11.03 (16)	37.23 (54)
FUEL	39.30 (57**)	15.86 (23)	11.72 (17)	8.27 (12)	14.48 (21)	10.34 (15)	8.27 (12)	39.30 (57)
PREDICTED P/Pc OXID	0.44	0.29	0.26	0.22	0.23	0.20	0.24	0.42
FUEL	0.45	0.23	0.22	0.19	0.29	0.23	0.18	0.43
FREQUENCY, HZ	STABLE	STABLE	STABLE	245	350	280	255	STABLE
PK/PK AMPLITUDE,								
$N/M^2 \times 10^4$ (PSI) OXID	--	4.82-11.72 (7-17)	6.89 (10)	49.64 (72)	6.21-16.54 (9-24)	23.44 (34)	33.09 (48)	8.27 (12)
FUEL	--	4.82 (7)	4.82 (7)	24.82 (36)	6.89 (10)	16.55 (24)	28.27 (41)	6.89 (10)

*DURING STABLE PART OF TEST

**REFERENCE

the discrepancy is greater than would be expected from instrumentation inaccuracies. Values of injector ΔP divided by P_c are also tabulated based on the predicted pressure drops. Tests were conducted with values as low as approximately 0.2 on each side of the injector.

Chugging was not evident as the chamber pressure was reduced from test to test until Test 7-8 where a chamber pressure of 57.92×10^4 N/m^2 (84 psia) was obtained for steady-state. On this test, chugging occurred for approximately 0.6 seconds after ignition at a frequency of about 300 Hz. As the chamber pressure was reduced on the successive tests, the duration of the chugging increased until at a chamber pressure of 46.88×10^4 N/m^2 (68 psia) chugging continued throughout the test. When the chamber pressure was increased on the next test to 50.33×10^4 N/m^2 (73 psia) and the mixture ratio was decreased to 1.5, continuous chugging occurred for 1.6 seconds but continued sporadically throughout the remaining duration of the test. Variation of the mixture ratio to 1.6 and 1.9 at 46.19×10^4 N/m^2 (67 psia) chamber pressure on the next two tests resulted in small changes in the chug amplitude. Chug frequencies of 200-300 Hz were noted. Oscillations at two frequencies were indicated during the early portions of some of the tests; however, the lower frequency persisted for less than 1 second after start.

Complete summaries of all steady-state performance data (average measured values and calculated values) compiled for Test Sequence 7, Runs 8-14 are presented in Ref. 29.

Application of Experimental Data to Model Verification

The White Sands test data presented in the previous section are sufficient to provide initial verification of the engineering model in a manner which is consistent with the model's anticipated normal usage. A total of seven verification analyses were evaluated based upon the integrated chamber low pressure tests summarized previously in Table 5 . Tests 7-8, 7-9, and 7-14 were used to represent examples of stable system behavior while tests 7-10, 7-11, and 7-12 provided examples of unstable engine operating conditions. The low amplitude chugging behavior encountered in test 7-10A was planned to serve as an illustration of marginally stable operating behavior.

MODEL INPUT DATA

Each of the seven verification analyses required the same basic input data to the computer program, namely:

1. Feed system configuration (Figs. 17 and 18).
2. Injector characteristics (Fig . 15, Tables 3 and 4).
3. Chamber geometry (Fig. 14 , Table 2) .
4. Steady-state engine operating conditions (Ref. 29 Appendix).

In order to determine the steady-state distributed energy release functions required by the stability model, an existing Distributed Energy Release combustion model (JANNAF computer program DER) was executed for each verification case. In all cases, the DER calculated performance was less than the measured engine performance. This difference between the calculated and experimental performance should not affect the stability calculations since performance is dependent upon the largest droplet diameter groups while stability is mainly dependent upon the smaller droplet groups.

Output from the DER computer calculations was curve-fitted with the steady-state equations employed by the stability model in order to obtain important combustion-related parameters. One of these parameters is the vaporization "time delay". Integrating the steady-state vaporization expressions given by Eq. 64 from the start plane for vaporization (X_0) to any given vaporization plane (X) yields:

$$\ln (\% \text{ unburned propellant}) = \ln(100) - \left[\frac{X - X_0}{\bar{\tau}\,\bar{V}}\right] \tag{138}$$

A plot of this equation along with DER calculated values for the fuel and oxidizer for test IHT 1-7-14 is shown in Fig. 20. A straight line was drawn through each curve for $X < 0.0635$ m (2.5 in.), since the vaporization rates corresponding to these distances are much greater than those for $X > 0.0635$ m (2.5 in.). Obtaining $\bar{\tau}\,\bar{V}$ from the slope of each curve and using the fact that $\bar{V}$ equals the average injection velocity enables the vaporization "time delays" to be calculated. Methods for obtaining other input data required by the stability model from the DER program output are outlined in Ref. 3.

Initial model verification calculations indicated that the following terms must be neglected in order to obtain agreement between calculated and experimental results:

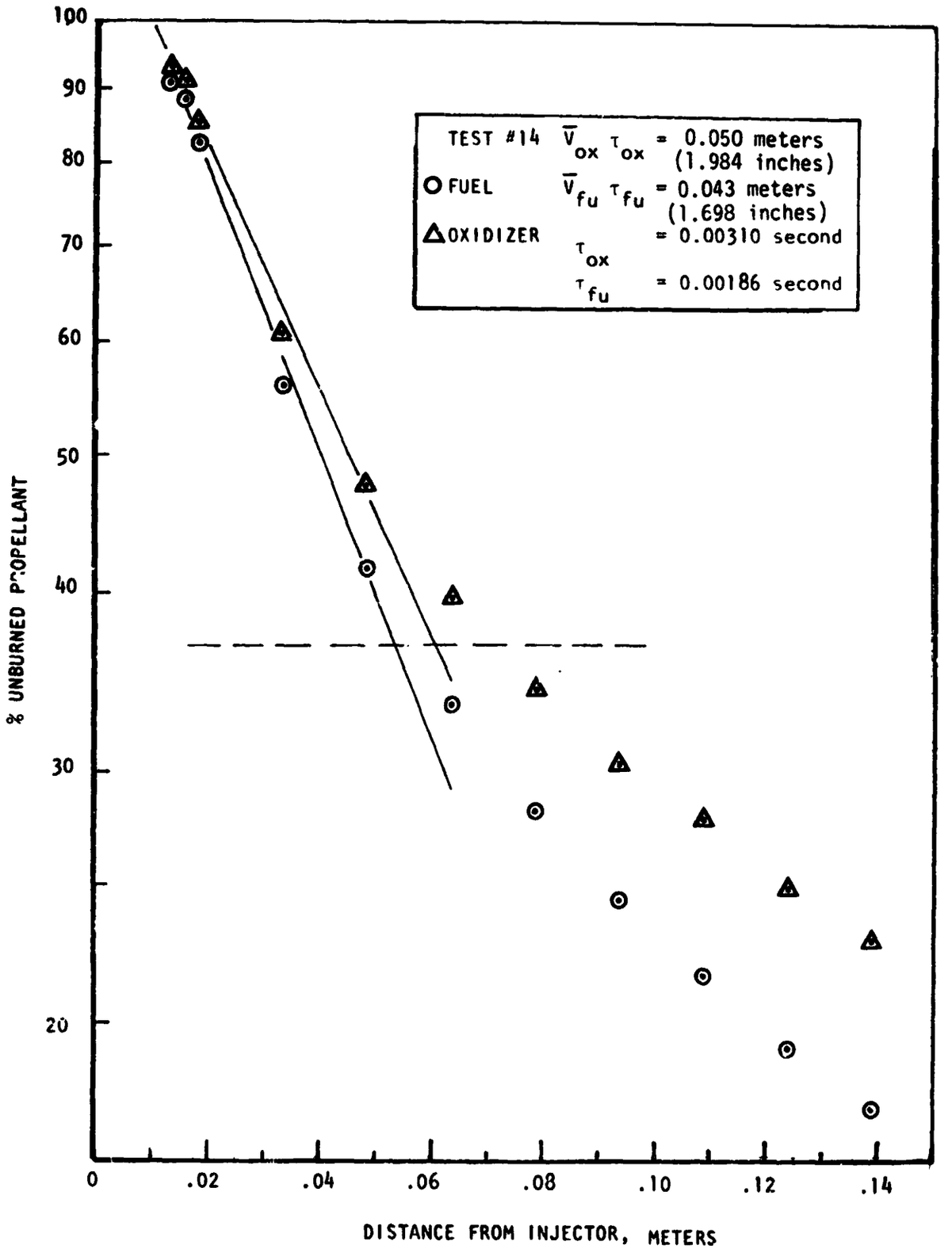

Figure 20. Determination of Vaporization Time Delays for Fuel and Oxidizer Based Upon WSTF Test IHT 1-7-14

1. Changes in the vaporization time delay due to changes in mixture ratio must be neglected, i.e., $\frac{\partial \bar{\tau}}{\partial MR} = 0$.
2. Changes in the nozzle admittance due to mixture ratio changes must be neglected, i.e., $\frac{\partial c^*}{\partial MR} = 0$.
3. The oscillatory relative velocity between the gas and the droplets must be neglected, i.e., $\tau_{DRAG} = 0$.

Since the vaporization "time delay" is actually temperature dependent instead of mixture ratio dependent, even though the temperature is a function of the mixture ratio, the stability model should be modified to reflect this dependence. Model calculations at the end of the program indicated that if this change from mixture ratio to temperature dependence is made in the model, agreement between calculated and experimental results can be maintained while including $(\frac{\partial \tau}{\partial T})$ and $(\frac{\partial c^*}{\partial MR})$ effects. Problems encountered when the oscillatory relative velocity effects are included in the model calculations have not been isolated but continuing effort will be directed towards including this important coupling term.

DETERMINATION OF KLYSTRON DISTANCE

One of the important input parameters required by the stability model is the Klystron distance. Since experimentally determined values for the Klystron distance for the OME system configuration are not presently available, and in lieu of actual combustion characterization test data, the Klystron distances were determined based on IHT 1-7-10 and 1-7-12 test data. The fuel and oxidizer Klystron distances were assumed to be equal and independent of engine operating conditions. These assumptions are probably invalid but were made for lack of actual combustion characterization test data.

Shown in Fig. 21 is the decrement for tests 10 and 12 as a function of the Klystron distance. The decrement (λ) is defined as minus the imaginary part of the complex frequency divided by the real part of the complex frequency and is a measure of how fast the wave will grow or decay. A positive value for the decrement indicates a damping or stable behavior, whereas a negative

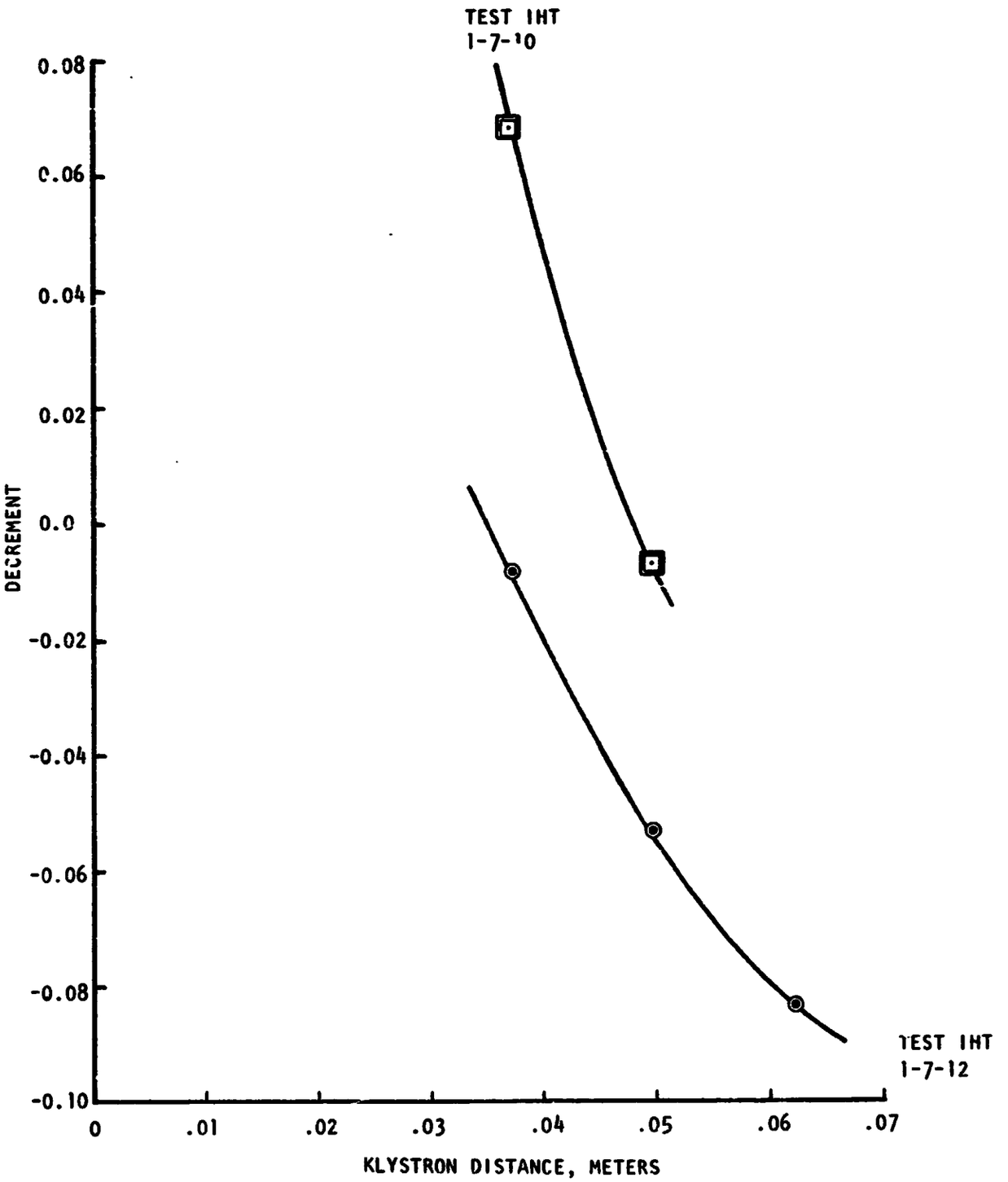

Figure 21. Determination of Klystron Distance Based upon WSTF Tests IHT 1-7-12 AND IHT 1-7-10

C-2

value indicates an increasing amplitude or unstable behavior. Marginal stability or instability corresponds to a decrement value near zero.

Since tests 10 and 12 were experimentally unstable, Fig. 21 yields the result that the Klystron distance must be greater than 0.0495 m (1.95 in.). For model verification, a Klystron distance of 0.0508 m (2 in.) was selected based on the information presented in Fig. 21.

COMPARISON BETWEEN CALCULATED AND EXPERIMENTAL RESULTS

Execution of the complete engineering model results in the prediction of the oscillatory frequency and information related to the stability or damping coefficient (decrement) of that frequency for the pressure-fed propulsion system. For each given test case, the frequency and stability predicted by the engineering model can be compared with the experimental data. Shown in Table 6 are the tabulated experimental data and calculated results. Comparison between calculated and experimental results indicate that the model is in agreement with the experimental data in predicting stable or unstable operation for all tests except IHT 1-7-11. Also, the value for the decrement for test IHT 1-7-10A should be closer to the neutral stability value of zero. Comparison of the experimental and calculated frequencies for the unstable tests yields the result that the calculated instability frequencies are much lower than the experimental values. This discrepancy in frequency could be due to assumptions in modeling the feed system or to omitting certain combustion effects.

Figure 22 presents the experimental and calculated results as functions of the fuel and oxidizer injector pressure drops. The experimental data can be separated into stable and unstable regions, i.e., if the fuel and/or oxidizer delta pressure is below a certain value, the engine was experimentally unstable. Based on this fact and the calculated results presented in Table 6 , Fig. 22 indicates that the model calculations are not sensitive enough to the oxidizer injector pressure loss. Based on tests 9 and 10

TABLE 6 . COMPARISON OF CALCULATED AND EXPERIMENTAL RESULTS

TEST NO.	EXPERIMENTAL FREQUENCY (Hz)	CALCULATED	
		FREQUENCY	DECREMENT
8	Stable	216.4	0.1370
9	Stable	209.6	0.0417
10	245	207.1 281.0	-0.0078 0.1024
10A	Marginally Stable (350)	152.1 175.8 211.3 247.3	0.1431 0.2194 0.1353 0.1535
11	280	198.6 219.8 261.4 293.2	0.1748 0.1598 0.1159 0.0695
12	255	174.3 212.8 280.4	0.1901 -0.0533 0.09566
14	Stable	264.8 314.8	0.2613 0.2020

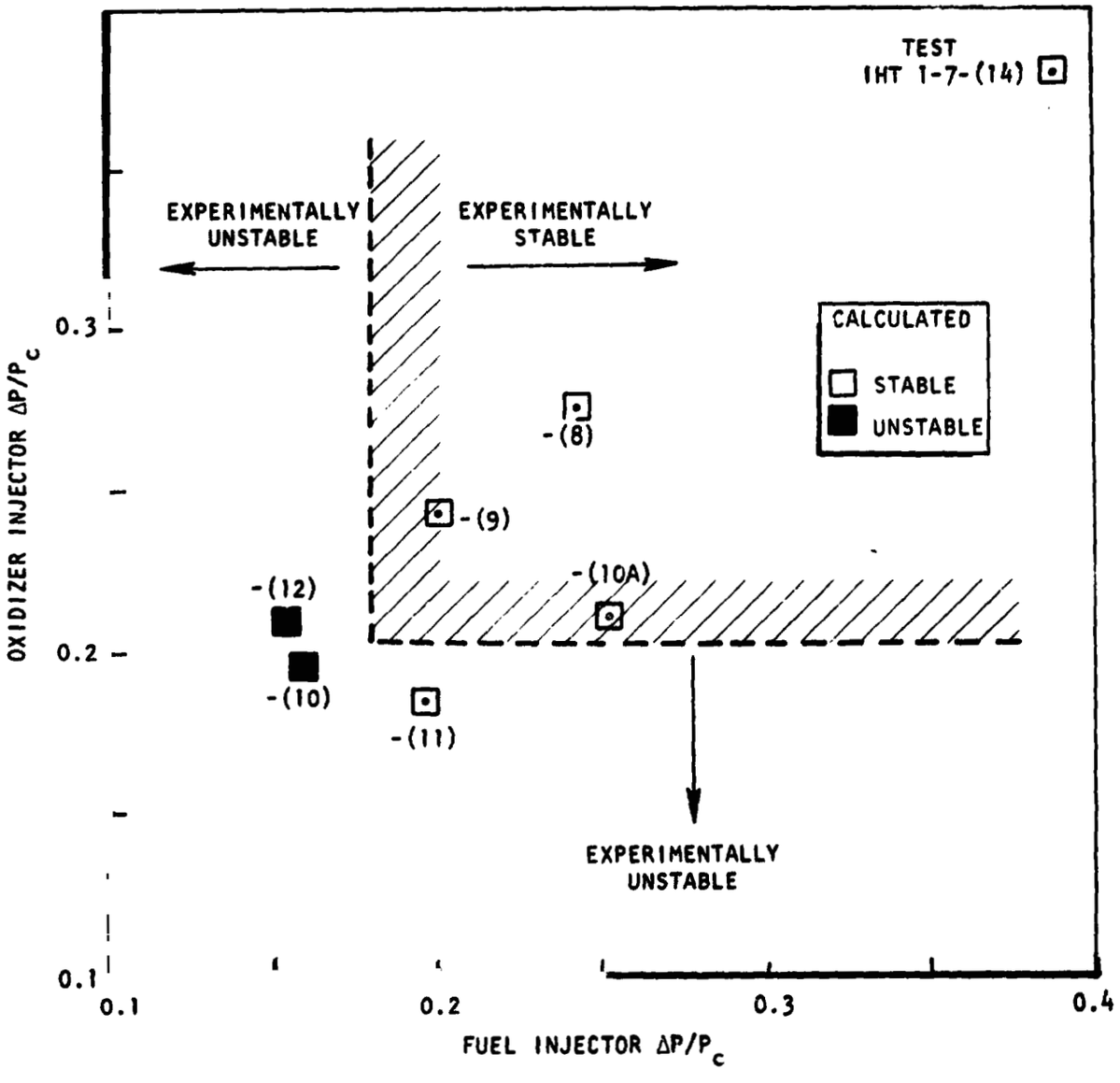

Figure 22. Comparison of Feed System Coupled Stability Model Calculations and WSTF Experimental Data

(or 12), the model predicts the correct trend with respect to fuel delta pressure but examination of tests 10A and 11 shows that the model does not predict the correct trend with respect to oxidizer delta pressure. This insensitivity to oxidizer delta pressure could be due to the particular hydrodynamic modeling of the oxidizer system or due to using the same Klystron distance for the oxidizer and fuel. It should be noted that the Klystron distance was determined based on tests 10 and 12 which are controlled by the fuel system. Also, the omission of certain combustion effects could, and probably are, affecting the model predictions. Final determination of the models inability to predict correctly the experimental results of tests 11 and 10A cannot be made until after combustion characterization studies have been completed. A limited number of calculations have shown that the model is quite sensitive to changes in the hydrodynamic system and certain combustion parameters.

SECTION V

CONCLUSIONS AND RECOMMENDATIONS

The Feed System Coupled Stability Model (FSCSM) has been formulated, checked out and successfully executed. It has been shown to be capable of analyzing feed system/engine coupled instabilities in pressure-fed, storable propellant, propulsion systems over a frequency range of 10 to 1000 Hz. The model has been constructed in a generalized manner in order that it may be readily applicable to present and future engine and propulsion systems.

Based upon the limited number of model verification analyses conducted thus far using the OME system as a working basis, the model appears to predict correctly the stability or instability of a given engine system. As expected by the theoretical analysis, the Klystron constant was determined to have a significant effect on the stability prediction. With respect to the predicted unstable tests, the frequencies calculated by the model were found to be much lower than the experimentally determined frequencies (213 Hz vs. 255 Hz and 207 Hz vs. 245 Hz). These results are due in part to the assumptions used in modeling the feed system as well as to the omission of certain combustion effects. The calculated frequencies were found to be highly sensitive to the feed system input data, particularly to the lengths of the various line segments and to the injector manifold volume. In addition, the value of the decrement was directly related to the magnitude of the injector ΔP. Comparison of the available experimental and calculated results indicated that the model was not sensitive enough to the oxidizer injector pressure loss.

A number of areas exist where modifications or possible improvements to FSCSM can be made. These are listed below:

1. Input data required by the model should be simplified. This could be accomplished in two steps. First, modify the output of the steady-state DER program to calculate and print out in a logical sequence the pertinent data to be used as input to the combustion and chamber dynamics subprograms. Next, change the hydrodynamics subprogram to accept line segment ΔP's as input data and calculate values of resistances and acoustic velocities internally.

2. More accurate feed system formulations should be investigated to include the effects of various nonlinearities. This would involve the use of the complete continuity and momentum equations instead of the simplified "waterhammer" description.

3. Improvements in the combustion and chamber dynamics model formulations should be studied. First, the velocity coupling terms should be reviewed. These were neglected during model verification due to their extreme sensitivity in affecting the model results. In addition, more realistic methods of evaluating the effect of mixture ratio on nozzle admittance should be determined. Improved methods of calculating the vaporization time delays as functions of pressure, temperature, mixture ratio, etc., should also be investigated.

   Inclusion of the full set of spray equations (continuity, momentum, etc.) would enable the Klystron constant to be determined more readily as a function of the propellant properties and/or injector geometry. This would also yield more realistic expressions from which the vaporization rates and droplet velocities could be calculated. Although this would tend to increase the complexity of the chamber dynamics equations, the solution method for determining the complex frequency and decrement (stability rating) would not be affected.

Finally, to incorporate certain types of non-linearities into the combustion dynamics formulation, the combustion coefficients should be made functions of the local peak-to-peak pressure amplitude. Then, investigation of stability or instability for a finite disturbance could be made and the actual peak-to-peak amplitudes determined for unstable disturbances.

4. Actual OME subscale test data should be obtained yielding combustion characterization test parameters and detailed feed system information to provide a more rigorous verification of the FSCSM. The experimental test program should be structured into two phases. The first phase would be used to check out the hydrodynamics model formulation. It would involve perturbing the pressure in the test chamber under non-combustion conditions and measuring local oscillatory pressures and flowrates at selected points along the length of the feed system. The second phase would be used to verify the combustion and chamber dynamics models. This would consist of pulsing the feed system at a known frequency and measuring the combustor response.

5. Additional areas exist where improvements in the model could aid in better understanding of typical feed system coupled instabilities. These include:

    a. Multi-dimensional chamber and manifold descriptions
    b. Coupling of pressure response with injector passage resonance

A multi-dimensional model would be very useful in analyzing instabilities where response in the chamber is not uniform across the injector face. This would include analyzing the effect of feed system coupling on chamber radial and tangential modes of instability as well as including the proper feed system effect in the design and analysis of acoustic cavities. Previously, feed system contributions to chamber

resonant modes of instability have usually been ignored. However, some flow oscillations can occur across the injector face for even very high frequency oscillations. In some cases, feed system modifications may be the method used to stabilize this type of instability. In other cases accurately including the feed system effect could make design of damping devices more reliable.

Another type of instability that occasionally occurs is a feed system resonance involving only the injector flow path coupling with some pressure response feedback. These instabilities are generally high frequency (observed instabilities have been from 4400 to 14,000 Hz). The injector resonant response characteristic can be accurately modeled, but the feedback loop involving chamber combustion or some other generation of pressure oscillations has not been simulated. This makes evaluation of various modifications somewhat qualitative. If the pressure feedback loop could be accurately simulated, the determination of required system modifications would be more reliable.

SECTION VI

REFERENCES

1. Boehnlein, J. J.: "Generalized Propulsion System Model," R-8445, Rockwell International, Rocketdyne Division, Canoga Park, California, 1971.

2. Kahn, D. R.: "Engineering Model Characterization Evaluation Interim Report," ASR 74-372, Rockwell International, Rocketdyne Division, Canoga Park, California, December 1974.

3. Schuman, M. D. et al.: "OME Feed System Coupled Stability Investigation - Computer User's Manual," Rockwell International, Rocketdyne Division, Canoga Park, California, July 1975.

4. Ezekiel, F. D.: Control Engineering, May 1958, 111-112.

5. Summerfield, M.: "A Theory of Unstable Combustion in Liquid Propellant Rocket Systems," ARS Journal, Vol. 21, No. 5, September 1951, 108-114.

6. Crocco, Luigi, and Sin-I Cheng: "Theory of Combustion Instability in Liquid Propellant Rocket Motors," AGARDograph No. 8, Butterworths Sci. Publ., 1956.

7. Hurrell, H. G.: "Analysis of Injection Velocity Effects on Rocket Motor Dynamics and Stability," NASA TR R-43, 1959.

8. Wenzel, L. M. and J. R. Szuch: "Analysis of Chugging in Liquid-Bipropellant Rocket Engines Using Propellants With Different Vaporization Rates," NASA TN D-3080, October 1965.

9. Zinn, B. T. and E. A. Powell: "Nonlinear Combustion Instability in Liquid-Propellant Rocket Engines," Thirteenth Symposium (International) on Combustion, August 1970, 491-503.

10. Szuch, J. R.: "Digital Computer Program for Analysis of Chugging Instabilities," NASA TN D-7026, December 1970.

11. Lores, M. E. and B. T. Zinn: "Nonlinear Longitudinal Combustion Instability in Rocket Motors," Combustion Science and Technology, Vol. 7, 1973, 245-256.

12. Priem, R. J. and M. F. Heidmann: "Propellant Vaporization as a Design Criterion for Rocket-Engine Combustion Chambers," NASA TR R-67, 1960.

13. Combs, L. P.: "Liquid Rocket Performance Computer Model With Distrib... Energy Release," NASA CR-114462, June 1972.

14. Zajac, L. J.: "Correlation of Spray Dropsize Distribution and Injector Variables," R-8455, Rockwell International, Rocketdyne Division, Canoga Park, California, 1969.

15. Nurick, W. H.: "Study of Spray Disintegration of Accelerating Flow Fields," NASA CR-114479, June 1972.

16. Zajac, L. J.: "Droplet Breakup in Accelerating Gas Flows, Part I - Primary Atomization, Part II - Secondary Atomization," NASA CR-134478 (Part I), NASA CR-134479 (Part II), October 1973.

17. Fenwick, J. R. and G. J. Bugler: "Oscillatory Flame-Front Flowrate Amplification Through Propellant Injection Ballistics (The Klystron Effect)," ICRPG 3rd Combustion Conference, CPIA No. 138, Vol. 1, October 1966, 417-427.

18. Goldsmith, M. and S. S. Penner: Jet Propulsion, Vol. 24, July-August 1954, p. 245.

19. Williams, F. A.: Combustion Theory, Addisor Wesley, Reading, Mass., 1965.

20. Combs, L. P., W. D. Chadwick, and D. T. Campbell: "Liquid Rocket Performance Computer Model With Distributed Energy Release," Interim Final Report, NASA CR-111000, September 1970.

21. Ranz, W. E. and W. R. Marshall, Jr.: Chem. Eng. Progress, Vol. 48, 1952, 141-146 and 173-180.

22. Heidmann, M. F.: "Amplification by Wave Distortion of the Dynamic Response of Vaporization Limited Combustion," NASA TN D-6287, May 1971.

23. Kenworthy, M. J.: "Augmentor Combustion Stability Investigation," AFAPL-TR-74-61, August 1974.

24. Linow, F. R.: Combustion Characterization Test Plan, ASR 74-333, Rockwell International, Rocketdyne Division, Canoga Park, California, October 1974.

25. Wilkenson, J. H.: The Algebraic Eigenvalue Problem, Oxford University Press, Ely House, London, 1967.

26. "ICRPG One-Dimensional Equilibrium Reference Program - Preliminary Description of ODE, a Computer Program for the Calculation of Chemical Equilibrium Composition With Applications," ICRPG Performance Standardization Working Group, July 1968.

27. Ralston, A.: A First Course in Numerical Analysis, McGraw-Hill Book Co., New York, 1965.

28. Muller, D. E.: "A Method for Solving Algebraic Equations Using a Computer," MTAC, Vol. 10, 1956, pp. 208-215.

29. Kahn, D. R.: "Engineering Model Verification Plan," ASR 75-108, Rockwell International, Rocketdyne Division, Canoga Park, California, April 1975.

30. Space Shuttle Orbital Maneuvering Engine/Reusable Thrust Chamber Program, NASA Contract NAS9-12802, Task XII Data Dump (Phase II), OME Integrated Thrust Chamber Test Report, Rocketdyne ASR 74-229, August 1974.

31. Sutton, R. D.: "Spray Combustion Processes in Steady and Nonsteady Ph.D. Thesis, University of California, Berkeley, California, 1971.

32. Bell, W. A. and B. T. Zinn: "The Prediction of Three-Dimensional Liquid Propellant Rocket Nozzle Admittances," NASA CR-121129.

APPENDIX A

FEED SYSTEM HYDRODYNAMICS MODEL EQUATIONS

In this appendix, the system of 57 equations describing the generalized feed system shown in Fig. 7 is presented. The equations are given in the linearized, La Place transformed format required by the frequency response subroutine. The derivation of the equations is based upon the mathematical formulation outlined in Section II.

$$P_1 + (R_1 + a_1)\,\dot{w}_1 + [P_1 + (R_1 - a_1)\,\dot{w}_1]\,e^{-2T_1 s} = 0 \qquad \text{(A-1)}$$

$$P_1 - a_3\dot{w}_3 - [P_2 + (R_3 - a_3)\,\dot{w}_4]\,e^{-T_3 s} = 0 \qquad \text{(A-2)}$$

$$P_2 + (R_3 + a_3)\,\dot{w}_4 - [P_1 + a_3\dot{w}_3]\,e^{-T_3 s} = 0 \qquad \text{(A-3)}$$

$$P_1 - (R_2 + a_2)\,(\dot{w}_1 - \dot{w}_3) - [P_1 - (R_2 - a_2)\,(\dot{w}_1 - \dot{w}_3)]\,e^{-2T_2 s} = 0 \qquad \text{(A-4)}$$

$$P_2 - a_5\dot{w}_6 - [P_3 + (R_5 - a_5)\,\dot{w}_7]\,e^{-T_5 s} = 0 \qquad \text{(A-5)}$$

$$P_2 - a_4\,(\dot{w}_4 - \dot{w}_6) - [P_8 + (R_4 - a_4)\,\dot{w}_{15}]\,e^{-T_4 s} = 0 \qquad \text{(A-6)}$$

$$P_8 + (R_4 + a_4)\,\dot{w}_{15} - [P_2 + a_4\,(\dot{w}_4 - \dot{w}_6)]\,e^{-T_4 s} = 0 \qquad \text{(A-7)}$$

$$P_3 + (R_5 + a_5)\,\dot{w}_7 - [P_2 + a_5\,\dot{w}_6]\,e^{-T_5 s} = 0 \qquad \text{(A-8)}$$

$$P_3 - a_6\,\dot{w}_7 - [P_4 + (R_6 - a_6)\,\dot{w}_8]\,e^{-T_6 s} = 0 \qquad \text{(A-9)}$$

$$P_4 - (R_7 + a_7)\,(\dot{w}_8 - \dot{w}_{10}) - [P_4 - (R_7 - a_7)\,(\dot{w}_8 - \dot{w}_{10})]\,e^{-2T_7 s} = 0 \qquad \text{(A-10)}$$

$$P_4 - a_8\,\dot{w}_{10} - [P_5 + (R_8 - a_8)\,\dot{w}_{11}]\,e^{-T_8 s} = 0 \qquad \text{(A-11)}$$

$$P_5\,(R_8 + a_8)\,\dot{w}_{11} - [P_4 + a_8\,\dot{w}_{10}]\,e^{-T_8 s} = 0 \qquad \text{(A-12)}$$

$$P_5 - a_9\,\dot{w}_{11} - [P_6 + (R_9 - a_9)\,\dot{w}_{12}]\,e^{-T_9 s} = 0 \qquad \text{(A-13)}$$

$$P_6 + (R_9 + a_9)\,\dot{w}_{12} - [P_5 + a_9\,\dot{w}_{11}]\,e^{-T_9 s} = 0 \qquad \text{(A-14)}$$

$$P_6 - a_{10}\,\dot{w}_{12} - [P_7 + (R_{10} - a_{10})\,\dot{w}_{13}]\,e^{-T_{10} s} = 0 \qquad \text{(A-15)}$$

$$P_7 \bullet (R_{10} + a_{10})\,\dot{w}_{13} - [P_6 + a_{10}\,\dot{w}_{12}]\,e^{-T_{10} s} = 0 \qquad \text{(A-16)}$$

$$P_7 - Z_o s\,\dot{w}_{14} - R_o\,\dot{w}_{14} = P_o \qquad \text{(A-17)}$$

$$sP_7 - \left(\frac{c^2}{gV}\right)_o \dot{w}_{13} + \left(\frac{c^2}{gV}\right)_o \dot{w}_{14} + \left(\frac{c^2}{gV}\right)_o K_o\,sP_7 = \left(\frac{c^2}{gV}\right)_o K_o\,sP_o \qquad \text{(A-18)}$$

$$P_8 + a_{14}\,\dot{w}_{17} - [P_{12} - (R_{14} - a_{14})\,\dot{w}_{24}]\,e^{-T_{14} s} = 0 \qquad \text{(A-19)}$$

$$P_{12} - (R_{14} + a_{14})\,\dot{w}_{24} - [P_8 - a_{14}\,\dot{w}_{17}]\,e^{-T_{14} s} = 0 \qquad \text{(A-20)}$$

$$P_8 - a_{11}\,(\dot{w}_{15} + \dot{w}_{17}) - [P_9 + (R_{11} - a_{11})\,\dot{w}_{18}]\,e^{-T_{11} s} = 0 \qquad \text{(A-21)}$$

$$P_9 + (R_{11} + a_{11})\,\dot{w}_{18} - [P_8 + a_{11}\,(\dot{w}_{15} + \dot{w}_{17})]\,e^{-T_{11} s} = 0 \qquad \text{(A-22)}$$

$$P_9 - (R_{13} + a_{13})\,(\dot{w}_{18} - \dot{w}_{19}) - [P_9 - (R_{13} - a_{13})\,(\dot{w}_{18} - \dot{w}_{19})]\,e^{-2T_{13} s} = 0 \qquad \text{(A-23)}$$

$$P_9 - a_{12}\,\dot{w}_{19} - [X + R_{12} - a_{12})\,\dot{w}_{20}]\,e^{-T_{12} s} = 0 \qquad \text{(A-24)}$$

$$P_{11} + (R_{15} + a_{15})\,\dot{w}_{22} + [P_{11} + (R_{15} - a_{15})\,\dot{w}_{22}]\,e^{-2T_{15} s} = 0 \qquad \text{(A-25)}$$

$$P_{11} - a_{16}\,\dot{w}_{22} - [P_{12} + (R_{16} - a_{16})\,(\dot{w}_{24} + \dot{w}_{25})]\,e^{-T_{16} s} = 0 \qquad \text{(A-26)}$$

$$P_{12} + (R_{16} + a_{16})\,(\dot{w}_{24} + \dot{w}_{25}) - [P_{11} + a_{16}\,\dot{w}_{22}]\,e^{-T_{16}s} = 0 \qquad \text{(A-27)}$$

$$P_{13} + (R_{22} + a_{22})\,\dot{w}_{34} + [P_{13} + (R_{22} - a_{22})\,\dot{w}_{34}]\,e^{-2T_{22}s} = 0 \qquad \text{(A-28)}$$

$$P_{13} - a_{24}\,\dot{w}_{36} - [P_{17} + (R_{24} - a_{24})\,\dot{w}_{37}]\,e^{-T_{24}s} = 0 \qquad \text{(A-29)}$$

$$P_{13} - (R_{23} + a_{23})\,(\dot{w}_{34} - \dot{w}_{36}) - [P_{13} - (R_{23} - a_{23})\,(\dot{w}_{34} - \dot{w}_{36})]\,e^{-2T_{23}s} = 0 \qquad \text{(A-30)}$$

$$P_{12} - (R_{17} + a_{17})\,\dot{w}_{25} - [P_{14} - a_{17}\,\dot{w}_{26}]\,e^{-T_{17}s} = 0 \qquad \text{(A-31)}$$

$$P_{14} + a_{17}\,\dot{w}_{26} - [P_{12} - (R_{17} - a_{17})\,\dot{w}_{25}]\,e^{-T_{17}s} = 0 \qquad \text{(A-32)}$$

$$P_{17} - a_{21}\,(\dot{w}_{37} - \dot{w}_{38}) - [P_{14} + (R_{21} - a_{21})\,\dot{w}_{27}]\,e^{-T_{21}s} = 0 \qquad \text{(A-33)}$$

$$P_{14} + (R_{21} + a_{21})\,\dot{w}_{27} - [P_{17} + a_{21}\,(\dot{w}_{37} - \dot{w}_{38})]\,e^{-T_{21}s} = 0 \qquad \text{(A-34)}$$

$$P_{14} - a_{18}\,(\dot{w}_{26} + \dot{w}_{27}) - [P_{15} + (R_{18} - a_{18})\,\dot{w}_{29}]\,e^{-T_{18}s} = 0 \qquad \text{(A-35)}$$

$$P_{15} + (R_{18} + a_{18})\,\dot{w}_{29} - [P_{14} + a_{18}\,(\dot{w}_{26} + \dot{w}_{27})]\,e^{-T_{18}s} = 0 \qquad \text{(A-36)}$$

$$P_{15} - (R_{19} + a_{19})(\dot{w}_{29} - \dot{w}_{31}) - [P_{15} - (R_{19} - a_{19})(\dot{w}_{29} - \dot{w}_{31})]\,e^{-2T_{19}s} = 0 \qquad \text{(A-37)}$$

$$P_{15} - a_{20}\,\dot{w}_{31} - [Y + (R_{20} - a_{20})\,\dot{w}_{32}]\,e^{-T_{20}s} = 0 \qquad \text{(A-38)}$$

$$P_{16} + (R_{20} + a_{20})\,\dot{w}_{32} - [P_{15} + a_{20}\,\dot{w}_{31}]\,e^{-T_{20}s} = 0 \qquad \text{(A-39)}$$

$$P_{17} - a_{25}\,\dot{w}_{38} - [P_{18} + (R_{25} - a_{25})\,\dot{w}_{39}]\,e^{-T_{25}s} = 0 \qquad \text{(A-40)}$$

$$P_{18} + (R_{25} + a_{25})\,\dot{w}_{39} - [P_{17} + a_{25}\,\dot{w}_{38}]\,e^{-T_{25}s} = 0 \qquad \text{(A-41)}$$

$$P_{18} - a_{26}\,\dot{w}_{39} - [P_{19} + (R_{26} - a_{26})\,\dot{w}_{40}]\,e^{-T_{26}s} = 0 \qquad \text{(A-42)}$$

$$P_{19} + (R_{26} + a_{26})\,\dot{w}_{40} - [P_{18} + a_{26}\,\dot{w}_{39}]\,e^{-T_{26}s} = 0 \qquad \text{(A-43)}$$

$$P_{19} - (R_{27} + a_{27})(\dot{w}_{40} - \dot{w}_{42}) - [P_{19} - (R_{27} - a_{27})(\dot{w}_{40} - \dot{w}_{42})]\,e^{-2T_{27}s} = 0 \qquad \text{(A-44)}$$

$$P_{19} - a_{28}\,\dot{w}_{42} - [P_{20} + (R_{28} - a_{28})\,\dot{w}_{43}]\,e^{-T_{28}s} = 0 \qquad \text{(A-45)}$$

$$P_{20} + (R_{28} + a_{28})\,\dot{w}_{43} - [P_{19} + a_{28}\,\dot{w}_{42}]\,e^{-T_{28}s} = 0 \qquad \text{(A-46)}$$

$$P_{20} - a_{29}\,\dot{w}_{43} - [P_{21} + (R_{29} - a_{29})\,\dot{w}_{44}]\,e^{-T_{29}s} = 0 \qquad \text{(A-47)}$$

$$P_{21} + (R_{29} + a_{29})\,\dot{w}_{44} - [P_{20} + a_{29}\,\dot{w}_{43}]\,e^{-T_{29}s} = 0 \qquad \text{(A-48)}$$

$$P_{21} - a_{30}\,\dot{w}_{44} - [P_{22} + (R_{30} - a_{30})\,\dot{w}_{45}]\,e^{-T_{30}s} = 0 \qquad \text{(A-49)}$$

$$P_{22} + (R_{30} + a_{30})\,\dot{w}_{45} - [P_{21} + a_{30}\,\dot{w}_{44}]\,e^{-T_{30}s} = 0 \qquad \text{(A-50)}$$

$$P_{22} - Z_F s\,\dot{w}_{46} - R_F\,\dot{w}_{46} = P_F \qquad \text{(A-51)}$$

$$s\,P_{22} - \left(\frac{c^2}{gV}\right)_F (\dot{w}_{45} - \dot{w}_{46}) + \left(\frac{c^2}{gV}\right)_F K_F\,sP_{22} = \left(\frac{c^2}{gV}\right)_F K_F\,sP_F \qquad \text{(A-52)}$$

$$P_4 + (R_6 + a_6)\,\dot{w}_8 - [P_3 + a_6\,\dot{w}_7]\,e^{-T_6 s} = 0 \qquad \text{(A-53)}$$

$$P_{10} + (R_{12} + a_{12})\,\dot{w}_{20} - [P_9 + a_{12}\,\dot{w}_{19}]\,e^{-T_{12} s} = 0 \qquad \text{(A-54)}$$

$$P_{17} + (R_{24} + a_{24})\,\dot{w}_{37} - [P_{13} + a_{24}\,\dot{w}_{36}]\,e^{-T_{24} s} = 0 \qquad \text{(A-55)}$$

$$X = P_{10} \qquad \text{(A-56)}$$

$$Y = P_{16} \qquad \text{(A-57)}$$

NOTE: $a_N = \dfrac{C_N}{A_N g}$

APPENDIX B

COMBUSTION MODEL EQUATIONS

KLYSTRON EFFECT

The dynamics of the liquid propellant jet from the injector face to any location in the chamber are described by the continuity and momentum equations:

$$\frac{\partial}{\partial t}\left(A_j \rho_j\right) + \frac{\partial}{\partial x}\left(A_j \rho_j v_j\right) = 0 \qquad \text{(B-1)}$$

$$\frac{\partial}{\partial t}\left(A_j \rho_j u_j\right) + \frac{\partial}{\partial x}\left(A_j \rho_j v_j^2\right) = -A_j \frac{\partial p}{\partial x} \qquad \text{(B-2)}$$

Assuming

$$\rho_j = \text{constant} \qquad \text{(B-3)}$$

$$\frac{\partial p}{\partial x} = 0 \qquad \text{(B-4)}$$

$$\phi = \bar{\phi} + \tilde{\phi} \qquad (\phi \text{ any variable}), \qquad \text{(B-5)}$$

where

$$\bar{\phi} = f(x) \qquad \text{(time average value)} \qquad \text{(B-6)}$$

$$\tilde{\phi} = \phi' e^{-i\omega t} \qquad \text{(oscillatory value)} \qquad \text{(B-7)}$$

$$\tilde{\phi}' = g(x), \qquad \text{(B-8)}$$

the time average continuity and momentum equations become:

$$\frac{d}{dx}\left(\bar{A}_j \bar{v}_j\right) = 0 \qquad \text{(B-9)}$$

$$\frac{d}{dx}\left(\bar{A}_j \bar{v}_j^2\right) = 0 \qquad \text{(B-10)}$$

or

$$\bar{v}_j = \text{constant} \qquad \text{(B-11)}$$

$$\bar{A}_j = \text{constant} \qquad \text{(B-12)}$$

The first-order oscillatory continuity and momentum equations can be written as

$$\frac{\partial \tilde{A}_j}{\partial t} + \bar{A}_j \frac{\partial \tilde{v}_j}{\partial x} + \bar{v}_j \frac{\partial \tilde{A}_j}{\partial x} = 0 \qquad \text{(B-13)}$$

$$\frac{\partial \tilde{v}_j}{\partial t} + \bar{v}_j \frac{\partial \tilde{v}_j}{\partial x} = 0 \qquad \text{(B-14)}$$

Combining Eqs. B-7 and B-14 yields

$$v_j'(-i\omega) + \bar{v}_j \frac{dv_j'}{dx} = 0 \qquad \text{(B-15)}$$

which can be integrated to yield

$$v_j' = (v_j')_{inj}\, e^{i\omega x/\bar{v}_j} \qquad \text{(B-16)}$$

Since

$$\left(\frac{\tilde{\dot{m}}}{\bar{\dot{m}}}\right)_{inj} = \left(\frac{\tilde{v}_j}{\bar{v}_j}\right)_{inj} , \qquad \text{(B-17)}$$

the oscillatory jet velocity can be written as

$$\tilde{v}_j = \bar{v}_j\, e^{i\omega x/\bar{v}_j} \left(\frac{\tilde{\dot{m}}}{\bar{\dot{m}}}\right)_{inj} \qquad \text{(B-18)}$$

Substituting Eqs. B-7 and B-16 into Eq. B-13 yields

$$A_j'(-i\omega) + \bar{A}_j\, (v_j')_{inj}\, e^{i\omega x/\bar{v}_j} \left(\frac{i\omega}{\bar{v}_j}\right) + \bar{v}_j \frac{dA_j'}{dx} = 0 \qquad \text{(B-19)}$$

Integrating Eq. B-19 and employing Eq. B-17 yields the jet area

$$\tilde{A}_j = -\bar{A}_j \left(\frac{i\omega x}{\bar{v}_j}\right) e^{i\omega x/\bar{v}_j} \left(\frac{\tilde{\dot{m}}}{\bar{\dot{m}}}\right)_{inj} . \tag{B-20}$$

The mass flowrate of the jet is

$$\dot{m}_j = A_j \rho_j v_j \tag{B-21}$$

Therefore, the oscillatory flowrate is

$$\frac{\tilde{\dot{m}}_j}{\bar{\dot{m}}_j} = \frac{\tilde{A}_j}{\bar{A}_j} + \frac{\tilde{v}_j}{\bar{v}_j} . \tag{B-22}$$

Combining Eqs. B-18 , B-20, and B-22 gives

$$\frac{\tilde{\dot{m}}_j}{\bar{\dot{m}}_{inj}} = e^{i\omega x/\bar{v}_j} \left[1 - \frac{i\omega x}{\bar{v}_j}\right] \left(\frac{\tilde{\dot{m}}}{\bar{\dot{m}}}\right)_{inj} . \tag{B-23}$$

DROPLET VAPORIZATION

For the fuel or oxidizer spray, the droplet continuity equation can be written as

$$\frac{d}{dx}(A\rho_k v_k) = -A N_k \dot{m}_{vap_k} \tag{B-24}$$

and the vaporization rate is (Ref. 12)

$$\dot{m}_{vap_k} = \frac{\pi D_k k_{f_k} Nu_{H_k} Z_k}{c_{pv_k}} . \tag{B-25}$$

where ρ_k is the spray density (mass of spray per unit chamber volume), N_k is the number of droplets per unit chamber volume, and

$$Z_k \equiv \frac{c_{p_{v_k}} Nu_{m_k} p MW_{v_k} D_{v_k}}{k_{f_k} Nu_{H_k} \Re T_{f_k}} \ln \left(\frac{p}{p-p_{v_k}}\right) \qquad \text{(B-26)}$$

Noting that

$$\rho_k = N_k m_k = N_k \rho_{\ell_k} \frac{\pi D_k^3}{6} \qquad \text{(B-27)}$$

the droplet number flowrate can be written as

$$\dot{N}_k = v_k A N_k = \frac{A v_k \rho_k}{m_k} \qquad \text{(B-28)}$$

Therefore, Eq. B-24 can be written as

$$\frac{d}{dx}(m_k \dot{N}_k) = -\frac{\dot{N}_k}{v_k} \dot{m}_{vap_k} \quad . \qquad \text{(B-29)}$$

For steady-state combustion models, the preceding equation (along with Eq. B-25) is numerically integrated allowing the droplet diameter, D_k, to vary along the length of the combustor and maintaining constant droplet number flowrate ($\dot{N}_k$). Combs' (Ref. 20) has shown that changing from a variable droplet diameter to a variable droplet number flowrate yields approximately the same results for steady-state vaporization. Therefore, in order to simplify the integration for stability analysis, the droplet diameter was held constant and the droplet number flowrate was assumed to vary.

Summing Eq. B-24 over all fuel or oxidizer droplet size groups yields

$$\sum_k \frac{d}{dx}(A\rho_k v_k) = -A \sum_k \rho_k \frac{\dot{m}_{vap_k}}{m_k} = -A \sum_k \frac{\rho_k (6) Z_\kappa k_{f_k} Nu_{H_k}}{\rho_{\ell_k} D_k^2 c_{p_{v_k}}} \qquad \text{(B-30)}$$

which can be written as

$$\frac{d}{dx}(A\rho_s v_s) = -\frac{A\rho_s}{\tau_s} = -A \dot{m}_{vap_s} \quad , \qquad \text{(B-31)}$$

where

$$\rho_s \equiv \sum_k \rho_k \tag{B-32}$$

$$v_s \equiv \frac{1}{\rho_s} \sum_k (\rho_k v_k) \tag{B-33}$$

$$\frac{1}{\tau_s} \equiv \frac{1}{\rho_s} \sum_k \frac{\rho_k (6) Z_k \, k_{f_k} \, Nu_{H_k}}{\rho_{\ell_k} \, D_k^2 \, c_{p_{v_k}}} \tag{B-34}$$

Letting Z_k, k_{f_k}, $c_{p_{v_k}}$ be independent of k and assuming

$$\tau_s = f(t) \tag{B-35}$$

yields:

$$\tau_s = \frac{\rho_{\ell_s} \, c_{p_{v_s}} \, D_s^2}{(6) Z_s \, k_{f_s} \, Nu_{H_s}} \quad , \tag{B-36}$$

where

$$D_s^2 = (\dot{m}_s)_{inj} \Big/ \sum_k \left(\frac{\dot{m}_k}{D_k^2} \right)_{inj} \quad . \tag{B-37}$$

From Eq. B-31

$$\frac{d(A\rho_s v_s)}{A\rho_s v_s} = - \frac{dx}{\tau_s v_s} \tag{B-38}$$

Integrating Eq. B-38 between x_0 and x

$$A\rho_s v_s = (\dot{m}_s)_{x=x_0} \exp \left[- \int_{x_0}^{x} \frac{dx}{\tau_s v_s} \right] \tag{B-39}$$

Substituting Eq. B-39 into Eq.B-31 yields the fuel or oxidizer spray vaporization rate:

$$\dot{m}_{vap_s} \frac{(\dot{m}_s)_{x=x_o}}{A\tau_s v_s} \exp\left[-\int_{x_o}^{x} \frac{dx}{\tau_s v_s}\right] \tag{B-40}$$

Using perturbation techniques, the time average vaporization rate can be written as

$$\bar{\dot{m}}_{vap_s} = \frac{(\bar{\dot{m}}_s)_{x=x_o}}{A\bar{\tau}_s \bar{v}_s} \exp\left[-\frac{(x-x_o)}{\bar{\tau}_s \bar{v}_s}\right] \tag{B-41}$$

and the oscillatory vaporization rate can be written as

$$\tilde{\dot{m}}_{vap_s} = \bar{\dot{m}}_{vap_s} \left\{ \frac{(\tilde{\dot{m}}_s)_{x=k_s}}{(\bar{\dot{m}}_s)_{x=x_o}} - \frac{\tilde{\tau}_s}{\bar{\tau}_s} - \frac{\tilde{v}_s}{\bar{v}_s} + \int_{x_o}^{x} \left(\frac{\tilde{\tau}_s}{\bar{\tau}_s} + \frac{\tilde{v}_s}{\bar{v}_s}\right) \frac{dx}{\bar{\tau}_s \bar{v}_s} \right\} \tag{B-42}$$

Assuming

$$v_s \approx (v_s)_{x=x_{k_s}} \tag{B-43}$$

yields

$$\frac{\tilde{v}_s}{\bar{v}_s} = \left(\frac{\tilde{v}_s}{\bar{v}_s}\right)_{x=x_{k_s}} \tag{B-44}$$

Letting ρ_{ℓ_s}, $c_{p_{v_s}}$, and k_{f_s} be constant, the oscillatory time delay can therefore be expressed as

$$\frac{\tilde{\tau}_s}{\bar{\tau}_s} = \frac{2\tilde{D}_s}{\bar{D}_s} - \frac{\tilde{z}_s}{\bar{z}_s} - \frac{\widetilde{Nu}_{H_s}}{\overline{Nu}_{H_s}} + \left(\frac{\partial \tau_s}{\partial MR}\right) \frac{\widetilde{MR}}{\bar{\tau}_s} \tag{B-45}$$

DROPLET VELOCITY

The droplet drag equation can be written as

$$m_k \frac{dv_k}{dt} = F_k \quad , \tag{B-46}$$

where

$$F_k = \frac{\pi}{8} \rho D_k^2 |v-v_k|(v-v_k)C_{D_k} \tag{B-47}$$

Letting

$$C_{D_k} = 24\left(\frac{\mu}{D_k \rho |v-v_k|}\right)\alpha_k \tag{B-48}$$

the droplet drag equation becomes

$$\frac{dv_k}{dt} = \frac{(18)\alpha_k \mu}{\rho_{\ell_k} D_k^2}(v-v_k) \quad . \tag{B-49}$$

Defining

$$\tau_{drag_k} \equiv \frac{\rho_{\ell_k} D_k^2}{(18)\alpha_k \mu} \tag{B-50}$$

the oscillatory droplet drag equation is

$$\frac{d\tilde{v}_k}{dt} = \frac{(\tilde{v} - \tilde{v}_k)}{\tau_{drag_k}} \quad . \tag{B-51}$$

The following expressions are assumed:

$$\tilde{v} = v' e^{-i\omega t} \tag{B-52}$$

$$\tilde{v}_k = R_{v_k} v' e^{-i\omega t} \tag{B-53}$$

Hence,

$$R_{v_k}\, v'(-i\omega) = \frac{v'}{\tau_{drag_k}} (1-R_{v_k}) \tag{B-54}$$

or

$$R_{v_k} = \frac{1+i\omega\, \tau_{drag_k}}{\left[1 + (\omega\tau_{drag_k})^2\right]} \tag{B-55}$$

NUSSELT NUMBER

It may be observed that one of the dominant terms in the oscilla time delay is the Nusselt number. For longitudinal modes, the Nusselt number is (Ref. 21)

$$Nu_H = 2.0 + 0.6\, Pr^{1/3} \left[\frac{\rho D_k}{\mu} |v-v_R|\right]^{1/2} \tag{B-56}$$

Letting

$$F_\rho \equiv \left(\frac{\rho}{\bar{\rho}}\right)^{1/2}, \quad F_v \equiv \left[\frac{|v-v_k|}{c\Delta M}\right]^{1/2}, \tag{B-57}$$

where

$$\Delta M \equiv \left[\frac{|v-v_k|}{c}\right]_{\text{steady state}}, \tag{B-58}$$

the Nusselt number can be written as

$$Nu_H = 2.0 + 0.6Pr^{1/3} \left[\frac{\bar{\rho}\,\bar{D}_k}{\mu} c\Delta M\right]^{1/2} F_\rho F_v \left(\frac{D_k}{\bar{D}_k}\right)^{1/2}. \tag{B-59}$$

Expanding the preceding equation into time average and oscillatory parts yields

$$\overline{Nu}_H = 2.0 + 0.6\, Pr^{1/3} \left[\frac{\bar{\rho}\,\bar{D}_k}{\mu} c\Delta M\right]^{1/2} \bar{F}_\rho \bar{F}_v \tag{B-60}$$

$$\frac{\widetilde{Nu}_H}{\overline{Nu}_H} = \left(\frac{\overline{Nu}_H - 2}{\overline{Nu}_H}\right) \left[\frac{1}{2}\left(\frac{\widetilde{D}_k}{\bar{D}_k}\right) + \frac{\tilde{F}_\rho}{\bar{F}_\rho} + \frac{\tilde{F}_v}{\bar{F}_v}\right] \tag{B-61}$$

From the definition of F_v and the droplet velocity equations:

$$F_v = \left\{ \left[\bar{v} - \bar{v}_k + \tilde{v} - R_{v_k} \tilde{v} \right]^2 \frac{1}{(\bar{v}-\bar{v}_k)^2} \right\}^{1/4} \tag{B-62}$$

$$F_v = \left[\left| 1 + \left(\frac{\tilde{v}}{\bar{c}} \right) \left(\frac{1-R_{v_k}}{\Delta M} \right) \right| \right]^{1/2} . \tag{B-63}$$

Letting

$$\frac{\tilde{F}_v}{\bar{F}_v} = R_{F_v} \frac{\tilde{v}}{\bar{c}} \quad , \text{ and} \tag{B-64}$$

$$\frac{\tilde{F}_\rho}{\bar{F}_\rho} = R_{F_\rho} \frac{\tilde{\rho}}{\bar{\rho}} \quad , \tag{B-65}$$

the following equation can be determined:

$$\frac{\tilde{\overline{Nu}}_H}{\overline{Nu}_H} = \left(\frac{\overline{Nu}_H - 2}{\overline{Nu}_H} \right) \left[\frac{1}{2} \left(\frac{\tilde{D}_k}{\bar{D}_k} \right) + R_{F_\rho} \left(\frac{\tilde{\rho}}{\bar{\rho}} \right) + R_{F_v} \left(\frac{\tilde{v}}{\bar{c}} \right) \right] . \tag{B-66}$$

For small perturbations in the pressure, the linear response factors and the time average values are

$$\bar{F}_\rho = 1 \quad , \quad \bar{F}_v = 1 \tag{B-67}$$

$$R_{F_\rho} = \frac{1}{2} \quad , \quad R_{F_v} = \frac{1}{2} \left(\frac{1-R_{v_k}}{\Delta M} \right) . \tag{B-68}$$

OSCILLATORY DROPLET TEMPERATURE

The oscillatory combustion time delay requires the evaluation of the heat transfer blockage term which is related to the combustion gas and liquid vapor properties. Since the vapor pressure at the droplet surface is related to the droplet temperature, the blockage term also depends on the oscillatory droplet surface temperature. For a single droplet, the temperature inside the droplet can be described by the energy equation

$$\frac{\partial}{\partial t}\ (\rho c_p T) = \frac{1}{r^2}\ \frac{\partial}{\partial r}\ \left[r^2 k_{eff}\ \frac{\partial T}{\partial r}\right] + \frac{\partial p}{\partial t} \qquad \text{(B-69)}$$

where k_{eff} is the effective liquid thermal conductivity. For zero recirculation inside the droplet, k_{eff} is the standard liquid thermal conductivity. For infinite recirculation, k_{eff} is also infinite.

Since

$$\rho c_p T = \rho c_v T + p \qquad \text{(B-70)}$$

and assuming

$$\rho = \text{constant},\quad c_v = \text{constant},\quad k_{eff} = \text{constant}, \qquad \text{(B-71)}$$

$$\alpha = \frac{k_{eff}}{\rho c_v}\ , \qquad \text{(B-72)}$$

the energy equation can be written as

$$\frac{\partial T}{\partial t} = \frac{\alpha}{r^2}\ \frac{\partial}{\partial r}\ \left[r^2\ \frac{\partial T}{\partial r}\right] \qquad \text{(B-73)}$$

The oscillatory part of the preceding equation is

$$T'\ (-i\omega) = \frac{\alpha}{r^2}\ \frac{d}{dr}\left[r^2\ \frac{dT'}{dr}\right]\ , \qquad \text{(B-74)}$$

where

$$T = \bar{T} + \tilde{T} = \bar{T} + T' e^{-i\omega t} \tag{B-75}$$

and the solution is

$$T' = (T')_{r=r_s} \left(\frac{r_s}{r}\right) \frac{\sinh \sqrt{\frac{-i\omega}{\alpha}}\, r}{\sinh \sqrt{\frac{-i\omega}{\alpha}}\, r_s} \tag{B-76}$$

Differentiating the preceding equation and evaluating at the droplet surface yields

$$\frac{1}{T'_s}\left(\frac{dT'}{dr}\right)_s = -\left(\frac{1}{r_s}\right) + \sqrt{\frac{-i\omega}{\alpha}}\ \mathrm{ctnh}\left(\sqrt{\frac{-i\omega}{\alpha}}\ r_s\right) \tag{B-77}$$

Since the heat transfer rate to the droplet surface is

$$Q'_s = \left[4\pi r_s^2\, k_{eff}\left(\frac{dT'}{dr}\right)_{r_s}\right] = R_{T_s}\, T'_s \quad , \tag{B-78}$$

the response factor can be evaluated as:

$$R_{T_s} = (4\pi\, r_s^2\, k_{eff}) \left[-\frac{1}{r_s} + \sqrt{\frac{-i\omega}{\alpha}}\ \mathrm{ctnh}\left(\sqrt{\frac{-i\omega}{\alpha}}\ r_s\right)\right] \tag{B-79}$$

HEAT TRANSFER BLOCKAGE TERM

From the analysis of the gas film surrounding a vaporizing droplet, the droplet heating rate can be expressed as (Ref. 12):

$$Q_s = Zk_f\, Nu_H \left[\frac{(T-T_s)}{(e^Z-1)} - \frac{\Delta H_{vap}}{c_{p_{v_f}}}\right] \pi\, D_s \quad , \tag{B-80}$$

where the heat transfer blockage term is

$$Z = \frac{c_{p_{v_f}}\, Nu_m\, PMW_{v_f}\, \mathscr{D}_{v_f}}{k_f Nu_H R\, T_f} \ln\left(\frac{p}{p-p_v}\right) \tag{B-81}$$

Assuming that the time average droplet temperature is at "wet bulb" conditions [$(\partial \bar{T}_s/\partial t = 0]$ and the following variables are constant

$$c_{p_{v_f}}, \quad \frac{p M W_v \mathcal{L}_f v_f}{k_f R \bar{T}_f}, \quad \frac{Nu_m}{Nu_H}, \tag{B-82}$$

the oscillatory heat transfer blockage term can be written as

$$\frac{Z'}{\bar{Z}} = \left(\frac{p'_v}{\bar{p}_v} - \frac{p'}{\bar{p}}\right) \left(\frac{\bar{p}_v}{\bar{p}-\bar{p}_v}\right) \Bigg/ \ln \left(\frac{\bar{p}}{\bar{p}-\bar{p}_v}\right) \tag{B-83}$$

Letting

$$\beta_Z \equiv \left(\frac{\bar{p}_v}{\bar{p}-\bar{p}_v}\right) \Bigg/ \ln \left(\frac{\bar{p}}{\bar{p}-\bar{p}_v}\right), \text{ and} \tag{B-84}$$

$$\frac{p'_v}{\bar{p}_v} \equiv \xi_{p_v} \frac{T'_s}{\bar{T}_s}, \tag{B-85}$$

$$\frac{\Delta H'_{vap}}{\Delta \bar{H}_{vap}} \equiv \xi_{\Delta H_v} \frac{T'_s}{\bar{T}_s}, \tag{B-86}$$

the oscillatory droplet heating rate can be written as

$$Q'_s = \frac{(\pi D_s)\, \bar{\bar{z}} k_f \bar{Nu}_H}{(e^{\bar{Z}} - 1)} \left[T' - T'_s + \frac{\bar{\Delta H}_{vap}}{c_{p_{v_f}}} e^{\bar{Z}} Z' + \frac{\bar{\Delta H}_{vap}}{c_{p_{v_f}}} \xi_{\Delta H_v} (e^{\bar{Z}} - 1) \frac{T'_s}{\bar{T}_s} \right] \tag{B-87}$$

The oscillatory heat transfer blockage term then becomes

$$Z' = \bar{Z} \beta_Z \left(\xi_{p_v} \frac{T'_s}{\bar{T}_s} - \frac{p'}{\bar{p}} \right) \tag{B-88}$$

Combining the preceding equations with the heat transfer rate given in the preceding section and letting

$$T' = \bar{T} \left(\frac{\gamma-1}{\gamma}\right) \frac{p'}{\bar{p}} \tag{B 89}$$

the heat transfer blockage term becomes:

$$\begin{aligned} \frac{Z'}{\bar{Z}} \frac{1}{\beta} \Bigg\{ & \frac{2\alpha\rho_k c_{v_k} (e^{\bar{Z}}-1)\bar{T}_s}{\bar{Z} k_f \, Nu_H} \left[-1 + \sqrt{\frac{-i\omega}{\alpha}} \frac{D_k}{2} \operatorname{ctnh} \left(\sqrt{\frac{-i\omega}{\alpha}} \frac{D_s}{2} \right) \right] \\ & + \bar{T}_s - \frac{\overline{\Delta H_{vap}}}{c_{p_{v_f}}} e^{\bar{Z}} \bar{Z}\beta \, \xi_{p_v} - \frac{\overline{\Delta H_{vap}}}{c_{p_{v_f}}} \xi_{\Delta H_v} (e^{\bar{Z}}-1) \Bigg\} \\ = & \left\{ \xi_{p_v} \bar{T} \left(\frac{\gamma-1}{\gamma}\right) - \bar{T}_s + \frac{\overline{\Delta H_{vap}}}{c_{p_{v_f}}} \xi_{\Delta H_v} (e^{\bar{Z}}-1) \right. \\ & \left. - \frac{2\alpha\rho_k c_{p_{v_k}} (e^{\bar{Z}}-1)\bar{T}_s}{\bar{Z} k_f \, Nu_H} \left[-1 + \sqrt{\frac{i\omega}{\alpha}} \frac{D_k}{2} \operatorname{ctnh} \left(\sqrt{\frac{i\omega}{\alpha}} \frac{D_k}{2} \right) \right] \right\} \left(\frac{p'}{\bar{p}}\right) \end{aligned} \tag{B-90}$$

Combining the preceding expressions, and expressions presented in the model formulation section, with the general vaporization rate expression (p. II-25) yields the combustion coefficients:

$$c_{1_s} = R_{m_s} - R_{u_s} - 2 R_{D_s} + \left(\frac{\overline{Nu}_s - 2}{\overline{Nu}_s} \right) \frac{R_{D_s}}{2} \tag{B-91}$$

$$c_{4_s} = R_{F_{\rho_s}} \left(\frac{\overline{Nu}_s - 2}{\overline{Nu}_s} \right) \tag{B-92}$$

$$c_{6_s} = -\left(\frac{\partial \bar{\tau}_s}{\partial MR}\right) \frac{1}{\bar{\tau}_s} \qquad \text{(B-93)}$$

$$c_{8_s} = R_{Fu_s}\left(\frac{\overline{Nu}_s - 2}{\overline{Nu}_s}\right) \qquad \text{(B-94)}$$

$$c_{9_s} = 2\,R_{D_s} - \left(\frac{\overline{Nu}_s - 2}{\overline{Nu}_s}\right) \frac{R_{D_s}}{2} + R_{u_s} \qquad \text{(B-95)}$$

$$c_{12_s} = -\,c_{4_s} \qquad \text{(B-96)}$$

$$c_{14_s} = -\,c_{6_s} \qquad \text{(B-97)}$$

$$c_{16_s} = -\,c_{8_s} \qquad \text{(B-98)}$$

$$c_{2_s} = c_{3_s} = c_{5_s} = c_{7_s} = c_{10_s} = c_{11_s} = c_{13_s} = c_{15_s} = 0 \qquad \text{(B-99)}$$

where the subscript s denotes the fuel or oxidizer and

$$R_{m_s} = G_{inj_s}\left(1 - \frac{i\omega\, x_{k_s}}{\bar{v}_s}\right) \qquad \text{(B-100)}$$

$$R_{u_s} = G_{inj_s} \qquad \text{(B-101)}$$

$$R_{D_s} = \left[b_s - a_s \frac{i\omega\, x_{imp_s}}{\bar{v}_s}\right] G_{inj_s} \qquad \text{(B-102)}$$

It should be noted that the oscillatory heat blockage term has been neglected based on work presented in Refs. 22 and 23 which indicates that this term is not important at low frequencies.

APPENDIX C

CHAMBER MODEL EQUATIONS

In this appendix, chamber model equations are derived from basic flow equations. Complete derivation of the basic equations is presented in Ref. 31. Assumptions used in the derivation of the basic equations are: (1) ideal gas flow is valid state equation; (2) dilute sprays occupy a negligible fraction of chamber volume; (3) the spray can be represented by a finite number of dropsize groups; each dropsize group contains a large number of locally identical drops; and, each size group constitutes a separate liquid phase and exchange terms between liquid phases are not included; (4) drag contributes only kinetic energy to the spray energy equation; (5) secondary "shear" breakup of drops is not included; (6) negligible coupling between diffusion and thermal gradients; and (7) no body forces.

The following equations can be formulated for the gas phase:

Gas Continuity

$$\frac{\partial \rho}{\partial t} + \nabla \cdot (\rho \vec{u}) = \sum_n \sum_j \left(N_j^n \dot{m}_{vap_j}^n \right) \tag{C-1}$$

Gas Momentum

$$\frac{\partial}{\partial t} (\rho \vec{u}) + \nabla \cdot (\rho \vec{u}; \ \vec{u}) = -\nabla p + \nabla \cdot \underline{\underline{\tau}} - \sum_n \sum_j \left[N_j^n \left(\vec{F}_j^n - \dot{m}_{vap_j}^n \vec{u}_j^n \right) \right] \tag{C-2}$$

Equation of State

$$p = \rho R T \tag{C-3}$$

Shear Stress

$$\underline{\underline{\tau}} = -\mu_{eff} \left[\nabla \vec{u} + (\nabla \vec{u})^t - \frac{2}{3} (\nabla \cdot \vec{u}) \underline{\underline{I}} \right] \tag{C-4}$$

Gas Energy

$$\frac{\partial}{\partial t}\left[\rho\left(h + \frac{u^2}{2}\right)\right] + \nabla \cdot \left[\rho \vec{u}\left(h + \frac{u^2}{2}\right)\right]$$

$$= -\nabla \cdot \vec{q} + \nabla \cdot (\vec{u}\underline{\tau}) + \frac{\partial p}{\partial t}$$

$$+ \sum_n \sum_j \left\{ N_j^n \left[\dot{m}_{vap_j}^n \left(h_j + \frac{(u_j^n)^2}{2} \right) - Q_j^n - \vec{u}_j^n \cdot \vec{F}_j^n \right] \right\} \qquad \text{(C-5)}$$

Gas Mixture Ratio

$$\frac{\partial}{\partial t}(\rho MR) + \nabla \cdot (\rho \vec{u}\, MR)$$

$$- \rho \mathcal{D}_{eff} \left[\nabla^2 MR - \frac{2|\nabla MR|^2}{MR + 1} \right]$$

$$- (\nabla MR) \cdot \nabla(\rho \mathcal{D}_{eff}) =$$

$$(2\,MR + 1) \left[\sum_n^{ox} \sum_j N_j^n \dot{m}_{vap_j}^n \right] - (MR)^2 \left[\sum_n^{fu} \sum_j N_j^n \dot{m}_{vap_j}^n \right] \qquad \text{(C-6)}$$

Heat Transfer Rate

$$\vec{q} = -k_{eff} \nabla T - \sum_i (\rho \mathcal{D}_{eff})\, h_i \nabla y_i \qquad \text{(C-7)}$$

Drag Force

$$\vec{F}_j^n = \frac{\pi}{8} \left\{ \rho (D_j^n)^2 \left| \vec{u} - \vec{u}_j^n \right| (\vec{u} - \vec{u}_j^n)\, C_{D_j}^n \right\} \qquad \text{(C-8)}$$

Assuming

$$\mu_{eff} \sim 0, \quad k_{eff} \sim 0, \quad \mathcal{D}_{eff} \sim 0, \tag{C-9}$$

$$\vec{F}_j^n \sim 0, \quad Q_j^n \sim 0, \quad \vec{u}_j^n \equiv \vec{u},$$

The preceding equations can be simplified for longitudinal modes to:

Gas Continuity

$$A \frac{\partial \rho}{\partial t} + \frac{\partial}{\partial x} (A \rho v) = A \left[\dot{m}_{vap_{ox}} \quad \dot{m}_{vap_{fu}} \right] \tag{C-10}$$

Gas Momentum

$$A \frac{\partial}{\partial t} (\rho v) + \frac{\partial}{\partial x} (A \rho v^2) = - A \frac{\partial p}{\partial x} + A \left[\dot{m}_{vap_{ox}} + \dot{m}_{vap_{fu}} \right] v \tag{C-11}$$

Gas Energy

$$A \frac{\partial}{\partial t} \left[\rho \left(h + \frac{v^2}{2} \right) \right] + \frac{\partial}{\partial x} \left[A \rho v \left(h + \frac{v^2}{2} \right) \right]$$

$$= A \frac{\partial p}{\partial t} + A \left[\dot{m}_{vap_{ox}} \left(h_{ox} + \frac{v^2}{2} \right) \right. \tag{C-12}$$

$$\left. + \dot{m}_{vap_{fu}} \left(h_{fu} + \frac{v^2}{2} \right) \right]$$

Equation of State

$$p = \rho R T \tag{C-13}$$

Gas Mixture Ratio

$$A \frac{\partial}{\partial t} (\rho \, MR) + \frac{\partial}{\partial x} (A \rho \, v \, MR) = A(2 \, MR + 1) \left(\dot{m}_{vap_{ox}} \right) - A(MR)^2 \left(\dot{m}_{vap_{fu}} \right) \tag{C-14}$$

Assuming

$$h = \left(\frac{c_p}{R}\right)_{\emptyset} RT + (h_{ref})_{\emptyset} + \left(\frac{\partial h}{\partial MR}\right)_{\emptyset} (MR - MR_{\emptyset}), \tag{C-15}$$

$$\left(\frac{c_p}{R}\right)_{\emptyset} = \frac{\gamma_{\emptyset}}{(\gamma_{\emptyset} - 1)} \quad , \text{ and} \tag{C-16}$$

$$R = R_{\emptyset} + \left(\frac{\partial R}{\partial MR}\right)_{\emptyset} (MR - MR_{\emptyset}), \tag{C-17}$$

and substituting these relations into the preceding longitudinal equations, yields the following modified longitudinal equations:

Gas Continuity

$$A \frac{\partial \rho}{\partial t} + \frac{\partial}{\partial x} (A \rho v) = A (\dot{m}_{vap_{ox}} + \dot{m}_{vap_{fu}}) \tag{C-18}$$

Gas Momentum

$$\rho \frac{\partial v}{\partial t} + \rho v \frac{\partial v}{\partial x} + \frac{\partial p}{\partial x} = 0 \tag{C-19}$$

Equation of State

$$p = \rho T \left[R_{\emptyset} + \left(\frac{\partial R}{\partial MR}\right)_{\emptyset} (MR - MR_{\emptyset}) \right] \tag{C-20}$$

Gas Energy

$$A \frac{\partial p}{\partial t} + Av \frac{\partial p}{\partial x} + \gamma_{\emptyset} p \frac{\partial}{\partial x} (Av) =$$

$$(\gamma_{\emptyset} - 1) A \left\{ \dot{m}_{vap_{ox}} \left[\Delta h_{ox} - \left(\frac{\partial h}{\partial MR}\right)_{\emptyset} (2 MR + 1) \right] \right. \tag{C-21}$$

$$\left. + \dot{m}_{vap_{fu}} \left[\Delta h_{fu} + \left(\frac{\partial h}{\partial MR}\right)_{\emptyset} (MR)^2 \right] \right\}$$

Gas Mixture Ratio

$$\rho \frac{\partial MR}{\partial t} + \rho v \frac{\partial MR}{\partial x} = (MR + 1) \left[\dot{m}_{vap_{ox}} - (MR) \dot{m}_{vap_{fu}} \right] \tag{C-22}$$

Because of the complexity in solving nonlinear partial differential equations perturbation techniques were used to simplify the governing dynamic equations. Assuming

$$\phi = \bar{\phi} + \tilde{\phi} \quad (\phi \text{ any variable}), \tag{C-23}$$

where

$$\bar{\phi} = f(x) \tag{C-24}$$

and

$$\tilde{\phi} = g(x, t), \tag{C-25}$$

each perturbation quantity was taken to be of order (ϵ), where (ϵ) is a small ordering parameter that is a measure of the wave amplitude. The perturbation expressions for each of the independent variables were substituted back into the nonlinear partial differential equations, where all terms of order (ϵ^2) or higher are neglected. The resulting time-averaged equations can be solved for the time-averaged variables and the oscillatory equations can be solved by assuming solutions of the form

$$\tilde{\phi} = \phi' e^{-i\omega t} \tag{C-26}$$

where $\phi' = f(x)$ and ω is the complex frequency. The resulting equations form a system of ordinary differential equations in terms of the variables ϕ's and can be numerically integrated by employing boundary conditions and iteration techniques.

Following this approach the perturbation equations were expressed as:

$$\rho \equiv \bar{\rho} \left[1 + \rho' e^{-i\omega t}\right] \tag{C-27}$$

$$v \equiv \bar{v} + c_g v' e^{-i\omega t} \tag{C-28}$$

$$T = \bar{T} \left[1 + T' e^{-i\omega t}\right] \tag{C-29}$$

$$p = \bar{p}\left[1 + p' e^{-i\omega t}\right] \tag{C-30}$$

$$MR = \overline{MR} + MR' e^{-i\omega t} \tag{C-31}$$

$$\dot{m}_{vap_{ox}} = \bar{\dot{m}}_{vap_{ox}} + \dot{m}'_{vap_{ox}} e^{-i\omega t} \tag{C-32}$$

$$\dot{m}_{vap_{fu}} = \bar{\dot{m}}_{vap_{fu}} + \dot{m}'_{vap_{fu}} e^{-i\omega t} \tag{C-33}$$

The time-averaged equations were determined to be:

Gas Continuity

$$\frac{d}{dx}\left(A \bar{\rho} \bar{v}\right) = A\left(\bar{\dot{m}}_{vap_{ox}} + \bar{\dot{m}}_{vap_{fu}}\right) \tag{C-34}$$

Gas Momentum

$$\bar{\rho}\,\bar{v}\,\frac{d\bar{v}}{dx} + \frac{d\bar{p}}{dx} = 0 \tag{C-35}$$

Equation of State

$$\bar{p} = \bar{\rho} R_{\emptyset} \bar{T}\left[1 + \frac{1}{R_{\emptyset}}\left(\frac{\partial R}{\partial MR}\right)_{\emptyset}\left(\overline{MR} - MR_{\emptyset}\right)\right] \tag{C-36}$$

Gas Energy

$$A\bar{v}\,\frac{d\bar{p}}{dx} + \gamma_{\emptyset}\bar{p}\,\frac{d}{dx}\left(A\bar{v}\right) =$$

$$(\gamma_o - 1)\,A\left\{\bar{\dot{m}}_{vap_{ox}}\left[\Delta h_{ox} - \left(\frac{\partial h}{\partial MR}\right)_{\emptyset}\left(2\overline{MR} + 1\right)\right]\right. \tag{C-37}$$

$$\left. + \bar{\dot{m}}_{vap_{fu}}\left[\Delta h_{fu} + \left(\frac{\partial h}{\partial MR}\right)_{\emptyset}\left(\overline{MR}\right)^2\right]\right\}$$

Gas Mixture Ratio

$$\bar{\rho}\,\bar{v}\,\frac{d\,\overline{MR}}{dx} = \left(\overline{MR} + 1\right)\left[\bar{\dot{m}}_{vap_{ox}} - \overline{MR}\,\bar{\dot{m}}_{vap_{fu}}\right] \tag{C-38}$$

The oscillatory equations are given by:

Gas Continuity

$$\rho' \left(\frac{-i\omega}{c_{\phi}}\right) + \frac{dv'}{dx} + \frac{v'}{A\bar{\rho}} \frac{d(A\bar{\rho})}{dx}$$

$$+ \left(\frac{\bar{v}}{c_{\phi}}\right) \frac{d\rho'}{dx} + \frac{\rho'}{A\bar{\rho}\, c_{\phi}} \frac{d}{dx} (A\bar{\rho}\, \bar{v}) = \frac{(\dot{m}'_{vap_{ox}} + \dot{m}'_{vap_{fu}})}{\bar{\rho}\, c_{\phi}} \qquad \text{(C-39)}$$

Gas Momentum

$$v' \left(\frac{-i\omega}{c_{\phi}}\right) + \frac{v'}{c_{\phi}} \frac{d\bar{v}}{dx} + \frac{\bar{v}}{c_{\phi}} \frac{dv'}{dx} - \frac{\rho'}{\bar{\rho}\, c_{\phi}^2} \frac{d\bar{p}}{dx}$$

$$+ \frac{p'}{\bar{\rho}\, c_{\phi}^2} \frac{d\bar{p}}{dx} + \frac{\bar{p}}{\bar{\rho}\, c_{\phi}^2} \frac{dp'}{dx} = 0 \qquad \text{(C-40)}$$

Equation of State

$$p' = \rho' + T' + \frac{\bar{\rho}\,\bar{T}}{\bar{p}} \left(\frac{\partial R}{\partial MR}\right)_{\phi} MR' \qquad \text{(C-41)}$$

Gas Energy

$$p' \left(\frac{-i\omega}{c_{\phi}}\right) + \left(\frac{\bar{v}}{c_{\phi}}\right) \left[\frac{dp'}{dx} + \frac{p'}{\bar{p}} \frac{d\bar{p}}{dx}\right]$$

$$+ \frac{v'}{\bar{p}} \frac{d\bar{p}}{dx} + \gamma_{\phi} \left[\frac{dv'}{dx} + \frac{v'}{A} \frac{dA}{dx}\right]$$

$$+ \frac{\gamma_{\phi}\, p'}{A\, c_{\phi}} \frac{d}{dx} (A\, \bar{v}) = \frac{(\gamma_{\phi} - 1)}{\bar{p}\; c_{\phi}} \left\{ \dot{m}'_{vap_{ox}} \left[\Delta h_{ox} \right.\right. \qquad \text{(C-42)}$$

$$- \left(\frac{\partial h}{\partial \overline{MR}}\right)_{\emptyset} \quad (2\,\overline{MR} + 1) \Big] + \dot{m}'_{vap_{fu}} \quad \Big[\Delta h_{fu}$$

$$+ \left(\frac{\partial h}{\partial \overline{MR}}\right)_{\emptyset} (\overline{MR})^2 \Big] \quad - 2\,\bar{\dot{m}}_{vap_{ox}} \left(\frac{\partial h}{\partial \overline{MR}}\right)_{\emptyset} \quad MR'$$

$$+ 2\,\bar{\dot{m}}_{vap_{fu}} \quad \overline{MR} \quad \left(\frac{\partial h}{\partial \overline{MR}}\right)_{\emptyset} MR' \Big\}$$

Gas Mixture Ratio

$$MR' \left(\frac{-i\omega}{c_{\emptyset}}\right) + \left(\frac{\bar{v}}{c_{\emptyset}}\right) \frac{d\,MR'}{dx} + \left[\left(\frac{\bar{v}}{c_{\emptyset}}\right) \rho' + v'\right] \frac{d\,\overline{MR}}{dx}$$

$$= \frac{(\overline{MR} + 1)}{\bar{\rho}\, c_{\emptyset}} \left[\dot{m}'_{vap_{ox}} - \overline{MR}\ \dot{m}'_{vap_{fu}}\right] \qquad \text{(C-43)}$$

$$+ \frac{1}{\bar{\rho}\, c_{\emptyset}} \left[\bar{\dot{m}}_{vap_{ox}} - (2\,\overline{MR} + 1)\, \bar{\dot{m}}_{vap_{fu}}\right] (MR')$$

The boundary conditions for the steady-state differential equations are

$$\begin{aligned} @ \quad x &= x_0 \\ \bar{p}_{x_0} &= p_c \\ \bar{v}_{x_0} &= \bar{v}_{x=0} \\ \overline{MR}_{x_0} &= MR_{x=0} \quad (\text{if } \bar{v}_{x=0} \neq 0) \\ (A\bar{\rho}\ \bar{v})_{x_0} &= (\bar{\dot{m}})_{x=0} \quad (\text{if } \bar{v}_{x=0} \neq 0) \end{aligned} \qquad \text{(C-44)}$$

Assuming small Mach numbers, i.e., $M^2 << 1$, the steady-state differential equations can be integrated between the start plane for vaporization (x_0) and any location (x) to yield

$$\bar{p} = \text{constant} = \bar{p}_c \tag{C-45}$$

$$\overline{MR} = \frac{\left(\frac{\overline{MR}}{1+\overline{MR}}\right)_{x=0} (A\bar{\rho}\,\bar{v})_{x=0} + (\bar{\dot{m}}_{ox})_{inj} (1 - \phi_{ox})}{\left(\frac{1}{1+\overline{MR}}\right)_{x=0} (A\bar{\rho}\,\bar{v})_{x=0} + (\bar{\dot{m}}_{fu})_{inj} (1 - \phi_{fu})} \tag{C-46}$$

where

$$\phi_s = e^{-(x-x_0)/\bar{\tau}_s\,\bar{v}_s} \tag{C-47}$$

$$\begin{aligned}\bar{v} = \frac{(Av)_{x=0}}{A} + \frac{(\gamma_\phi - 1)}{\gamma_\phi\,\bar{p}\,A} \Bigg\{ & (\bar{\dot{m}}_{ox})_{inj} (1 - \phi_{ox})\,\Delta h_{ox} \\ & + (\bar{\dot{m}}_{fu})_{inj} (1 - \phi_{fu})\,\Delta h_{fu} + (A\bar{\rho}\,\bar{v}\,\overline{MR})_{x=0} \left(\frac{\partial h}{\partial \overline{MR}}\right)_\phi \\ & - \overline{MR} \left(\frac{\partial h}{\partial \overline{MR}}\right) \Big[(A\bar{\rho}\,\bar{v})_{x=0} + (\bar{\dot{m}}_{ox})_{inj} (1 - \phi_{ox}) \\ & + (\bar{\dot{m}}_{fu})_{inj} (1 - \phi_{fu}) \Big] \Bigg\}\end{aligned} \tag{C-48}$$

$$\bar{\rho} = \frac{1}{A\bar{v}} \Big\{ (A\bar{\rho}\,\bar{v})_{x=0} + (\bar{\dot{m}}_{ox})_{inj} (1 - \phi_{ox}) + (\bar{\dot{m}}_{fu})_{inj} (1 - \phi_{fu}) \Big\} \tag{C-49}$$

$$\bar{T} = \frac{\bar{p}}{\bar{\rho}\,R_\phi \left[1 + \frac{1}{R_\phi} \frac{\partial R}{\partial MR}_\phi (MR - MR_\phi)\right]} \tag{C-50}$$

If the gaseous injection velocity is equal to zero ($\bar{v}_{x=0} = 0$), the steady-state mixture ratio and density at $x = x_0$ are determined by

$$\overline{MR}_{x_0} = \left(\frac{\bar{\dot{m}}_{ox}}{\bar{\dot{m}}_{fu}}\right)_{inj} \left(\frac{\bar{\tau}_{fu}\ \bar{v}_{fu}}{\bar{\tau}_{ox}\ \bar{v}_{ox}}\right) \tag{C-51}$$

$$(\bar{\rho})_{x_0} \frac{(\gamma_\phi - 1)}{\gamma_\phi\ \bar{p}} \left\{ \overline{MR}_{x_0} \left[\Delta h_{ox} - \overline{MR}_{x_0} \left(\frac{\partial h}{\partial \overline{MR}}\right)_\phi \right] \right. \tag{C-52}$$

$$\left. + \Delta h_{fu} - \overline{MR}_{x_0} \left(\frac{\partial h}{\partial \overline{MR}}\right)_\phi \right\} = \overline{MR}_{x_0} + 1$$

These equations were developed by taking the limit as $x \to x_0$ from a downstream distance.

The boundary conditions for the oscillatory differential equations are

$$\begin{aligned} @\ x &= 0 \\ p' &= \Delta p \\ v' &= (v')_{x=0} \end{aligned} \tag{C-53}$$

From these boundary conditions and the oscillatory differential equations the oscillatory conditions at the start plane for vaporization (x_0) can be determined and are:

$$p'_{x_0} = \left[\Delta p \cos\left(\eta \frac{\omega x_0}{c_\phi}\right) + i\gamma_\phi \eta (v')_{x=0} \sin\left(\eta \frac{\omega x_0}{c_\phi}\right) \right] e^{-\frac{i\omega}{c_\phi} \eta^2 \frac{\bar{v}_{x=0}}{c_\phi} x_0} \tag{C-54}$$

where

$$\eta \equiv \sqrt{\frac{\bar{\rho}_{x_0} c_\phi^2}{\gamma_\phi\ \bar{p}}} \tag{C-55}$$

$$v'_{x_0} = \left[\frac{i}{\gamma_\phi} \frac{\Delta p}{n} \sin\left(n \frac{\omega x_0}{c_\phi}\right) + (v')_{x=0} \cos\left(n \frac{\omega x_0}{c_\phi}\right) \right] e^{\frac{i\omega}{c_\phi} n^2 \frac{\bar{v}_{x=0}}{c_\phi} x_0} \quad \text{(C-56)}$$

$$p'_{x_0} = \frac{p'_{x_0}}{\gamma_\phi} \quad \text{(C-57)}$$

$$MR'_{x_0} = (MR')_{x=0} e^{\left(\frac{i\omega}{c_\phi}\right)\left(\frac{c_\phi}{\bar{v}_{x=0}}\right) x_0} \quad \text{(C-58)}$$

$$T'_{x_0} = p'_{x_0} - \rho'_{x_0} - \frac{1}{\bar{R}_{x_0}} \left(\frac{\partial R}{\partial \overline{MR}}\right)_\phi MR'_{x_0} \quad \text{(C-59)}$$

If the gaseous injection velocity is equal to zero ($\bar{v}_{x=0} = 0$), the oscillatory mixture ratio at x_0 is determined by

$$MR'_{x_0} \left[\frac{(\bar{m}_{fu})_{inj}}{A \bar{\rho}_{x_0} c_\phi} (1 + \overline{MR}_{x_0}) - \frac{i\omega}{c_\phi} (\bar{\tau}_{fu} \bar{v}_{fu}) \right]$$

$$= \frac{(\overline{MR}_{x_0} + 1)}{A \bar{\rho}_{x_0} c_\phi} (\bar{m}_{fu})_{inj} \overline{MR}_{x_0} \left(\frac{\dot{m}'_{vap_{ox}}}{\bar{m}_{vap_{ox}}} \quad \frac{\dot{m}'_{vap_{fu}}}{\bar{m}_{vap_{fu}}} \right) \quad \text{(C-60)}$$

$$- (v'_{x_0}) \overline{MR}_{x_0} \frac{(\overline{MR}_{x_0} + 1)}{(\overline{MR}_{x_0} + 2)} \left(1 - \frac{\overline{MR}}{\overline{MR}_{inj}}\right)$$

This equation was developed by taking the limit of the mixture ratio equation as $x \to x_0$ from a downstream distance.

The nozzle admittance based on upstream conditions is

$$A_{N_U} = \gamma_\phi \left(\frac{v'}{\bar{p}\bar{\tau}}\right)_{x=\ell} \quad \text{(C-61)}$$

and the nozzle admittance based on downstream conditions is calculated based on the following analysis.

The gas flowrate of the nozzle inlet plane is

$$\dot{m} = \frac{p\, A_t\, g}{c^*} = A\rho\, v \tag{C-62}$$

where the characteristic velocity is

$$c^* = \frac{\sqrt{g\gamma\, RT}}{\gamma \left[\frac{2}{\gamma+1}\right]^{(\gamma+1)/2(\gamma-1)}} \tag{C-63}$$

For short nozzles, the oscillatory mass flowrate can be written as

$$\frac{\dot{m}'}{\bar{\dot{m}}} = \frac{\rho'}{\bar{\rho}} + \frac{v'}{\bar{v}} = \frac{p'}{\bar{p}} - \frac{1}{2}\,\frac{T'}{\bar{T}} - \left(\frac{\partial \bar{c^*}}{\partial \bar{MR}}\right)\,\frac{MR'}{\bar{c^*}} \tag{C-64}$$

Assuming

$$\frac{\rho'}{\bar{\rho}} = \frac{1}{\gamma}\,\frac{p'}{\bar{p}}\ ,\quad \frac{T'}{\bar{T}} = \left(\frac{\gamma-1}{\gamma}\right)\,\frac{p'}{\bar{p}}\ , \tag{C-65}$$

the nozzle admittance for a short nozzle can be written as

$$A_{N_s} = \bar{\rho}\,\bar{c}\,\bar{v}\,\left[\frac{(\gamma-1)}{2\gamma\,\bar{p}} - \left(\frac{\partial \bar{c^*}}{\partial \bar{MR}}\right)\,\frac{MR'}{\bar{c^*}\,p'}\right] \tag{C-66}$$

Assuming

$$A_N = A_{N_s} \left(\frac{A_N}{A_{N_s}} \right)_{MR = \text{constant}} \tag{C-67}$$

the nozzle admittance becomes

$$A_N = \left[1 - \left(\frac{\partial \overline{c^*}}{\partial \overline{MR}} \right) \frac{MR' \, \overline{p}}{\overline{c^*} \, p'} \left(\frac{2\gamma}{\gamma - 1} \right) \right] A_{N_{MR = \text{constant}}} \tag{C-68}$$

where $A_{N_{MR = \text{constant}}}$ can be calculated using the admittance program developed by Bell (Ref. 32).

APPENDIX D

REPORTS RESULTING FROM CONTRACT NAS9-14315

As a result of work performed under Contract NAS9-14315, "Orbital Maneuvering Engine, Feed System-Coupled Stability Investigation," the following reports have been produced. They are listed in chronological order. The subject matter of each report is summarized.

1. Linow, F. R.: "Combustion Characterization Test Plan," ASR 74-333, Rocketdyne Division, Rockwell International, Canoga Park, CA, October 1974. Describes in detail the test objectives, test hardware, test procedures, and data requirements necessary to obtain empirical characterization of stability-related propellant injection parameters and sensitive operating conditions for OME-type combustor hardware.

2. Kahn, D. R.: "Engineering Model Characterization Evaluation Interim Report," ASR 74-372, Rocketdyne Division, Rockwell International, Canoga Park, CA, December 1974. A summary of the effort conducted during Phase I of Contract NAS9-14315. Includes a detailed assessment of the available techniques for modeling the propulsion system's hydrodynamics, combustion dynamics, and chamber dynamics, and presents recommendations for the characterization technique to be used in each of these areas. A plan for incorporating the recommended techniques into an overall engineering model is also described.

3. Kahn, D. R.: "Engineering Model Verification Plan," ASR 75-108, Rocketdyne Division, Rockwell International, Canoga Park, CA, April 1975. Summarizes the White Sands Test Facility hot-fire test operating data to be employed in the verification of the OME Feed System-Coupled Stability Model. The report contains details of Rocketdyne's thrust chamber and injector, as well as schematics of the fuel and oxidizer feedline configuration used during these tests. Application of the experimental data to model verification is described and the final verification plan is presented.

4. Kahn, D. R., Schuman, M. D., Hunting, J. K., and K. W. Fertig: "Orbital Maneuvering Engine, Feed System-Coupled Stability Investigation, Final Report," R-9807, Rocketdyne Division, Rockwell International, Canoga Park, CA, September 1975. This report summarizes all technical effort conducted during each phase of the program, and is contained within the present volume.

5. Schuman, M. D., Fertig, K. W., Hunting, J. K., and D. R. Kahn: "Orbital Maneuvering Engine, Feed System-Coupled Stability Investigation, Computer User's Manual," R-9808, Rocketdyne Division, Rockwell International, Canoga Park, CA, September 1975. Presents complete documentation of the Feed System-Coupled Stability Model. The report presents the mathematical formulation of the model and a detailed description of the computer program. The latter includes the structure of the main program and all subroutines, instructions for data input, interpretation of program output data, and detailed analyses of program operation. Appendixes present program flow charts, computer code listings, and sample case input/output data.